Modeling of Transient Gas-Solid Reactions in a Fixed Bed Reactor

by

Baba El-Yakubu Jibril

A Thesis Presented to the

FACULTY OF THE COLLEGE OF GRADUATE STUDIES

KING FAHD UNIVERSITY OF PETROLEUM & MINERALS

DHAHRAN, SAUDI ARABIA

In Partial Fulfillment of the
Requirements for the Degree of

MASTER OF SCIENCE

In

CHEMICAL ENGINEERING

June, 1996

INFORMATION TO USERS

This manuscript has been reproduced from the microfilm master. UMI films the text directly from the original or copy submitted. Thus, some thesis and dissertation copies are in typewriter face, while others may be from any type of computer printer.

The quality of this reproduction is dependent upon the quality of the copy submitted. Broken or indistinct print, colored or poor quality illustrations and photographs, print bleedthrough, substandard margins, and improper alignment can adversely affect reproduction.

In the unlikely event that the author did not send UMI a complete manuscript and there are missing pages, these will be noted. Also, if unauthorized copyright material had to be removed, a note will indicate the deletion.

Oversize materials (e.g., maps, drawings, charts) are reproduced by sectioning the original, beginning at the upper left-hand corner and continuing from left to right in equal sections with small overlaps. Each original is also photographed in one exposure and is included in reduced form at the back of the book.

Photographs included in the original manuscript have been reproduced xerographically in this copy. Higher quality 6" x 9" black and white photographic prints are available for any photographs or illustrations appearing in this copy for an additional charge. Contact UMI directly to order.

UMI

A Bell & Howell Information Company
300 North Zeeb Road, Ann Arbor MI 48106-1346 USA
313/761-4700 800/521-0600

MODELING OF TRANSIENT GAS-SOLID REACTIONS IN A FIXED-BED REACTOR

BY

BABA EL-YAKUBU JIBRIL

A Thesis Presented to the

FACULTY OF THE COLLEGE OF GRADUATE STUDIES

KING FAHD UNIVERSITY OF PETROLEUM & MINERALS

DHAHRAN, SAUDI ARABIA

In Partial Fulfillment of the
Requirements for the Degree of

MASTER OF SCIENCE

In

CHEMICAL ENGINEERING

June, 1996

KING FAHD UNIVERSITY OF PETROLEUM & MINERALS
DHAHRAN, SAUDI ARABIA

COLLEGE OF GRADUATE STUDIES

This thesis, written by

BABA EL-YAKUBU JIBRIL

under the direction of his thesis committee, and approved by all the members, has been presented and accepted by the Dean, College of Graduate Studies, in partial fulfillment of the requirement for the degree of

MASTER OF SCIENCE IN CHEMICAL ENGINEERING

Thesis committee

M.A. Hastaoglu
Dr. Mehmet A. Hastaoglu
(Chairman)

Prof. Hussien K. Abdel Aal
(Member)

A. J. Al Amer
Dr. Adnan J. Al-Amer
(Member)

Dr. Ramazan Kahraman
(Member)

Dr. Dulaihan K. Al-Harbi
(Department Chairman)

Dr. Ala Al-Rabeh
(Dean College of Graduate Studies)

Date: 23-6-96

COLLEGE OF GRADUATE STUDIES

To my grandmother

Hajiya Rahana,

who put me on 'the way'...., to Dhahran,.....,
but was not destined to see me again.
May her soul rest in peace.

ACKNOWLEDGMENT

I must thank the almighty Allah for guiding me all along and His noble prophet Muhammad (S.A.W) who propounded the complete message.

Much of the credit of this work must go to my abled advisor, Dr. M. A. Hastaoglu, whose method of teaching and our discussions on this work made easy easier. He was always ready to offer a helping hand. He encouraged me to contact him any time, and insisted that "there is no hour that is odd". I remain grateful.

I am also grateful to my thesis committee members; Professor H. K. Abdel-Aal, Dr. A. J. Al-Amer and Dr. R. Kahraman. Their support and guidance were great sources of encouragement. I thank the management of KFUPM/RI division I for providing the naphtha hydrodesulfurization experimental data used in the validation of the model. I thank Dr. Ibrahim Ashour for rendering the abstract into Arabic and Mr. A. I. Abba and Mr. U. A. El-Nafaty for their assistance. I appreciate the support and encouragement of my other friends and colleagues whose names cannot be specifically mentioned here.

I fully appreciate the financial support and facilities supplied by KFUPM and am grateful to the Chemical Engineering Department for all the help given to me.

I remain indebted to my parents for their love and understanding. I owe a deep sense of gratitude to my grandmother, Hajiya Rahana, who put me on 'the way' to Dhahran, but was not destined to see me again. May her soul rest in peace. I profusely thank my wife, Jamilah, for having put up with my long absence without complain.

TABLE OF CONTENT

LIST OF FIGURES

THESIS ABSTRACT

NAME OF STUDENT	**BABA EL-YAKUBU JIBRIL**
TITLE OF STUDY	**Modeling of Transient Gas -Solid Reactions in Fixed-Bed Reactors**
MAJOR FIELD	**Chemical Engineering**
DATE OF DEGREE	**June, 1996**

Transient gas-solid reactions taking place in a fixed bed reactor have been modeled. Three levels of process space are used: the bed, pellets and grains in meter, millimeter and micron sizes respectively. This kind of a rigorous model is very rare in literature.

The multi-component mixture traveling down the reactor through the void spaces enters the gas film around the pellets and into its pores. The product gases travel in reverse order out of the pellets and down the reactor. Both radial and axial directions are included. Heat transfer follows a similar path. Also convective heat transfer is considered at the bed wall. Mass fluxes are approximated via "dusty gas model". Convective transfer coefficients are used for transport into the pellets. All transport and thermophysical parameters are used as transient.

Highly nonlinear partial differential equations for heat and mass transfer are approximated as finite difference equations. The pellet and bed equations are solved using an iterative alternating-direction-implicit method with considerable savings in storage and computation time. Thomas algorithm was used to solve for component concentrations and temperature from the resulting tridiagonal matrices.

Pellet model has been validated with four selected gas-solid reactions. Due to lack of transient experimental data the bed model is validated using steady state experimental data of catalytic hydrodesulfurization reaction with Langmuir-Hinshelwood mechanism. The model gave a conversion of 99.98% compared to experimental value of 99.90% for thiophene at steady state. Steady state average temperature was predicted within 0.5 %. In both cases the model has successfully predicted the experimental data. It has also been verified via a mass balance approach. The model has been tested for stability with qualified success. Some parametric studies were performed. The response of the model to perturbation in feed inlet conditions are also shown herein.

This model could be used for the studies of short-lived processes, e.g. start-up and shutdown, predictive and control simulation, etc.

MASTER OF SCIENCE DEGREE

KING FAHD UNIVERSITY OF PETROLEUM AND MINERALS

DHAHRAN, SAUDI ARABIA

JUNE, 1996

ملخص الرسالة

أســم الطـالب : بابا اليعقوب جبريل

عنوان الرسالـه : النمذجة الديناميه للتفاعلات بين الغاز والمواد الصلبه في مفاعلات ذات مهد ثابت

التخصص العام : هندسه كيميائيه

تاريـخ الدرجه : يونيه ١٩٩٦ م

التفاعلات الديناميه بين الغاز والماده الصلبه في مفاعل ذي مهد ثابت قد تم نمذجته .ثلاثة مستويات فراغيه للعمليه أستخدمت وهي المهدوالحبه الكبيره ووجداتها على التوالي متر مليمتر ، ميكرو متر . هذا النوع من النمط التفصيلي قليلا ما يوجد في المنشورات العلميه .

الخليط متـعدد المواد مـن الغـاز يمـر من أعلـى إلـى أسفل مـن خلال المسـام وخلال الشريـط الغـازي (الفيلـم الغـازي) حـول الحبـه الكبيره (pellet) منها الى المسام الداخليه . المنتج الغازي يخرج من المسام ويمر من أعلى المفاعل إلى أسفل . كلا الأتجاهين القطري والرأسي قد تم إدراجها في الدراسه .

إنتقال الحراره تبع نفس المسار المشابه . وأنتقال الحراره بالحمل أيضاً قد اخذ في الأعتبار عند حائط المهد . معدل أنتقال الماده قد قرب بواسطة نمط غازي (dusty gas model). معاملات الحراره بالحمل أستخدمت لنقل الماده خلال الحبه الكبيره . معاملات النقل والثرموديناميكيه المستخدمه كانت ديناميه .

معادلات تفاعليه جزئيه غير خطيه لنقل الماده والحراره قد قربت بمعادلات جبريه بأستخدام طريقه الفروق المحدده . هذه المعادلات قد حُلت والنتائج قد خُزنت هي وزمن الحاسبات .نمط الحبه الكبيره قد أختبرت توافقيته لأربع تفاعلات غازيه مع صلبه مختاره - هذا النمط قد أختبر توافقيه لنتائج ساكنه عمليه وذلك لعدم وجود نتائج ديناميه معمليه ومن هذه النتائج التي أستخدمت أزالة الكبريت بواسطة الهيدرجه في وجود عامل حفزي بواسطة نمط لو نجهاير - هينشيلوود - النمط أعطى تحويل قيمته ٩٨، ٩٩ ٪ مقارنه لقيمة عمليه ٩، ٩٩٪ لمادة الثيوفين عند الحاله الساكنه . ودرجة الحراره المتوسطه للحاله الساكنه حسبت بمقدار خطأ ٥ ر٠ ٪ في كلتا الحالتين النمط تمكن بنجاح من حساب القيم العمليه . وقد تحقق من ذلك بواسطة أتزان الماده . النمط قد أختبر للأتزان بنجاح وصفي . بعض الدراسات الخاصه بالمعاملات قد أجريت . أستجابة النمط لاضطراب في ظروف التغذيه قد قدمت في هذا البحث .

هذا النمط يمكن استخدامه لدراسات على العمليات مثل بداية التشغيل والتوقف ومحاكات التحكم ...الخ

درجة الماجستير في العلوم

جامعة الملك فهد للبترول والمعادن

(الظهران) المملكه العربيه السعوديه

يونيه ١٩٩٦

CHAPTER 1

INTRODUCTION

1.1 GENERAL

Most gas-solid reactions, catalytic and non-catalytic can, to some extent, be conducted in almost any vessel that contains the solid and withstands the temperature and pressure of the reaction. The choice of a fixed-bed reactor or any other appropriate means becomes important where the objective is to conduct the reaction profitably. Fixed-bed reactor is among the commonest reactor types extensively used for a large number of processes; catalytic and non-catalytic reactions and mass and heat transfer operations (Froment et al., 1987). The main advantages of this type of reactor are its simplicity in construction and ease of operation.

Gas-solid reactions in fixed-bed reactors are frequently encountered in the chemical process industries. Examples of these include, hydrodesulfurization of petroleum feedstock, carbon desulfurization, coal gasification, roasting of pyrites, combustion of solid fuel, and pyrolysis. Reactions taking place in a matrix can also be considered as a fixed-bed configuration. These include waste incineration, underground gasification, and soil conditioning. This class of reactions finds wide application also in petrochemical industry. The most important are regeneration of coked catalyst by oxygen-containing gases, reduction or reoxidation of nickel (reforming) or ammonia-synthesis (on iron).

Perhaps the most important question to ask when initiating a design project for a fixed-bed reactor is whether or not the reactor is really suitable for the purpose at hand. The next important point is a picture of its transient behavior for short-lived processes, e.g. start-up and shutdown. In order to answer these questions for decision-making processes, predictive and control simulation or scale-up purposes, an accurate mathematical model describing the processes taking place is very important. The solution of the necessary equations governing heat and mass transfer, which are a set of highly nonlinear partial differential equations will supply values for the dependent variables of the system for decision making.

Due to the importance of these system-dependent-variables, modeling of the reactor has been a subject of rigorous studies by various researchers. However, important as it is, development of generalized models of multicomponent and multireaction schemes that describe the transient phenomena of the reactor is very rare in the literature. Almost all of the works reviewed were carried out either for a specific reaction or a group of similar reactions and are generally for steady state models. In most transient studies, mass and energy fluxes in the radial direction are neglected in most of them. This makes them unsuitable for the study of short-lived phenomena, for instance, when the feed is stopped during the shutdown of the reactor.

As a result of the foregoing, an attempt is made here to develop a detailed mathematical model that describes the transient behavior for gas-solid reactions, both microscopically in the pellet and macroscopically in the bed of the reactor. The microscopic model for the pellet is based on pore or grain model, describing diffusion, reaction, and pore structure evolution in the pellets developed earlier (Abba and Hastoaglu, 1995). This is to be used together with macroscopic

continuum fixed-bed reactor equations to model the transient phenomena that take place in gas-solid reactions. It is both necessary and important to include such level of details in the model because, in presenting a mathematical model describing the transient behavior of a fixed-bed reactor, there are many important mechanisms necessary for an accurate analysis of transport phenomena occurring in such reactors. The use of simplifying assumptions to remove some of the complexity in the model may lead to misleading conclusions.

On this basis it is suggested that the only procedure for obtaining valid fixed-bed reactor profiles is to include all important factors in the derivation of equations. In addition, stability seems to be connected to the behavior of the pellet equation rather than the bed equation (McGruire and Lapidus, 1965). In this work, all important factors are included in both the heat and mass transfer equations in the pellet and the bed.

The important physical properties of the system are estimated based on the assumption of continuum in the bed. The critical temperature and pressure, gas heat capacity, heat of formation and the constants which are required for the calculation of various physical data are taken from the literature. The individual viscosities are determined from the method of Thodos (Reid et al., 1977) and the effective value is estimated by the Wilkes approximation. The diffusivities are determined by Chapman and Enskog method (Bird et al., 1977). For the thermal conductivity, Wassiljewa equation (Reid et al., 1977) is used. The mass and heat transfer coefficients are determined from the Chilton-Colburn analogy based on Rowe and Claxton (1965) correlation.

The model is validated in two ways: i) using some experimental data available in the literature and ii) overall material balance on the bed.

1.2 RESEARCH OBJECTIVES

The objectives of this research are to:

a) Formulate multicomponent gas-solid -multireaction schemes among gases and solids in a transient fixed bed reactor where:

i) The radial and axial directions are considered.

ii) There are three spaces within the bed which are:

- the bed (dimension in meters),
- the pellet space (dimension in centimeters), and
- the grain or pore space (with dimension in microns)

iii) The bed operation is nonisothermal. It is either heated or cooled from the side walls or by the incoming feed.

iv) The structural parameters such as bed porosity, pellet size, pore size undergo changes during reactions.

v) The gas velocity and pressure depend on position in the bed.

vi) All transport properties are transient

b) Prepare the set of governing partial differential equations for mass (for each component) and heat transfer. The auxiliary equations for transport parameters and other properties complement the main equations. The travel of the reaction front, a differential equation in the diffuse reaction zone for each solid component, is also considered.

c) Develop a finite difference solution strategy.

d) Solve the set of equations.

e) Verify the results obtained through the solution strategy.

f) Check the sensitivity and accuracy of the results.

1.3 ORGANIZATION OF THE THESIS

In this thesis a mathematical model is presented for describing the transient behavior of a fixed-bed reactor. This model includes most of the important mechanisms necessary for an accurate description of the transport phenomena occurring in such a reactor as emphasized in the objectives of this thesis.

After this introductory chapter, Chapters 2 and 3 show some essential preliminaries for the work. In Chapter 2 background information on fixed-bed reactor modeling is outlined. A brief review of some relevant works on the modeling is also given. Chapter 3 gives the model formulation. Here conservation equations which are highly non-linear partial differential equations (PDE's) are developed. The equations for transport and physical properties are also given.

In Chapter 4 the non-linear PDE's are converted into approximate algebraic difference equations for the solution of the model. An attempt is made in Chapter 5 to show the validity of the model by comparing its results with steady state experimental data of fixed-bed reactor hydrodesulfurization (HDS). On the pellet level the model has successfully predicted the experimental conversion/time data obtained for carbon gasification, metal oxide reduction, and wood pyrolysis obtained by TGA experiments. A simulation study of the HDS is presented and discussed in Chapter 6. Some concluding remarks, observations and recommendations for further work are given in Chapter 7.

Appendices A and B are included where, appendix A describes the Thomas algorithm, the technique used in the model and appendix B gives a brief description and flowchart of the program.

CHAPTER 2

BACKGROUND TO THE WORK AND LITERATURE REVIEW

2.1 BACKGROUND TO THE WORK

2.1.1 INTRODUCTION

The fixed-bed reactors are among the commonest types of reactors that are generally used in the process industry. This is chiefly due to some of its advantages over other types. Its construction is simple, essentially similar to that of a shell-and-tube heat exchanger (Doraiswamy and Sharma, 1984). In its crudest form the reactants simply flow through the solid packed in the tubes while the heat exchanging medium flows on the outside surface of the tubes. This also makes the reactor easy to operate, and therefore, generally employed for the majority of gas-solid reactions. One important area where the fixed-bed reactor is not used is in catalyst regeneration. Here, fluidized bed reactor is preferred for continuous regeneration of catalysts. In order to control the pronounced heat effect in some cases, multibed adiabatic reactor may be used. In this case direct or indirect interstage heat exchange could be employed for optimum operations (Froment et al., 1977). The heat exchange would be via a heat-exchanging fluid on the outside surface of the tubes or by inserting tubes that contain the heat-exchanging fluid into the bed. Further relevant discussion on this is given by Froment et al. (1977).

2.1.2 TYPICAL EXAMPLES OF GAS-SOLID REACTIONS

Gas-solid reactions; both catalytic and noncatalytic, constitute a class of very important reactions in use today. Catalytic gas-solid reactions occupy a prominent position in the chemical industry as a whole including refining, petrochemicals, etc. The noncatalytic reactions are equally important. These are prevalent in metallurgical operations, pollution abatement, and gasification among others.

Some examples of catalytic reactions are:

Ammonia synthesis	Iron as a catalyst
Oxidation of sulfur dioxide	Supported platinum or vanadium oxide
Isomerisation of xylenes	ZSM-5 Zeolite

The most general type of a single heterogeneous noncatalytic reaction can be represented by (Doraiswamy and Sharma 1984)

$$A + B = C + D$$

where A, B, C and D can each be either a solid or a gas; further, one of the reactants or products may not be present at all. Some specific type of the reactions are:

Type A (Reduction or roasting of ores):

Fluid and solid reactants $\rightarrow$ fluid and solid products

e.g. roasting of zinc ore

$$2ZnS(s) + 3O_2(g) \rightarrow 2ZnO(s) + 2SO_2(g)$$

Type B:

Fluid and solid reactants $\rightarrow$ solid products

e.g. nitrogenation of calcium carbide to produce cyanamide

$$N_2(g) + CaC_2(s) \rightarrow CaCN_2(s) + C(s)$$

Type C (decomposition reactions):

Solid reactants → fluid and solid products

e.g. decomposition of magnesium hydroxide

$$Mg(OH)_2(s) \rightarrow MgO(s) + H_2O(g)$$

Type D (gasification reaction):

Fluid and solid reactants → fluid products

e.g. gasification of carbon

$$C(s) + H_2O(g) \rightarrow CO(g) + H_2(g)$$

Type E (thermal decomposition reactions):

Solid reactants → fluid products

e.g. decomposition of ammonium chloride

$$NH_4Cl(s) \rightarrow NH_3(g) + HCl(g)$$

It is obvious that type A reaction is the one most commonly encountered in the process industry. In the subsequent discussion emphasis would be on this type of reaction although the model could handle types A, B, C, and D.

2.1.3 MACROSCOPIC MODEL FOR FIXED-BED REACTOR

The ultimate objective of reactor modeling is to arrive at the system variables of temperature, pressure, concentration, etc. that result in an optimal operation condition, for instance, highest conversion or selectivity. For this reason we need to develop a set of equations that relate the system variables, for example, to the conversion. Reasonable approximations become important because of the complex hydrodynamics involved in the fixed-bed. So the system of equations to be used must take these approximations into considerations. Many mathematical models for conservation of heat and mass in the reactor have been proposed in the literature.

2.1.3.1 CLASSIFICATION OF MODELS

In this section, we look at the classification of the fixed-bed reactor models as classified by Froment et al. (1977). These are mainly the pseudohomogeneous and heterogeneous models. The important line between them is the difference in consideration of the temperature and concentration between the bulk and solid. While the heterogeneous model distinguishes these two variables between the bulk and the solid surface, pseudohomogeneous one does not. Each class can further be subdivided into one-dimensional or two-dimensional models to account for the gradients in the reactor bed. In addition, unsteady-state operation could also be included which complicate the analysis extensively.

Pseudohomogeneous Model

The basic pseudohomogeneous model postulates plug flow through the bed. Uniform flow in a section perpendicular to flow is assumed, hence a one-dimensional model. There is, of course, some non-uniformity in a thin layer close to the wall when the heat is exchanged with the surrounding. This basic model is only an ideal case; in reality, there is at least some mixing or dispersion in the axial (z) or radial direction. The model becomes two-dimensional when dispersion in radial direction is considered. This is mainly because of the occurrence of temperature gradients.

Heterogeneous Model

The basic model of this category is a simple extension of the one in the pseudohomogeneous model. In this case, temperature and concentration gradients over the film surrounding the catalyst particles are considered. In order to move closer to reality, gradients inside the catalyst particle may be added to the previous

model. Finally, a closest model to reality is obtained by the addition of axial and radial gradients in the reactor as well as inter- and intraparticle local gradients. In this work, transient phenomena of the fixed-bed reactor would be investigated with the two-dimensional model.

2.1.4 APPROACHES TO THE REACTOR MODELING

The phenomena described above coupled with dispersion, must be quantitatively expressed for studying the system. There are different accepted approaches for the modeling of the fixed-bed reactor. The four main approaches described by Doraiswamy et al. (1984), are summarized in Figure 2.1.

The Quasicontinuum Model

The most generally accepted approach is the quasicontinuum model where the overall flow is considered to follow parallel streamlines although not necessarily at a uniform velocity. The gross concentration and temperature profiles in the bed are assumed to be continuous functions of axial and radial coordinates. The mixing caused by the presence of packing is modeled in terms of Fickian diffusion mechanism. But the diffusibity is termed 'effective' diffusivity or dispersion coefficient because it is a lumped effect of molecular and turbulent diffusion. In this work continuum model approach is used.

Another model, the cell model, accounting for the two-phase nature of the reactor, has also received considerable attention in the literature. In this case, each pellet along with its environment is considered as a small, completely mixed reactor or cell. A sequence of such cells connected in the direction of flow is assumed to approximate the heterogeneous one - dimensional model. In the two - dimensional

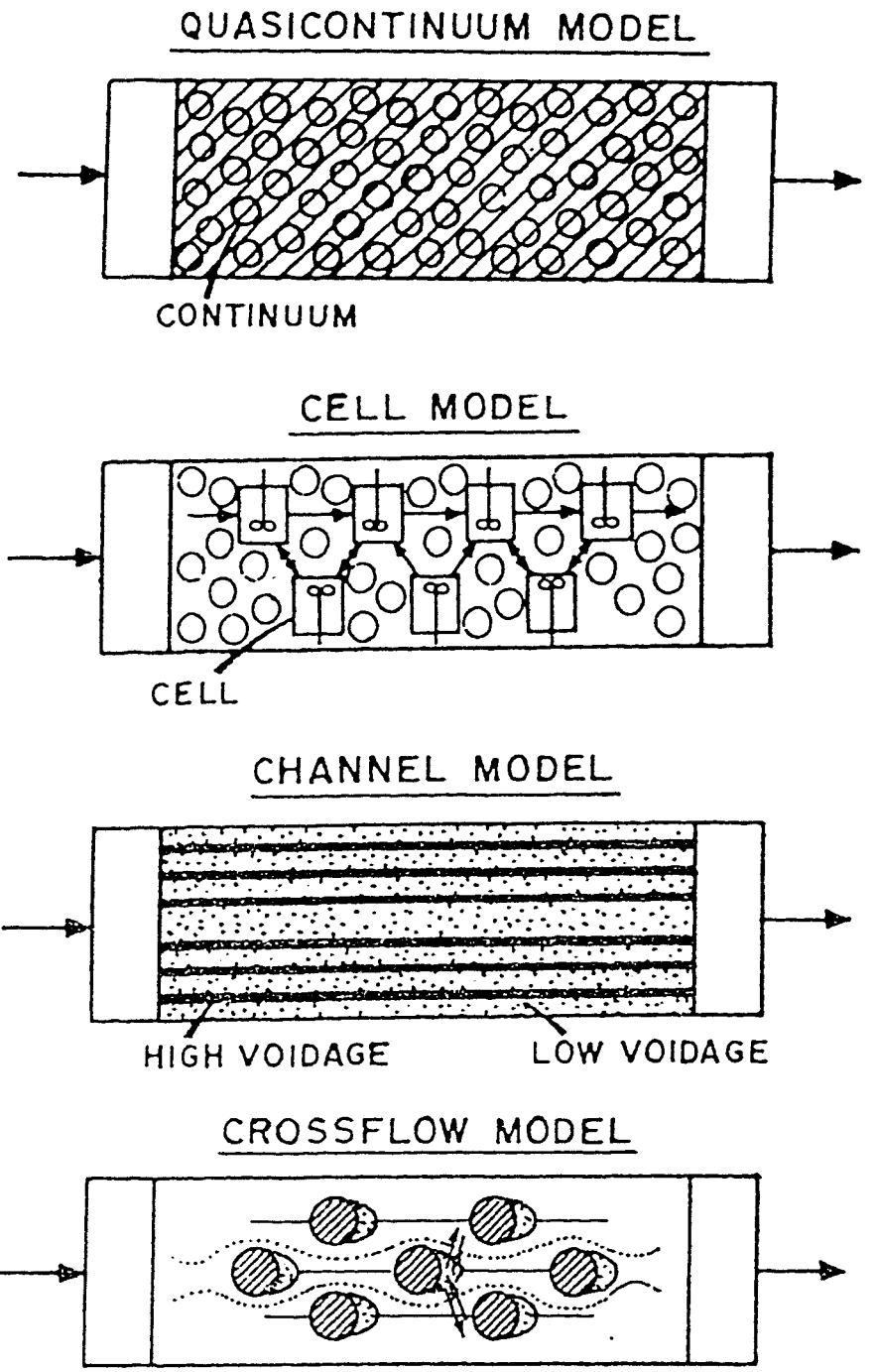

Figure 2.1 Models for describing different approaches for fixed-bed reactor (Doraiswamy et al. 1984).

model, the cells are additionally considered to be laterally connected.

The Channel Models

These are based on the observed distribution of local void volume in the bed. The void volume passes through alternate zones of maxima and minima in the radial direction. The channel model in its simplest form assumes that the packed bed is built up of coaxial cylindrical surfaces passing through a minimum voidage.

Crossflow Models

These are based on the idealization of the flow pattern in the bed. The whole region is classified into stagnant and flowing parts. The stagnant parts correspond to the wakes of the packing elements, and dispersion is introduced by assuming that there is an exchange of fluid between the stagnant and flowing regions throughout the bed. The physical situation gives rise to first-order differential equations as against the recurrence relations in mixing-cell models and second-order differential equations in the Fickian diffusion models. The models are described as initial value problems and avoid all the complications inherent in the existing models. However, the other models are conceptually simpler.

2.1.5 FIXED-BED REACTOR MICROSCOPIC MODEL

In addition to the fixed-bed macroscopic models, the microscopic model on the pellet level is also very important. This is particularly so when the solid is being reacted as the reaction continues. The models that have been developed for predicting the conversion as a function of time for solids undergoing reaction are both diverse and numerous. Basically two types of models have been considered; one in which the solid is assumed to be nonporous and one in which it is assumed

porous. These models and the examples of their application are described elsewhere (Doraiswamy and Sharma, 1984).

Pellet model is described below briefly (Szekely and Hastaoglu, 1976; Doraiswamy et al., 1984). The particle-pellet model postulates that the solid pellet consists of a number of small particles or grains which are surrounded by macrospores of the gas phase through which the gas has to diffuse to reach various grains (micron or submiron in size). The reaction occurs in each grain according to the sharp-interface model. A product layer forms with time around each grain and this in turn offers some resistance to mass and heat transfer. The mathematical analysis of such systems can be built up by first considering the rate of reaction of individual grains and then incorporating it in the mass balance of species in the macropores of the solid. A schematic diagram of the model is shown in Figure 2.2.

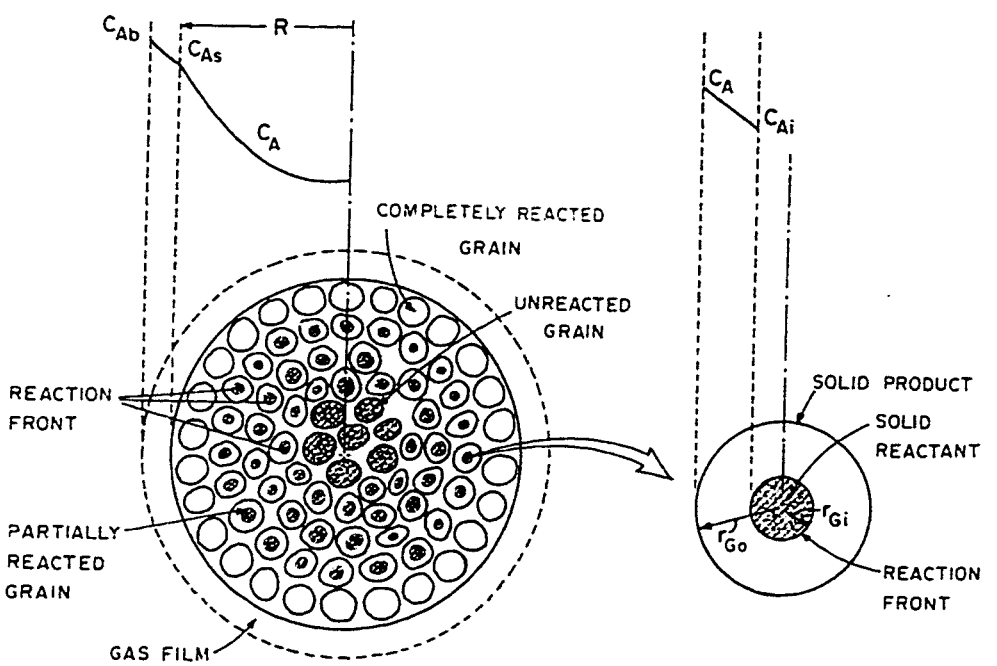

Figure 2.2 Schematic representation of the grain model for the reaction of a porous solid with a gas (Doraiswamy et al., 1984).

2.2 BRIEF REVIEW OF THE RELEVANT WORKS ON FIXED-BED REACTOR MODELING

Almost all the works reviewed were carried out for a specific system or a number of similar systems. A group of workers, (Efthimiadis et al., 1993) have reported a two-dimensional mathematical model for a fixed-bed reactor. They have specially modeled coal desulfurization reactions. They neglected the variation of temperature in the axial direction. Both experimental and steady state studies were performed. Their model was fairly accurate. It employed a comprehensive generalized pore model developed earlier by Yu et al. (1987). In a similar work, Sotirchos et al. (1989) have reported the effect of different pore models on the modeling of a fixed-bed reactor for desulfurization. The transient behavior of the model was considered. Froment et al. (1994) have reported a 1-D heterogeneous model for hydrodesulfurization of oil fractions. They studied both experimental and adiabatic aspects in modeling analysis.

Bhattacharya et al. (1986) have modeled char gasification in a fixed-bed reactor. Axial mixing of mass and energy as well as dispersion of mass were ignored. Their model was accurate only at the initial stage of the simulation. Hobbs et al. (1992) also have reported a one-dimensional unsteady-state model for coal gasification. Their model gave a fair representation of the reactor. They emphasized the importance of the char oxidation resistance to bulk film diffusion. Other detailed models have been applied very well to a variety of reactions as reported by Hastaoglu, (1995), Hastaoglu and Hassam, (1988) and Hastaoglu et al. (1988). They were applied to carbon gasification, metal oxide reduction, wood pyrolysis and catalytic carbon gasification. Another model for specific application is the one developed by Silveston et al. (1994). It was developed and applied for

SO_2 oxidation. Good agreement between transient simulation and experimental data obtained earlier was reported. Grozev et al. (1994) have recently reported unsteady state SO_2 oxidation that supported an earlier model prediction.

Ferreira et al. (1992) have developed a model to predict the dynamic behavior with large pore catalyst particles. They considered processes taking place in both the particles and the bed. The diffusive term in the bed was ignored. They used the method of lines for integration. Space coordinates were discretized via orthogonal collocation in finite elements. Another group have earlier employed collocation method (Segall et al., 1984). They emphasized the advantage of this method over the finite difference for reactor control purposes. They used data from catalyzed hydrogenolysis of n-butane to compare the orthogonal collocation with finite difference method. The conclusion they have drawn is that, the main drawback to this is the number of the collocation points which are usually small. This makes the system susceptible to instability.

Acharya et al. (1990) have reported a validated model for butene-1 dehydrogenation. Their results have compared well with experimental data. They assumed constant temperature and concentration gradients in the radial direction. The pellets remained isothermal during the analysis. Some models for reactor optimization on some specific reactions were also reported (Borio, et al. 1992; Cropley, 1990).

From the foregoing it is apparent that modeling of fixed-bed reactors for some specific systems have received considerable attention. In particular, significant work has been done in coal combustion and gasification processes. A number of models on these processes have appeared in the literature. The recent review by

Hobbs et al. (1993) is the most comprehensive one. It emphasized the modeling and research effort in combustion and gasification during the last 10 years. In that review 37 models are identified: six are zero-dimensional, 27 are one-dimensional, and four are two-dimensional. Twenty-one of these models are categorized as heterogeneous, which use separate solid and gas temperatures. The features and limitations common to these models are stated. Recently the same authors, Hobbs, et al. (1992) have developed a one-dimensional model which has removed some of the limitations. The most recent model for coal gasification and combustion is by Radulovic, et al. (1995). It is an improved version of the one-dimensional models developed earlier.

Many other workers have studied different aspects of fixed-bed reactors such as stability, multiplicity of solution, etc. Khandaralli et al. (1993) have studied the stability of a catalytic fixed-bed reactor using a steady state model. They presented a criterion for reactor stability which can be extended to different reaction schemes. The work gives an insight into the stability regimes of the model. Another interesting work on the reactor behavior is that of Almeida-Costa et al. (1994). They have reported a one-dimensional heterogeneous model for wrong-way analysis in the transient regime. They have emphasized the important impact of intraparticle convection on the occurrence of wrong-way behavior for the temperature of the solid phase.

Development of sophisticated models for the treatment of experimental data is very rare in the literature. Generally, simplified rate expressions have been used, as was done by Richard et al. (1994). They used statistical modeling with simplified rate expressions, owing to the highly complex nature of the problem. Another model was developed by Abdel-Hadi and Hsu (1981) for underground

coal gasification using the permeation method. The resulting equations were solved by finite-element method. They used a transient, 2-D Cartesian model. Another work by Wedel and Luss (1984) was also about a 1-D, two-phase model concentrating particularly on steady state multiplicity.

Due to the advantage of transient operation in increased conversion and selectivity (in many cases), some researchers have investigated reacting systems in the transient regimes. Bussche et al. (1993) have presented a simulation result of a fixed-bed reactor for methanol synthesis based on a heterogeneous one dimensional model. Different levels of transient modeling were compared thereby assessing the influence of some operating parameters. This study has given further insight into the complex behavior of the reversed flow reactor. Another group (Hoebink et al., 1994) has reported a two-dimensional heterogeneous model taking into account axial dispersion for both mass and enthalpy. The model could handle multicomponent in gases and multireaction network. They have also highlighted the importance of the homogeneous reaction in the void space. The intrapellet gradients are found to have a large impact on the rate of production. Apart from these few 1-D and 2-D models nobody seems to have attempted to present a generalized model.

It is as a result of the foregoing that an attempt is being made here to develop a detailed mathematical model that describes the transient behavior of a fixed-bed reactor for gas-solid reactions. It is based on the grain-pellet model, describing diffusion, reaction, and pore structure evolution in pellets. This is used together with macroscopic fixed-bed reactor equations to model the transient phenomena that take place in gas-solid reactions.

CHAPTER 3

MATHEMATICAL FORMULATION OF THE MODEL

3.1 INTRODUCTION

Transient modeling of a fixed-bed reactor is both difficult and challenging due to the complex hydrodynamics of the system. Difficult because even the solution of the steady-state form of the mass- and energy-conservation equations for the reactor has been found to be complex. Therefore, when transient conditions are considered the situation becomes even more difficult to solve (Smith, 1981). For any system, the transient behavior of the reactor must be known in sufficient detail; not only for the start-up or shut-down procedures, but also for possible changes in operation conditions. The challenge, therefore, is to understand the response of the system to such operation parameters, such as variation in feed composition, temperature and flow rate. The dynamic response of the system to these involuntary disturbances determines, for example, the control and safety strategy to be adopted.

In the formulation that follows, all necessary details with respect to the space levels in the system, are taken into consideration in order to come up with a comprehensive and generalized model for gas-solid reactions in a fixed-bed reactor. Continuum model is employed for the macroscopic bed equation while for the microscopic or pellet level equation, the particle-pellet model of Szekely and Evans (1970) was used.

3.2 THREE LEVEL SPACE IN THE FIXED BED

A fixed bed can be considered to consist of three levels of space for the purpose of catalytic/noncatalytic reactions. These are mainly i) the large space in the reactor, ii) the pellet, and iii) the grains. The bed space has large pellets and the void volume. Homogeneous reactions may take place within the bed pores or the pores inside the pellets. On the other hand, nonhomogeneous reactions take place mostly on the surface area within the pores, and this is considered to give major contribution in the system. At any rate, both Knudsen and molecular diffusion aspects are considered so that the model can handle beds with very fine pellets as well as coarse ones.

The single pellets, on the other hand, are studied very well (Hastaoglu, et al. 1988, Hastaoglu, 1995). The simulation within the pellets will be used, again in a transient, nonisothermal, nonisobaric manner. The pellets are considered to consist of fine grains to represent the available surface area of the pellet. Then, one must follow the reaction front within the grains. Therefore, these three spaces are tied together through their boundaries. The grain exchanges heat and mass with the rest of the pellet interior through its external surface area. The pellet does the same with the bed. Therefore the bed does not "see" the pellets except as source or sink through their external surfaces. The three levels of space are shown in Figure 3.1.

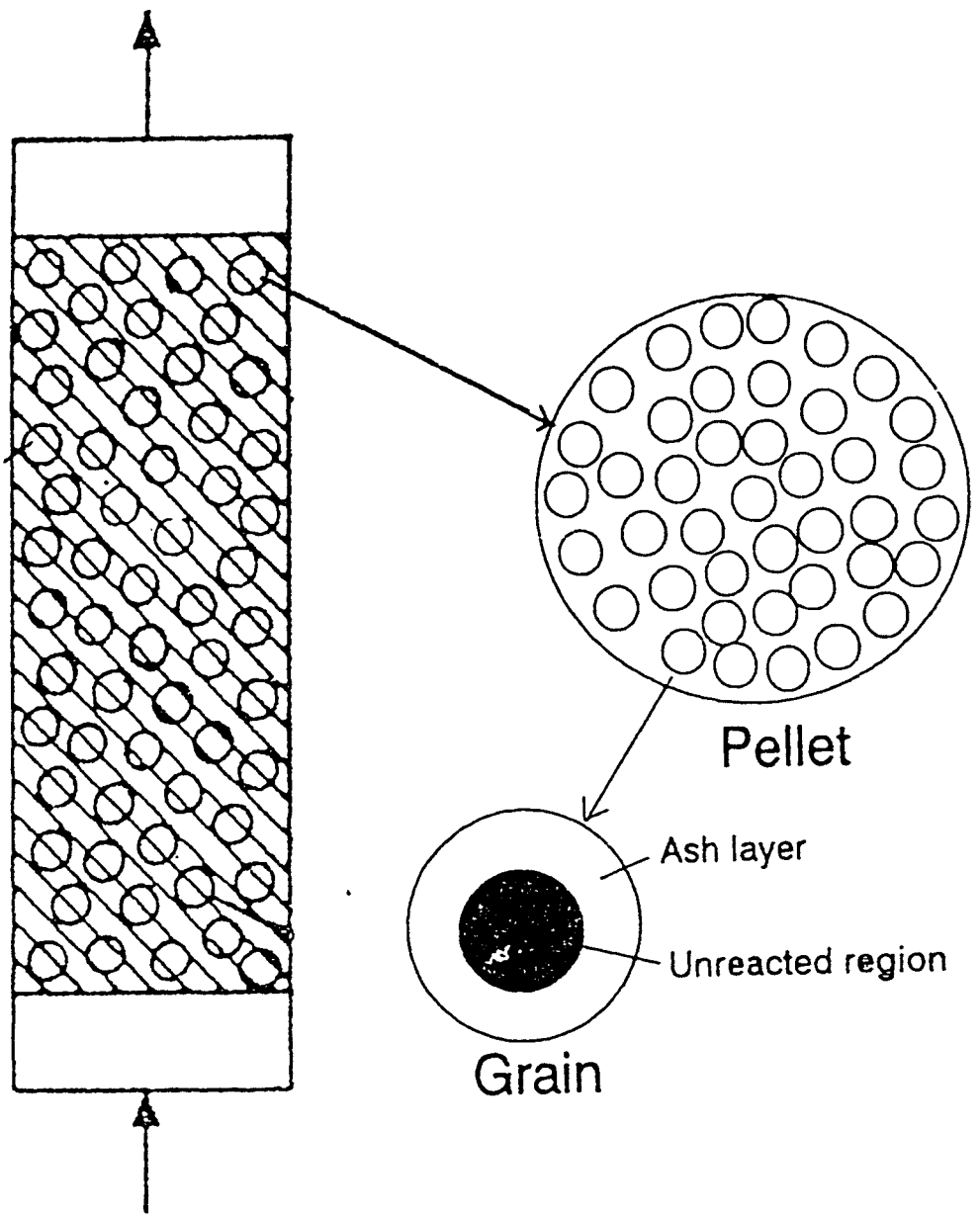

Figure 3.1 Schematic diagram of three levels of process space: fixed-bed, pellet and grain.

3.3 CONSERVATION EQUATIONS

3.3.1 Reaction Scheme

The necessary equations for reaction schemes are written for an example case of

$$A(gas) + bB(solid) \rightarrow cC(gas) + dD(solid) \qquad (1)$$

The stochiometric coefficient of A is made equal to one by dividing equation (1) by the original coefficient of A. Where b, c and d are new coefficients of B, C and D. The reaction in equation (1) represents a single reaction with four components taking part in the process.

A generalized system of reactions with many component can be represented with A as gaseous species and B as solid as follows (Abba and Hastaoglu, 1996).

Reaction 1:

$$a_{11}A_1 + a_{12}A_2 + \ldots + a_{1N_g-1}A_{N_g-1} + a_{1N_g}A_{N_g} + b_{11}B_1 + b_{12}B_2 + \ldots + b_{1N_S-1}B_{N_S-1} + b_{1N_S}B_{N_s} = 0$$

Reaction 2:

$$a_{21}A_1 + a_{22}A_2 + \ldots + a_{2N_g-1}A_{N_g-1} + a_{2N_g}A_{N_g} + b_{21}B_1 + b_{22}B_2 + \ldots + b_{2N_S-1}B_{N_S-1} + b_{2N_S}B_{N_s} = 0$$

Reaction 3:

$$a_{31}A_1 + a_{32}A_2 + \ldots + a_{3N_g-1}A_{N_g-1} + a_{3N_g}A_{N_g} + b_{31}B_1 + b_{32}B_2 + \ldots + b_{3N_S-1}B_{N_S-1} + b_{3N_S}B_{N_s} = 0$$

.....

Reaction i:

$$a_{i1}A_1 + a_{i2}A_2 + \ldots + a_{iN_g-1}A_{N_g-1} + a_{iN_g}A_{N_g} + b_{i1}B_1 + b_{i2}B_2 + \ldots + b_{iN_S-1}B_{N_S-1} + b_{iN_S}B_{N_s} = 0$$

.....

Reaction N_r:

$$a_{N_r1}A_1 + a_{N_r2}A_2 + \ldots + a_{N_rN_g-1}A_{N_g-1} + a_{N_rN_g}A_{N_g} + b_{N_r11}B_1 + b_{N_r2}B_2 + \ldots + b_{N_rN_S-1}B_{N_S-1} + b_{N_rN_S}B_{N_s} = 0$$

In general such a reaction scheme can be represented by

$$\sum_{j=1}^{N_g} a_{ji}A_i + \sum_{j=1}^{N_s} b_{ji}B_i = 0 \qquad i = 1, N_r \qquad (2)$$

where A is gaseous component as reactant or product. B stands for solid component as reactant or product. a and b are the coefficient of A and B respectively in a given reaction indicated by their subscript. The sign of a or b is negative for components that are products.

The rate expression for a general reaction can represented based on a pivot solid component or, as done here on a gas component A

$$\text{(Rate of reaction i)} = f_i \tag{3}$$

If more than one reactions are involved, the net rate of consumption of A_j could be found by

$$\text{(Net rate of reaction/consumption of } A_j) = \sum_{i=1}^{N_r} a_{ij} f_i \,. \tag{4}$$

The consumption of other components could be obtained using this rate. For any component that may be involved in the system without actually participating in the reaction, its coefficients in all reactions would be equal to zero. This is particularly applicable in a situation where a diluant is used to control a given reaction or combustion with air where N_2 is not taking part in the reaction. Similarly for inert solids coefficients b_{ik} would be zero.

3.3.2 Rate Expressions for Some Chemical Reactions

The accuracy of any mathematical model for a reactor depends entirely on the accuracy of the kinetic model of the reaction. In other words the main deficiencies in modeling of fixed-bed catalytic and noncatalytic processes originate from incomplete and inaccurate chemical kinetic (Froment, 1987). Special attention is given to the choice of the kinetic models used in this work. Some of the kinetic models tested are given below.

3.3.2.1 Chemical Reaction in Hyrodesulfurization

The following reaction is, in general, termed as hydrodesulfurization (HDS). It basically involves reaction of H_2 with a gas-liquid or gas phase containing "bound" sulfur to produce H_2S and an oil product relatively devoid of sulfur (Carberry, 1976; Luss and Hutchinson, 1971; Frye and Mosby, 1973; Schuit and Gates, 1973; Babcock et al., 1957).

Rate of thiophene conversion to butene as given by Satterfield and Robert (1968)

$$r_{HDS} = \frac{kK_T P_T P_{H_2}}{(1 + K_T P_T + K_{H_2S} P_{H_2S})^2} \quad \text{(moles/kg cat./sec)} \qquad (5)$$

where the values of k, K_T and K_{H_2S} are evaluated based on the following

$k_a = 3.6809$ mol/kg/s/(N/m^2) $\qquad E_a = 87.738$ kJ/mol

$K_{aT} = 1.14419 \times 10^{-12}$ m^2/N $\qquad E_{aT} = 83.2922$ kJ/mol

$K_{aH_2S} = 1.3518 \times 10^{-16}$ m^2/N $\qquad E_{aH_2S} = 120.2053$ kJ/mol.

These values of E's and K's are used for the evaluation of reaction rate constant and adsorption coefficient, respectively. On the other hand, there is another rate of thiophene conversion to butene as given by Froment and van Parijs (1984)

$$r_{HDS} = \frac{k_T K_T K_H^2 P_T P_H}{(1 + K_H P_H^{1/2} + K_T P_T + K_S P_S / P_H)^3} \text{ (kmol/kg cat./hr)} \qquad (6)$$

where the values of k_T, K_T, K_S and K_H are evaluated based on the following

$k_{aT} = 1.88 \times 10^{11}$ kmol/(kg hr) $\qquad E_{aT} = 125.2$ kJ/mole

$K_{aT} = 5.53 \times 10^{-4}$ $\qquad \Delta H = 44.6$ kJ/mol

$K_{aH} = 72.3$ $\qquad E_{aH} = 0.0$

$K_{aS} = 91.2$ $\qquad E_{aS} = 0.0$.

The rate of butene conversion to butane as given by Froment et al. (1984),

$$r_{HDG} = \frac{k_B K_B K^2{}_H P_B P_H}{(1 + K_H P_H^{1/2} + K_A P_A + K_B P_B)^3}, \quad \text{(kmol/kg cat./hr)} \qquad (7)$$

where k_B, K_B and K_H, K_A are evaluated based on equation (8) using

k_{aB}= 7.95x10^{11} kmol/(kg cat./h)

K_{aB}=0.0

K_{aA}= 4.02x10^{-4} ΔH =44.3kJ/mol

K_{aH}= 9.30x10^{-7} bar$^{1/2}$ ΔH =55.3kJ/mol

The reaction rate constant k and the adsorption coefficient are obtained from the following equations

$$k = k_a \exp(-\frac{E}{R_g T}) \qquad (8a)$$

$$K = K_a \exp(-\frac{\Delta H}{R_g T}) \qquad (8b)$$

The rate of thiophene conversion to butene as given by Chiuping Li et al. (1993), for first order kinetic of hydrodesulfurization reaction as

$$\ln\frac{C_o}{C_1} = -\ln(1 - X_S) = \frac{K_1}{WHSV} \qquad (9a)$$

and for a second order kinetic reaction, the conversion rate expression is given by

$$\frac{X_S}{1 - X_S} = \frac{K_2 C_O}{WHSV} \qquad (9b)$$

where

X_s = desulfurisation conversion

WHSV = Weight Hourly Space Velocity

R = 1.98 kcal/mol/k

K_2 = 2.31×10^{10} exp(-26. /RT)

C_O = sulfur concentration in the feed,

C_1 = sulfur concentration of the products.

3.3.2.2 Chemical Reaction in Gasification.

The rate of gasification reaction as given by Wu (1949) as

$$r_{gasication} = \frac{k_1 P_{CO_2}}{(1 + K_2 P_{CO} + K_3 P_{CO_2})} \tag{10}$$

where

$k_1 = 10.8\exp(-219{,}000/R_gT)$ mol/kPa m^2s

$K_2 = 3.26\text{x}10^{-11} \exp(253{,}000/R_gT)$ kPa^{-1}

$K_3 = 1.74\text{x}10^{-3} \exp(27{,}000/R_gT)$ kPa^{-1}.

3.3.3 Equation for the grain or micro-pores:

In some gas-solid reactions the solid matrix is continuously changing with the advance of the reaction. It is therefore necessary to formulate these changes; shrinkage or expansion (of the reaction front) of the grain. This would ultimately reflect the same change at the pellet level. For a solid component B_k, due to all the reactions that it takes part, the movement of the reaction front is given by

$$\frac{dr_{ck}}{dt} = -\frac{M_k}{\rho_k} \sum_i \frac{b_{ki}}{a_{ii}} f_i \tag{11}$$

3.3.4 Equations for the Pellet

Mass Transfer

$$\frac{\partial(\varepsilon C_j)}{\partial t} = -\nabla N_j + \sum F_i + \sum_{i=1}^{N_r} a_j s_i f_i \ , \quad j=1,N_g \tag{12}$$

where S_i (m^2/m^3) is the surface area for the reaction f_i.

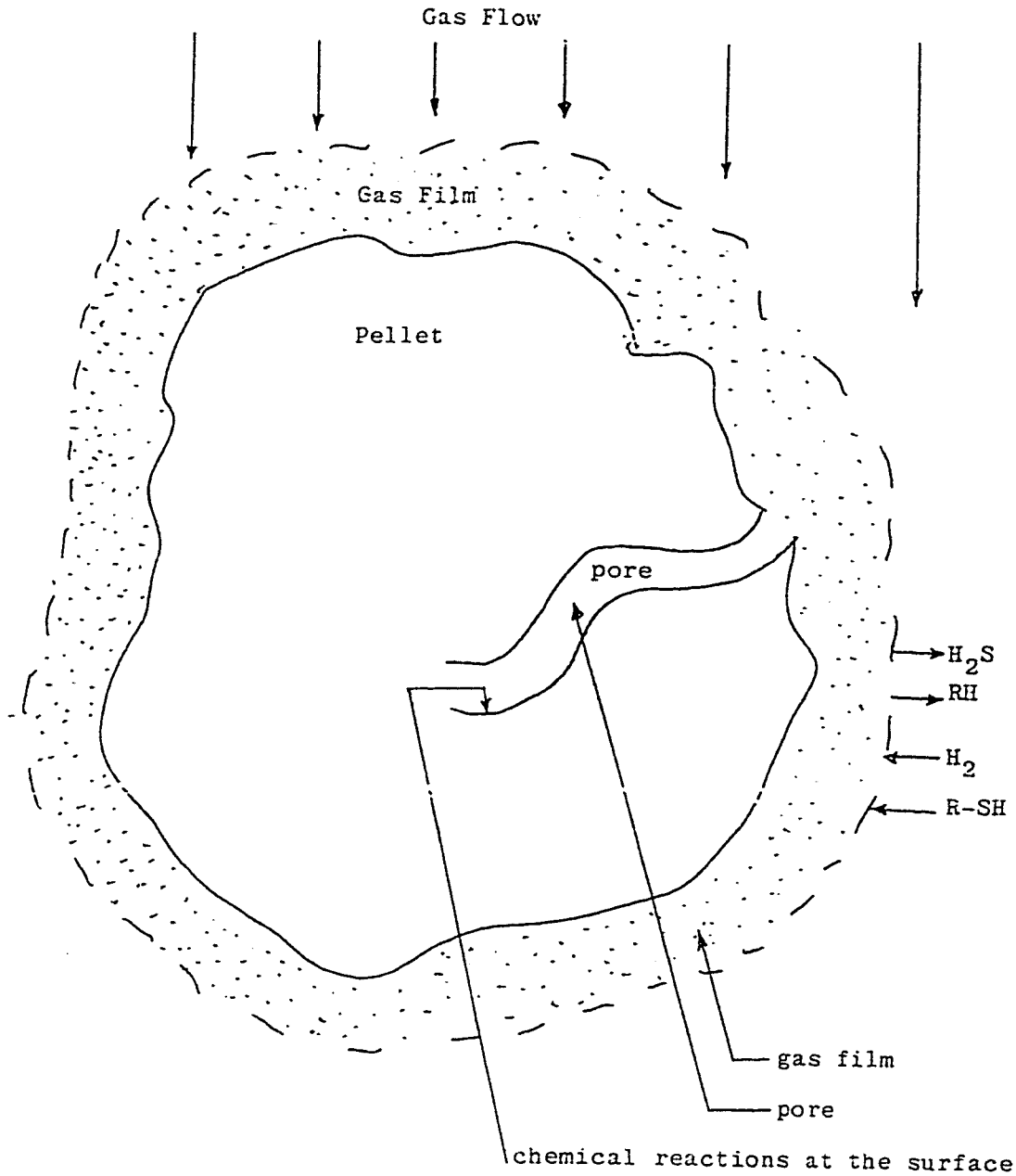

Figure 3.2. Schematic representation of the pellet and the flowing gas stream.

The following initial and boundary conditions complement the problem

$$t = 0;\ \ 0 \le R \le R_p:\ \ r_{cB} = r_{oB} = r_{gB},\ \ C_j = C_{jo} \tag{13a}$$

$$R = 0;\ \ N_G = 0 \tag{13b}$$

$$R = R_p;\ \ N_j = k_j (C_{js} - C_{jb}) \tag{13c}$$

Flux Equations

The mass fluxes of the components in the system (pellet pore and void space in the bed) are calculated by the use of the so-called "dusty-gas" flux equations for the transport of multicomponent mixtures of both diffusive and viscous components in porous media. If the thermal and surface diffusion terms are neglected, the equation is given as (Jackson, 1977; Mason, 1983),

$$\frac{N_i}{D^e_{i,k}} + \sum_{\substack{j=1 \\ j \neq i}}^{Ng} \frac{x_i N_j - x_j N_i}{D^e_{ij}} = -\frac{P}{R_g T}\nabla x_i - \frac{x_i}{R_g T}\left(1 + \frac{B_O P}{\mu_m D^e_{i,k}}\right)\nabla P \quad i=1,N_g \tag{14a}$$

where N_i is the flux of component i, D^e_{ki} is the effective Knudsen diffusion coefficient, D^e_{ij} is the effective binary bulk diffusion coefficient, B_o is a constant characteristics of the porous media

The diffusion is very important factor in heterogeneous chemical reactions. It is both necessary and important to employ such a comprehensive model (dusty-gas) to evaluate the fluxes. It gives accurate representation of the transport phenomena involved. It has been extensively used in modeling chemical reactions in porous catalyst as reviewed by Jackson (1977).

The flux of a component *i* can be written explicitly as follows

$$N_i = \frac{-\frac{P}{RT}\Delta x_i - \frac{x_i}{RT}\left(1 + \frac{B_o P}{\mu_m D_{ik}^e}\right)\nabla P + x_i \sum_{\substack{j=1 \\ j\neq i}}^{N_g} \frac{N_i}{D_{ij}^e}}{\frac{1}{D_{ik}^e} + \sum_{\substack{j=1 \\ j\neq i}}^{N_g} \frac{x_i}{D_{ij}^e}}, \quad i=1, N_g \qquad (14b)$$

This is an explicit expression, and the flux of each component on both the bed and pellet are calculated at each step of the simulation. Although N_i is written explicitly it requires that other fluxes are known. Therefore, at the beginning previous fluxes can be utilized for the fluxes at the right hand side of equation (14b). Then it is iterated a couple times using Gauss-Seidel iteration technique. Here any flux evaluated replaces its old value.

D_{ij} is obtained from Chapman and Enskog equation as given below

$$D_{ij} = 1.858 \times 10^{-7} T^{3/2} \frac{[(M_A + M_B)/M_B M_A]^{1/2}}{P \sigma_{AB}^2 \Omega_D}$$

where D_{ij} is the binary diffusion coefficient (m^2/s), T is temperature (K), P is pressure (atm), σ is the characteristic length (^oA) and Ω_D is the dimensionless diffusion collision integral. The other parameters are calculated from

$$D_{iK}^e = \frac{2\varepsilon^2 d_p}{3}\left(\frac{8R_g T}{\pi M}\right)^{1/2}, \quad D_{ij}^e = \varepsilon^2 D_{ij}, \quad B_0 = \frac{d_p^2}{8}. \qquad (15)$$

Local conversion of solid B_k

Local conversion of solid, B_k can be written in terms of the ratio of unreacted grain volume to initial grain volume as

$$x_{B_k} = 1 - \frac{r_{cB_k}^F}{r_{gB_k}^F} \qquad (16)$$

The overall conversion of solid B_k

The overall conversion of solid B_k in the pellet can be obtained by integrating local conversion given above over the pellet volume

$$X = \frac{\int_0^{Rp} x_{B_k} R^{F-1} dR}{\int_0^{Rp} R^{F-1} dR}. \qquad (17)$$

Heat Transfer

Transient heat transfer involves accumulation, conventive sensible heat, heats of homogeneous and heterogeneous reactions and thermal diffusion. These are written below:

$$C_p^e \frac{\partial T}{\partial t} = \nabla k^e \nabla T - \sum_j N_j C_{Pj} \nabla T - \sum_i F_i \Delta H_i - \sum s_i f_i \Delta H_i \qquad (18)$$

The initial and boundary conditions

$$t=0; \quad 0 \le R \le R_p : \; T = T_b \qquad (19a)$$

$$R = 0; \quad \nabla T = 0 \qquad (19b)$$

$$R = R_p ; \; -k^e \nabla T = h_c(T_s - T_b) + \sigma\theta(T_s^4 - T_b^4) \qquad (19c)$$

where T_S and T_P are pellet surface and bed temperatures at a bed location (R,Z). The mass and heat transfer equations are obtained by considering the balances over an element of a thin spherical shell.

3.3.5 *Equations for the Packed Tower*

The mass and energy balance equation for the fixed bed are obtained by considering an elemental section of a fixed bed reactor as shown in Figure 3.3. Consider this small volume element of radius r width Δr and height Δz, through which the reacting mixture flows. This volume contains both the (non) porous pellets and the surrounding fluid. The axial and radial velocities, temperature and concentration of the reacting fluid change continuously with the reaction. The conservation equations are described based on both the void and nonvoid cross-

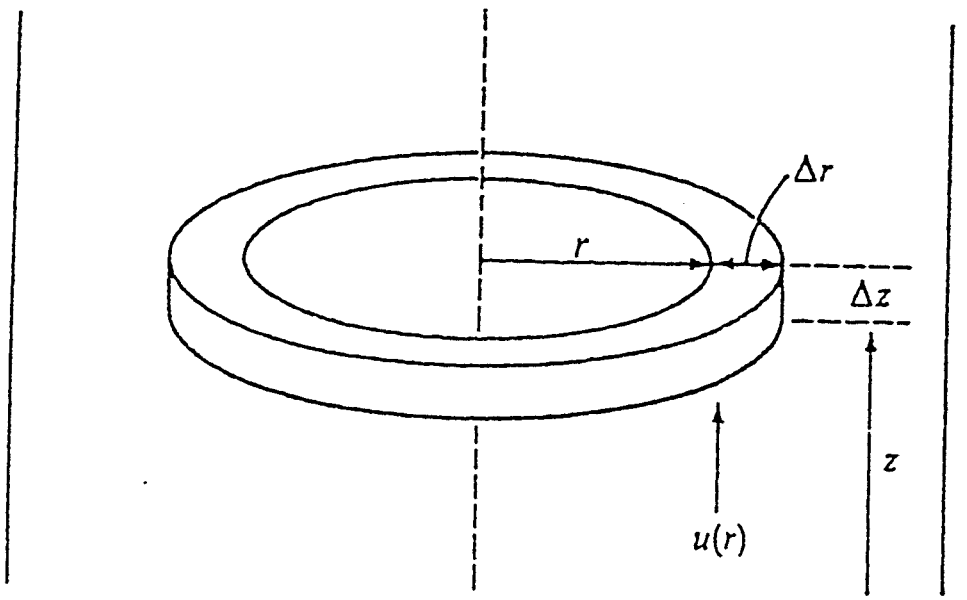

Figure 3.3 Annular Element in a Fixed-Bed Reactor.

sectional area as well as inlet and bed properties. The mass balance for a gas component C_i and heat balance equations are given below.

i) Mass

$$\frac{\partial(\varepsilon C_j)}{\partial t} = -\nabla M_{jr} - \nabla M_{jz} + \sum_{k=1}^{N_r} A_{rk} k_{cj}(C_j - C_{js}) + \sum F_i - v_z \frac{\partial C_j}{\partial z} \qquad (20)$$

ii) Heat

Conservation of heat on the gas

$$\varepsilon C_p C_t \frac{\partial T}{\partial t} = \frac{k}{r}\frac{\partial T}{\partial r} + \frac{\partial}{\partial r}(k\frac{\partial T}{\partial r}) + \frac{\partial}{\partial z}(k\frac{\partial T}{\partial z}) - C_p C_t v_z \frac{\partial T}{\partial z} + \sum F\Delta H +$$

$$-C_p(\frac{T}{r}\frac{\partial(N_r r)}{\partial r} + N_r\frac{\partial T}{\partial r}) - C_p(T\frac{\partial N_z}{\partial z} + N_z\frac{\partial T}{\partial z})$$

$$+[A_r\sum_{G}^{N_g} k_c(C_j - C_{js})C_{pj} + h_m + h_c](T_s - T) \qquad (21)$$

The initial and boundary conditions complementing equations (20) and (21) are

at $t = 0$: $T = T_o$; $C_j = C_{jo}$; $P = P_o$

at $R = 0$: $N_j = 0$; $q_r = 0$

at $R = R_w$: $N_j = 0$

at $R = R_w$: either $q_r = 0$, $q_r =$ given or $T = T_w$

at $z = 0$: $T = T_{in}$, $P = P_{in}$, $C_j = (C_j)_{in}$ (22)

3.4 TRANSPORT AND THERMOPHYSICAL PROPERTIES

The mathematical models, however accurate they may be, ultimately rely on thermophysical and transport parameters. A transport property approximated with a 10% error will more than reflect this error to results predicted. Therefore, correlations are invaluable in any modeling exercise. In the following some widely accepted correlations are used to evaluate the important properties.

The Transport Parameters

Chilton and Colburn (1934) correlations of heat and mass transfer coefficient provide very reliable means for evaluating heat and mass transfer coefficients. The correlations given below could be used to determine the value of mass transfer coefficient, depending on the value of the Reynolds number. On the basis of analogy of heat and mass transfer the heat transfer coefficient could be obtained by replacing Sh and Sc by Nu and Pr respectively in these equations.

i) The heat and mass transfer coefficients

$$Sh = 2.06Re^{0.425}Sc^{1/3}/\varepsilon \qquad Sc \le 168, \quad Re \le 5000$$

$$Sh = 20.4Re^{0.185}Sc^{1/3}/\varepsilon \qquad Sc \le 168, \quad Re \ge 5000$$

$$Sh = 1.09Re^{1/3}Sc^{1/3}/\varepsilon \qquad Sc \ge 168, \quad Re \ge 55$$

$$Sh = 0.25Re^{0.69}Sc^{1/3}/\varepsilon \qquad Sc \le 168, \quad Re \ge 55 \tag{23}$$

ii) Viscosity

The viscosities of the individual gas components could be obtained by (Reid and Sherwood, 1977).

$$\mu = [4.61T_r^{0.618} - 2.04\exp(-0.449T_r) + 1.94\exp(-4.058T_r) + 0.1]T_c^{-1/6}M^{1/2}P_c^{2/} \tag{24}$$

and for the mixture the following expression can be used.

$$\mu_m = \sum_i \frac{x_i\mu_i}{\sum_j x_j\phi_{ij}} \tag{25}$$

where $\phi_{ij} = \dfrac{[1+(\mu_i/\mu_j)^{1/2}(M_j/M_i)^{1/4}]^2}{[8(1+M_i/M_j)]^{1/2}}$.

iii) Specific Heat Capacity and Thermal Conductivity for multicomponent system can be found from

$$C_p^e = \sum_k \eta_{Bk}(1-\varepsilon)\rho_{Bk}C_{p_{Bk}} + \varepsilon C_i C_{P_g} \tag{27}$$

The thermal conductivity could be determined by replacing the viscosity with individual thermal conductivities in equation (25)

$$k^e = \sum_k \eta_{Bk}(1-\varepsilon)^2 k_{Bk} + \varepsilon^2 k_m \tag{28}$$

The individual heat capacity is obtained by

$$C_{pi} = A + BT + CT^2 + DT^3 \tag{29}$$

where the constants *A, B, C,* and *D* are given by Reid et al. (1977). *T* is in Kelvin, the unit of C_p is determined by the units of the constants. For mixtures C_p could be obtained by

$$C_{pm} = \sum_i x_i C_{pi} \ . \tag{30}$$

CHAPTER 4

NUMERICAL SOLUTION TECHNIQUE

INTRODUCTION

The set of the highly nonlinear, interrelated equations developed above are solved via numerical techniques. For this purpose an alternating-direction-implicit, iterative scheme has been developed. The grain and pellet spaces are solved first using bed parameters as boundary values. Here the heat and mass transfer equations written for each and every component are solved separately. The solution for the heat transfer equations are found to be more stable. Then, the mass transfer equations are solved with the new temperature profiles. This, therefore, has rendered the temperature aspect implicit. Since the heat and mass transfer equations are solved in an implicit manner, a couple of iterations are performed at each time step to stabilize the solution.

As implied above, the pellet and bed equations are linked together via boundary conditions. The bed parameters are used as boundary values for the pellet. The fluxes at the pellet surface are used as source or sink for the respective heat and mass transfer equations for the bed. Heat transfer equations for the pellet are discretized via implicit differencing and the resulting set of equations are solved using Thomas algorithm (Appendix A). The mass balance equations are solved using an iterative explicit technique as mentioned earlier.

The solution for the pellet and grain are stored and the heat and mass fluxes through the exterior surfaces of the pellet are calculated and stored for the future use. At this stage a similar procedure is developed again for the reactor bed. The solution of the bed equations are carried out using an implicit, alternating direction iterative approach as will be outlined later. The discretized equations and solution methodology for both pellet and bed are given in the following sections. Figure 4.2 shows the grid systems which are used for representation of the pellet and the reactor.

4.1 DIFFERENCE EQUATIONS

For numerical solution of a partial differential equation (PDE) with two (or more) dimensions, implicit schemes usually result in complex difference equations (DE). To avoid these complexities, and yet maintain the advantage of implicit solution, an Alternating-Direction-Implicit method is used. The basic idea is to alternate two difference equations (one direction implicit and the other direction explicit) which are used in turn over successive time steps (Carnanhan et al., 1969). The set of DE's are developed for the equations in this work based on Figure 4.2. The DE's and their associated boundary conditions are fed into Thomas algorithm for solution.

4.1.1 Discretization of Mass Transfer Equation

The continuity equation of all components in the bulk gas with a dummy component G as given in equation (20) could be reproduced here. (*) indicates the value of the variables at the next time step, i.e., $n+1$

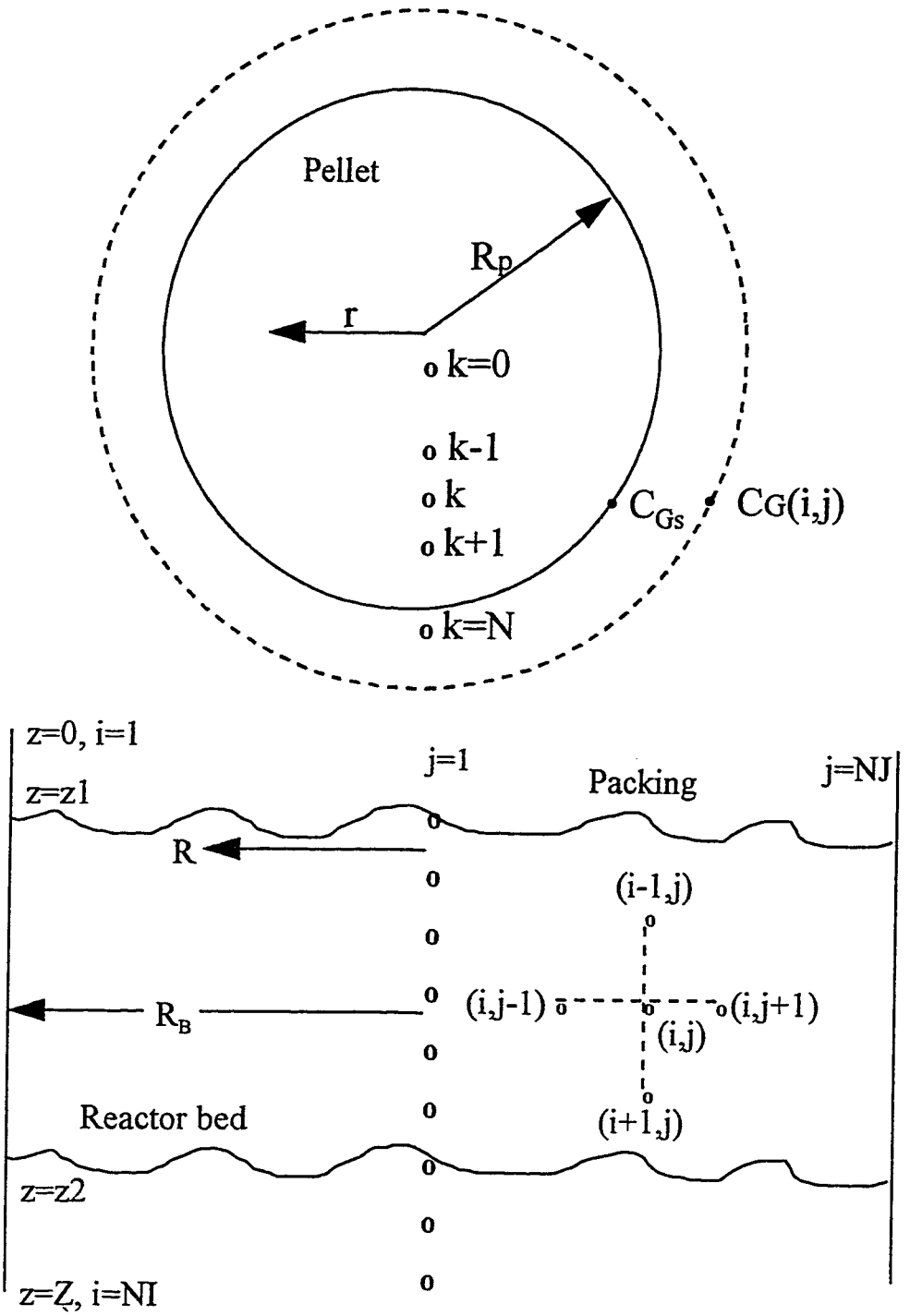

Figure 4.1 The grid system for the pellet and the reactor

$$\frac{\partial(\varepsilon C_G)}{\partial t} = -\nabla M_{Gr} - \nabla M_{Gz} + \sum_k A_r k_{cBk}(C_G - C_{Gs}) + \sum F - v_z \frac{\partial C_G}{\partial z} \qquad (20)$$

This can be discretized with implicit alternating direction approach as following, let us define $R_j = (j-1)\Delta r$, and $Z_i = (i-1)\Delta z$. For r-implicit and z-explicit case, we have, in general, the following terms at a grid (i,j)

1. $$\frac{\partial(\varepsilon C_G)}{\partial t} = \frac{(\varepsilon C_G)^* - (\varepsilon C_G)}{\Delta t}$$

2. $$-\frac{1}{r}\nabla(rM_{Gr}) = -\frac{1}{R_j}\frac{R_{j+1}M^*_{GRj+1j} - R_{j-1}M^*_{GRj-1j}}{2\Delta r}$$

3. $$\nabla M_{Gz} = \frac{M_{GZi+1,j} - M_{GZi-1,j}}{2\Delta z}$$

4. $$A_r k_c(C_G - C_{GS}) = A_{r_{ij}} k_{ci,j}(C_{Gi,j} - C_{GS_{i,j}})$$

5. $$F = F_{i,j}$$

6. $$v_z \frac{\partial C_G}{\partial z} = v_{z_{i,j}} \frac{C_{Gi+1,j} - C_{Gi-1,j}}{2\Delta z} \qquad (31)$$

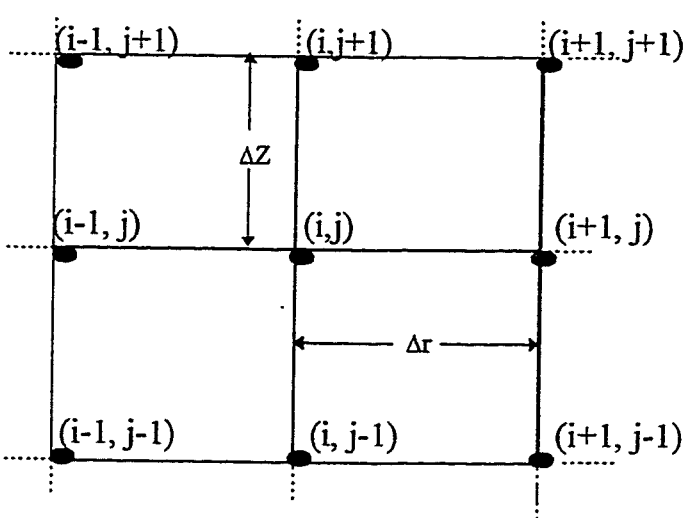

Figure. 4.2 General arrangement of grid points.

Therefore, equation (20) with r-implicit, becomes,

$$\frac{\varepsilon C_G^{\bullet} - \varepsilon C_G}{\Delta t} = -\frac{1}{R_j}\frac{R_{j+1}M_{GR_{i,j+1}}^{\bullet} - R_{j-1}M_{GR_{i,j-1}}^{\bullet}}{2\Delta r} - \frac{M_{GZi+1,j} - M_{GZi-1,j}}{2\Delta z}$$

$$+\sum A_{r_{ij}} k_{cBki,j}(C_{Gi,j} - C_{GSi,j}) + \sum F_{i,j} - v_{zi,j}\frac{C_{Gi+1,j} - C_{Gi-1,j}}{2\Delta z} \qquad (32)$$

For the z-implicit and r-explicit segment, we have;

$$\frac{\varepsilon C_G^{\bullet} - \varepsilon C_G}{\Delta t} = -\frac{1}{R_j}\frac{R_{j+1}M_{GRi,j+1} - R_{j-1}M_{GRi,j-1}}{2\Delta r} - \frac{M_{GZi+1,j}^{\bullet} - M_{GZi-1,j}^{\bullet}}{2\Delta z}$$

$$+A_{r_{ij}} k_{cBki,j}(C_{Gi,j} - C_{GSi,j}) + F_{i,j} - v_{zij}\frac{C_{Gi+1,j}^{\bullet} - C_{Gi-1,j}^{\bullet}}{2\Delta z} \qquad (33)$$

At the reactor central axis, $r = 0$, $M_{GR} = 0$. This produces undefined terms. Therefore one can use L'Hospital's approximation as $\frac{1}{R_j}\nabla(RM_{GR}) = 2\frac{\partial M_{GR}}{\partial R}$.

Then equation (20) is modified as

$$\frac{\partial(\varepsilon C_G)}{\partial t} = -2\frac{\partial M_{Gr}}{\partial r} - \frac{\partial M_{Gz}}{\partial z} + \sum A_r k_c(C_G - C_{Gs}) + \sum F - v_z\frac{\partial C_G}{\partial z} \qquad (34)$$

For r-implicit z-explicit segment, at the center, we have

$$\frac{(\varepsilon C_G)^{\bullet} - (\varepsilon C_G)}{\Delta t} = -\frac{M_{GR2,j}^{\bullet}}{\Delta R} - \frac{M_{GZi+1,1} - M_{GZi-1,1}}{2\Delta z} + \sum A_r k_{cj1}(C_{Gj1} - C_{GSj1}) + \sum F_{j1}$$

$$-v_{zi1}\frac{C_{Gi+1,1} - C_{Gi-1,1}}{2\Delta z} \qquad (35)$$

For r-explicit, z-implicit, at the center, we have

$$\frac{(\varepsilon C_G)^{\bullet} - (\varepsilon C_G)}{\Delta t} = -\frac{M_{GRi,2}}{\Delta R} - \frac{M^{\bullet}_{GZi+1,1} - M^{\bullet}_{GZi-1,1}}{2\Delta z} + \sum A_r k_{ci,1}(C_{Gi,1} - C_{GSi,1})$$

$$+ \sum F_{i,1} - (v_z)_{i,1} \frac{C_{Gi+1,1} - C_{Gi-1,1}}{2\Delta z} \qquad (36)$$

At $r = R_B$, $M_{GR} = 0$, r-implicit, and z-explicit

$$\frac{(\varepsilon C_G)^{\bullet} - (\varepsilon C_G)}{\Delta t} = \frac{1}{R_{NJ}} \frac{R_{NJ-1} M^{\bullet}_{GR_{i,NJ-1}}}{\Delta R} - \frac{M_{GZi+1NJ} - M_{GZi-1,NJ}}{2\Delta z}$$

$$+ \sum A_r k_{ci,NJ}(C_{Gi,NJ} - C_{GSi,NJ}) + \sum F_{i,NJ} - v_{zi,NJ} \frac{C_{Gi+1,NJ} - C_{Gi-1,NJ}}{2\Delta z} \qquad (37)$$

in all the preceding expressions, $C_{GS_{ij}}$ is taken as an average of the previous and present step values.

z-implicit and r-explicit

$$\frac{(\varepsilon C_G)^{\bullet} - (\varepsilon C_G)}{\Delta t} = \frac{1}{R_{NJ}} \frac{R_{NJ-1} M_{GRi,NJ-1}}{\Delta R} - \frac{M^{\bullet}_{GZi+1,NJ} - M_{GZi-1NJ}}{2\Delta z}$$

$$+ \sum A_r k_{ci,NJ}(C_{Gi,NJ} - C_{GSi,NJ}) + \sum F_{j,NJ} - v_{zi,NJ} \frac{C^{\bullet}_{Gi+1,NJ} - C^{\bullet}_{Gi-1,NJ}}{2\Delta z} \qquad (38)$$

At the entrance of the reactor where $z = 0$, the other conditions are; $T = T_{in}$, $P = P_{in}$, $C_G = C_{Gin}$. Thus, for the z-implicit and r-explicit, we have;

$$\frac{(\varepsilon C_G)^{\bullet} - (\varepsilon C_G)}{\Delta t} = -\frac{1}{R_j} \frac{R_{j+1} M_{GR1,j+1} - R_{j-1} M_{GR1,j-1}}{2\Delta R} - \frac{M_{GZ1,j}}{2\Delta z}$$

$$+ \sum A_r k_{c1,j}(C_{Gin1,j} - C_{GS1,j}) + \sum F_{1,j} \qquad (39)$$

Again at the entrance for the z-explicit and r-implicit, we have;

$$\frac{(\varepsilon C_G)^{\bullet}-(\varepsilon C_G)}{\Delta t} = -\frac{1}{R_j}\frac{R_{j+1}M^{\bullet}_{GR1,j+1}-R_{j-1}M^{\bullet}_{GR1,j-1}}{2\Delta R} - \frac{M_{GZ2,j}}{2\Delta z}$$
$$+\sum A_r k_{c1,j}(C_{Gin1,j}-C_{GS1,j}) + \sum F_{1,j} \qquad (40)$$

At the exit of the reactor where $z = Z$, we have for the z-implicit and z- explicit segment, we have;

$$\frac{(\varepsilon C_G)^{\bullet}-(\varepsilon C_G)}{\Delta t} = -\frac{1}{R_j}\frac{R_{j+1}M_{GRNI,j+1}-R_{j-1}M_{GRNI,j-1}}{2\Delta R}$$
$$+\frac{M_{GZNI-1,j}}{2\Delta z}+\sum A_r k_{cNI,j}(C_{GinNI,j}-C_{GSNI,j}) + \sum F_{NI,j} \qquad (41)$$

4.1.2 Discretization of Heat Transfer Equation

The equation for the conservation of heat for the bulk gas given in equation (21) is reproduced here for easy reference

$$\varepsilon C_p C_t \frac{\partial T}{\partial t} = \frac{k}{r}\frac{\partial T}{\partial r}+\frac{\partial}{\partial r}(k\frac{\partial T}{\partial r})+\frac{\partial}{\partial z}(k\frac{\partial T}{\partial z})-C_p C_t v_z \frac{\partial T}{\partial z}+\sum F\Delta H +$$
$$-C_p[\frac{T}{r}\frac{\partial(N_r r)}{\partial r}+N_r\frac{\partial T}{\partial r}]-C_p[T\frac{\partial N_z}{\partial z}+N_z\frac{\partial T}{\partial z}]$$
$$+a[k_c\sum_{G}^{N_g}(C_G-C_{Gs})C_{pG}+h_m+h_c](T_s-T) \qquad (21)$$

Now, each term could be discretized separately, using r-implicit and z-explicit

1. $$\varepsilon C_p C_t \frac{\partial T}{\partial t} = (\varepsilon C_p C_t)_{i,j} \frac{T_{i,j}^{\cdot} - T_{i,j}}{\Delta t}$$

2. $$\frac{k}{r}\frac{\partial T}{\partial r} = \frac{k_{avg}}{R_j}\frac{T^*_{i,j+1} - T^*_{i,j-1}}{2\Delta R}$$

3. $$\frac{\partial}{\partial r}(k\frac{\partial T}{\partial r}) = k_{avg_{i,j}}\frac{T^*_{i,j+1} - 2T^*_{i,j} + T^*_{i,j-1}}{(\Delta R)^2} + \frac{k_{mid\,i,j}}{R_i}\frac{T^*_{i,j+1} - T^*_{i,j-1}}{2\Delta R}$$

4. $$\frac{\partial}{\partial z}(k\frac{\partial T}{\partial z}) = k_{avg_{i,j}}\frac{T_{i+1,j} - 2T_{i,j} + T_{i-1,j}}{(\Delta z)^2} + \frac{k_{mid\,i,j}}{R_i}\frac{T^*_{i+1,j} - T^*_{i-1,j}}{2\Delta z}$$

5. $$C_p C_t v_z \frac{\partial T}{\partial z} = (C_p C_t v_z)_{i,j}\frac{T_{i+1,j} - T_{i-1,j}}{2\Delta z}$$

6. $$F\Delta H = F_{i,j}\Delta H_{i,j}$$

7. $$-C_P\,(\frac{T}{r}\frac{\partial(M_r r)}{\partial r} + M_r\frac{\partial T}{\partial r}) = -C_{p_{ij}}(\frac{T_{ij}}{R_j}\frac{R_{j+1}M_{rij+1} - R_{j-1}M_{rij-1}}{2\Delta R} + M_{rij}\frac{T_{ij+1} - T_{ij-1}}{2\Delta R})$$

8. $$-C_p(T\frac{\partial M_z}{\partial z} + M_z\frac{\partial T}{\partial z}) = -C_{p_{ij}}\,(T_{ij}\frac{M_{zi+1j} - M_{zi-1j}}{2\Delta z} + M_{rij}\frac{T_{i+1,j} - T_{i-1,j}}{2\Delta z})$$

9. $$k_c A_{rBk}\sum_G^{N_g}(C_G - C_{Gs})C_{pG} + (h_m + h_c)](T_s - T) =$$

$$k_{ci,j}A_{rBk}\sum_G^{N_g}(C_{Gi,j} - C_{Gsi,j})(C_{pG})_{i,j} + (h_m + h_c)_{i,j}](T_{s_{i,j}} - T_{i,j}) \qquad (42)$$

Then equation (21), (for r-implicit and z-explicit) becomes,

$$(\varepsilon C_p C_t)_{i,j}\frac{T_{i,j}^{\cdot} - T_{i,j}}{\Delta t} = +\frac{k_{avg}}{R_j}\frac{T^*_{i+1,j} - T^*_{i-1,j}}{2\Delta R} + k_{avg_{i,j}}(\frac{T^*_{i+1,j} - 2T^*_{i,j} + T^*_{i-1,j}}{(\Delta R)^2})$$

$$+k_{avg_{i,j}}(\frac{T_{i+1,j} - 2T_{i,j} + T_{i-1,j}}{(\Delta z)^2}) + k_{mid\,i,j}(\frac{T_{i+1,j} - T_{i-1,j}}{2\Delta z}) - (C_p C_t v_z)_{i,j}(\frac{T_{i+1,j} - T_{i-1,j}}{2\Delta z})$$

$$+F_{i,j}\Delta H_{i,j} - C_{p_{ij}}(T_{ij}\frac{M_{zi+1,j} - M_{zi-1,j}}{2\Delta z} + M_{ri,j}\frac{T_{i+1,j} - T_{i-1,j}}{2\Delta z})$$

$$+[k_{ci,j}A_{rBk}\sum_G^{N_g}(C_{Gi,j} - C_{Gsi,j})C_{pG_{i,j}} + (h_m + h_c)_{i,j}](T_{s_{i,j}} - T_{i,j}) \qquad (43)$$

and for z-implicit and r-explicit, we have

$$(\varepsilon C_p C_t)_{i,j}\frac{T_{i,j}^{\bullet}-T_{i,j}}{\Delta t}=\frac{k_{avg}}{R_j}\frac{T_{i,j+1}-T_{i,j-1}}{2\Delta R}+k_{avg_{i,j}}\left(\frac{T_{i,j+1}-2T_{i,j}+T_{i,j-1}}{(\Delta R)^2}\right)+\frac{k_{mid\,i,j}}{R_i}\left(\frac{T^{*}_{i,j+1}-T^{*}_{i,j-1}}{2\Delta R}\right)$$

$$+k_{avg_{i,j}}\left(\frac{T^{*}_{i+1,j}-2T^{*}_{i,j}+T^{*}_{i-1,j}}{(\Delta z)^2}\right)+\frac{k_{mid\,i,j}}{R_i}\left(\frac{T^{*}_{i+1,j}-T^{*}_{i-1,j}}{2\Delta z}\right)$$

$$-(C_p C_t v_z)_{i,j}\left(\frac{T_{i+1,j}-T_{i-1,j}}{2\Delta z}\right)+\sum F_{i,j}\Delta H_{i,j}$$

$$-C_{p_{ij}}\left(\frac{T_{ij}}{R_j}\frac{R_{j+1}M_{ri,j+1}-R_{j-1}M_{ri,j-1}}{2\Delta R}+M_{ri,j}\frac{T_{i,j+1}-T_{i,j-1}}{2\Delta R}\right)$$

$$-C_{p_{i,j}}\left(T^{*}_{i,j}\frac{M_{zi+1,j}-M_{zi-1,j}}{2\Delta z}+M_{ri,j}\frac{T^{*}_{i+1,j}-T^{*}_{i-1,j}}{2\Delta z}\right)$$

$$+[k_{ci,j}A_{rBki,j}\sum_{G}^{N_g}(C_{Gi,j}-C_{Gsi,j})C_{pG_{i,j}}+(h_m+h_c)_{i,j}](T_{s_{i,j}}-T_{i,j}) \quad (44)$$

At $r = 0$, equation (43) is recast using L'Hospital's rule to preventing undefined terms in the following form:

$$(\varepsilon C_p C_t)_{1,j}\frac{T_{1,j}^{\bullet}-T_{1,j}}{\Delta t}=k_{avg_{i,1}}\left(\frac{T_{i+1,1}-2T_{i,1}+T_{i-1,1}}{(\Delta z)^2}\right)$$

$$+\frac{k_{mid\,i,1}}{R_i}\left(\frac{T_{i+1,1}-T_{i-1,1}}{2\Delta z}\right)-(C_p C_t v_z)_{1,j}\left(\frac{T_{i+1,1}-T_{i-1,1}}{2\Delta z}\right)+\sum F_{i,1}\Delta H_{i,1}$$

$$-C_{p_{i,1}}\left(2T^{*}_{i,1}\frac{M_{ri,2}-M_{ri,1}}{\Delta R}+M_{ri,1}\frac{T^{*}_{i,2}-T^{*}_{i,1}}{\Delta R}\right)$$

$$-C_{p_{i,1}}\left(T_{i,1}\frac{M_{zi+1,1}-M_{zi-1,1}}{2\Delta z}+M_{ri,1}\frac{T_{i+1,1}-T_{i-1,1}}{2\Delta z}\right)$$

$$+[(k_c)_{1,j}A_{rBki,1}\sum_{G}^{N_g}(C_{Gi,1}-C_{Gsi,1})C_{pG_{1,j}}+(h_m+h_c)_{1,j}](T_{s_{i,1}}-T_{i,1}). \quad (45)$$

and for z-implicit and r-explicit, we have

$$(\varepsilon C_p C_t)_{i,1}\frac{T^{*}_{i,1}-T_{i,1}}{\Delta t}=2k_{avg_{i,1}}\left(\frac{T_{i,2}-T_{i,1}}{\Delta R}\right)+k_{avg_{i,1}}\left(\frac{T^{*}_{i+1,1}-2T^{*}_{i,1}+T^{*}_{i-1,1}}{(\Delta z)^2}\right)$$

$$+k_{mid\,i,1}\left(\frac{T^{*}_{i+1,1}-T^{*}_{i-1,1}}{2\Delta z}\right)-(C_p C_t v_z)_{i,1}\left(\frac{T^{*}_{i+1,1}-T^{*}_{i-1,1}}{2\Delta z}\right)+F_{i,1}\Delta H_{i,1}$$

$$-C_{p_{i,1}}(2T_{i,1}\frac{M_{ri,2}-M_{ri,1}}{\Delta R}+M_{ri,1}\frac{T_{i,2}-T_{i,1}}{\Delta R})$$

$$-C_{p_{i,1}}(T^{*}_{i,1}\frac{M_{zi+1,1}-M_{zi-1,1}}{2\Delta z}+M_{ri,1}\frac{T^{*}_{i+1,1}-T^{*}_{i-1,1}}{2\Delta z})$$

$$+[(k_c)_{1,j}A_{rBki,1}\sum_{G}^{N_g}(C_{Gi,1}-C_{Gsi,1})C_{pG_{i,1}}+(h_m+h_c)_{i,1}](T_{s_{i,1}}-T_{i,1}) \qquad (46)$$

Depending on the boundary condition imposed at the walls, $r = R_B$ there are three different scenarios: zero flux, finite flux and constant wall temperature. The relevant equations for each case are given below:

Case A: Zero flux at the wall

r-implicit,

$$(\varepsilon C_pC_t)_{i,NJ}\frac{T^{*}_{i,NJ}-T_{i,NJ}}{\Delta t}=k_{avg_{i,NJ}}(\frac{T_{i+1,NJ}-2T_{i,NJ}+T_{i-1,NJ}}{(\Delta z)^2})-(C_pC_tv_z)_{NI,j}(\frac{T_{i+1,NJ}-T_{i-1,NJ}}{2\Delta z})$$

$$+\sum F_{i,NJ}\Delta H_{i,NJ}-C_{p_{i,NJ}}\frac{T^{*}_{i,NJ}}{R_{NJ}}\frac{R_{NJ}M_{ri,NJ}-R_{NJ-1}M_{ri,NJ-1}}{2\Delta R}$$

$$-C_{p_{i,NJ}}(T_{i,NJ}\frac{M_{zi+1,NJ}-M_{zi-1,NJ}}{2\Delta z}+M_{ri,NJ}\frac{T_{i+1,NJ}-T_{i-1,NJ}}{2\Delta z})$$

$$+[k_{ci,NJ}A_{rBki,NJ}\sum_{G}^{N_g}(C_{Gi,NJ}-C_{Gsi,NJ})C_{pG_{i,NJ}}+(h_m+h_c)_{i,NJ}](T_{s_{i,NJ}}-T_{i,NJ}) \qquad (47)$$

z-implicit,

$$(\varepsilon C_pC_t)_{i,NJ}\frac{T^{*}_{i,NJ}-T_{i,NJ}}{\Delta t}=k_{avg_{i,NJ}}(\frac{T_{i,NJ-1}-T_{i,NJ}}{\Delta R})+k_{avg_{i,NJ}}(\frac{T^{*}_{i+1,NJ}-2T^{*}_{i,NJ}+T^{*}_{i-1,NJ}}{(\Delta z)^2})$$

$$-(C_pC_tv_z)_{i,NJ}(\frac{T^{*}_{i+1,NJ}-T^{*}_{i-1,NJ}}{2\Delta z})+\sum F_{i,NJ}\Delta H_{i,NJ}$$

$$-C_{p_{i,NJ}}\frac{T_{i,NJ}}{R_{NJ}}\frac{R_{NJ}M_{ri,NJ}-R_{NJ-1}M_{ri,NJ-1}}{\Delta R}$$

$$-C_{p_{i,NJ}}(T^{*}_{i,NJ}\frac{M_{zi+1,NJ}-M_{zi-1,NJ}}{2\Delta z}+M_{ri,NJ}\frac{T^{*}_{i+1,NJ}-T^{*}_{i-1,NJ}}{2\Delta z})$$

$$+[k_{ci,NJ}A_{rBki,NJ}\sum_{G}^{N_g}(C_{Gi,NJ}-C_{Gsi,NJ})C_{pG_{i,NJ}}+(h_m+h_c)_{i,NJ}](T_{si,NJ}-T_{i,NJ}) \quad (48)$$

Case B: Constant flux at the wall

For a constant flux, $-k_{avg}\frac{\partial T}{\partial r}=flux=Q$ or

$$k_{avg}\frac{T_{i,NJ+1}-T_{i,NJ-1}}{2\Delta R}=Q \quad \text{i.e.} \quad T_{i,NJ+1}=T_{i,NJ-1}-\frac{\Delta R}{k_{avg}}Q \quad (49)$$

the value of $T_{i,NJ+1}$ *and* $T^*_{i,NJ+1}$ in the next equation could be replaced by the same from equation (49), with implicit in the r-direction, we have

$$(\varepsilon C_pC_t)_{i,NJ}\frac{T^*_{i,NJ}-T_{i,NJ}}{\Delta t}=\frac{k_{avg}}{R_j}\frac{T^*_{i,NJ+1}-T^*_{i,NJ-1}}{2\Delta R}+k_{avg_{i,j}}(\frac{T^*_{i,NJ+1}-2T^*_{i,NJ}+T^*_{i,NJ-1}}{(\Delta R)^2})$$

$$+k_{mid_{i,NJ}}(\frac{T^*_{i,NJ+1}-T^*_{i,NJ-1}}{2\Delta R})+k_{avg_{i,NJ}}(\frac{T_{i+1,NJ}-2T_{i,NJ}+T_{i-1,NJ}}{(\Delta z)^2})$$

$$+k_{mid_{i,NJ}}(\frac{T_{i+1,NJ}-T_{i-1,NJ}}{2\Delta z})-(C_pC_tv_z)_{i,NJ}(\frac{T_{i+1,NJ}-T_{i-1,NJ}}{2\Delta z})+\sum F_{i,NJ}\Delta H_{i,NJ}$$

$$-C_{p_{i,NJ}}(\frac{T^*_{i,NJ}}{R_{NJ}}\frac{R_{NJ}M_{ri,NJ}-R_{NJ-1}M_{riNJ-1}}{\Delta R}+M_{ri,NJ}\frac{T^*_{i,NJ+1}-T^*_{i,NJ-1}}{2\Delta R})$$

$$-C_{p_{i,NJ}}(T_{i,NJ}\frac{M_{zi+1,NJ}-M_{zi-1,NJ}}{2\Delta z}+M_{ri,NJ}\frac{T_{i+1,NJ}-T_{i-1,NJ}}{2\Delta z})$$

$$+[k_{ci,NJ}A_{rBki,NJ}\sum_{G}^{N_g}(C_{Gi,NJ}-C_{Gsi,NJ})C_{pG_{i,NJ}}+(h_m+h_c)_{i,NJ}](T_{si,NJ}-T_{i,NJ}) \quad (50)$$

with implicitness in the z-direction, we have

$$(\varepsilon C_pC_t)_{i,NJ}\frac{T^*_{i,NJ}-T_{i,NJ}}{\Delta t}=\frac{k_{avg}}{R_j}\frac{T_{i,NJ+1}-T_{i,NJ-1}}{2\Delta R}+k_{avg_{i,NJ}}(\frac{T_{i,NJ+1}-2T_{i,NJ}+T_{i,NJ-1}}{(\Delta R)^2})$$

$$+k_{mid_{i,NJ}}(\frac{T_{i,NJ+1}-T_{i,NJ-1}}{2\Delta R})+k_{avg_{i,NJ}}(\frac{T^*_{i+1,NJ}-2T^*_{i,NJ}+T^*_{i-1,NJ}}{(\Delta z)^2})$$

$$k_{mid_{i,NJ}}(\frac{T^*_{i+1,NJ}-T^*_{i-1,NJ}}{2\Delta z})-(C_pC_tv_z)_{i,NJ}(\frac{T^*_{i+1,NJ}-T^*_{i-1,NJ}}{2\Delta z})+\sum F_{i,NJ}\Delta H_{i,NJ}$$

$$-C_{p_{i,NJ}}\left(\frac{T_{i,NJ}}{R_{NJ}}\frac{R_{NJ}M_{ri,NJ}-R_{NJ-1}M_{ri,NJ-1}}{\Delta R}+M_{ri,NJ}\frac{T_{i,NJ+1}-T_{i,NJ-1}}{2\Delta R}\right)$$

$$-C_{p_{i,NJ}}\left(T^{*}_{i,NJ}\frac{M_{zi+1,NJ}-M_{zi-1,NJ}}{2\Delta z}+M_{ri,NJ}\frac{T^{*}_{i+1,NJ}-T^{*}_{i-1,NJ}}{2\Delta z}\right)$$

$$+[k_{c\,i,NJ}A_{rBk\,i,NJ}\sum_{G}^{N_g}(C_{Gi,NJ}-C_{Gsi,NJ})C_{pG_{i,NJ}}+(h_m+h_c)_{i,NJ}](T_{si,NJ}-T_{i,NJ}). \quad (51)$$

Case C: Constant temperate at the wall

For a constant wall temperature, with $T_{i,NJ+1}=T^{*}_{i,NJ+1}=T_w$ in equation (52) with r-direction implicit, we have

$$(\varepsilon C_pC_t)_{i,NJ}\frac{T^{*}_{i,NJ}-T_{i,NJ}}{\Delta t}=+\frac{k_{avg}}{R_{NJ}}\frac{T^{*}_{i,NJ+1}-T^{*}_{i,NJ-1}}{2\Delta R}+k_{avg_{i,NJ}}\left(\frac{T^{*}_{i,NJ+1}-2T^{*}_{i,NJ}+T^{*}_{i,NJ-1}}{(\Delta R)^2}\right)$$

$$+k_{mid_{i,NJ}}\left(\frac{T^{*}_{i,NJ+1}-T^{*}_{i,NJ-1}}{2\Delta R}\right)+k_{avg_{i,NJ}}\left(\frac{T_{i,NJ+1}-2T_{i,NJ}+T_{i,NJ-1}}{(\Delta z)^2}\right)$$

$$+k_{mid_{i,NJ}}\left(\frac{T_{i+1,NJ}-T_{i-1,NJ}}{2\Delta z}\right)-(C_pC_tv_z)_{i,NJ}\left(\frac{T_{i+1,NJ}-T_{i-1,NJ}}{2\Delta z}\right)$$

$$+\sum F_{i,NJ}\Delta H_{i,NJ}$$

$$-C_{p_{i,NJ}}\left(\frac{T^{*}_{i,NJ}}{R_{NJ}}\frac{R_{NJ}M_{ri,NJ}-R_{NJ-1}M_{ri,NJ-1}}{\Delta R}+M_{ri,NJ}\frac{T^{*}_{i,NJ+1}-T^{*}_{i,NJ-1}}{2\Delta R}\right)$$

$$-C_{p_{i,NJ}}\left(T_{i,NJ}\frac{M_{zi+1,NJ}-M_{zi-1,NJ}}{2\Delta z}+M_{ri,NJ}\frac{T_{i+1,NJ}-T_{i-1,NJ}}{2\Delta z}\right)$$

$$+[k_{ci,NJ}A_{rBki,NJ}\sum_{G}^{N_g}(C_{Gi,NJ}-C_{Gsi,NJ})C_{pG_{i,NJ}}+(h_m+h_c)_{i,NJ}](T_{si,NJ}-T_{i,NJ}). \quad (52)$$

With z-direction implicit, we have

$$(\varepsilon C_pC_t)_{i,NJ}\frac{T^{*}_{i,NJ}-T_{i,NJ}}{\Delta t}=+\frac{k_{avg}}{R_{NJ}}\frac{T^{*}_{i,NJ+1}-T^{*}_{i,NJ-1}}{2\Delta R}+k_{avg_{i,NJ}}\left(\frac{T_{i,NJ+1}-2T_{i,NJ}+T_{i,NJ-1}}{2\Delta R}\right)$$

$$+k_{mid_{i,NJ}}\left(\frac{T_{i,NJ+1}-T_{i,NJ-1}}{2\Delta R}\right)+k_{avg_{i,NJ}}\left(\frac{T^{*}_{i,NJ+1}-2T^{*}_{i,NJ}+T^{*}_{i,NJ-1}}{2\Delta z}\right)$$

$$+k_{mid_{i,NJ}}\left(\frac{T_{i+1,NJ}-T_{i-1,NJ}}{2\Delta z}\right)-(C_pC_tv_z)_{i,NJ}\left(\frac{T_{i+1,NJ}-T_{i-1,NJ}}{2\Delta z}\right)+\sum F_{i,NJ}\Delta H_{i,NJ}$$

$$-C_{p_{i,NJ}}\left(\frac{T^{*}_{i,NJ}}{R_{NJ}}\frac{R_{NJ}M_{ri,NJ}-R_{NJ-1}M_{ri,NJ-1}}{\Delta R}+M_{ri,NJ}\frac{T^{*}_{i,NJ+1}-T^{*}_{i,NJ-1}}{2\Delta R}\right)$$

$$-C_{p_{i,NJ}}\left(T_{i,NJ}\frac{M_{zi+1,NJ}-M_{zi-1,NJ}}{2\Delta z}+M_{ri,NJ}\frac{T_{i+1,NJ}-T_{i-1,NJ}}{2\Delta z}\right)$$

$$+[k_{ci,NJ}A_{rBki,NJ}\sum_{G}^{N_g}(C_{Gi,NJ}-C_{Gsi,NJ})C_{pG_{i,NJ}}+(h_m+h_c)_{i,NJ}](T_{si,NJ}-T_{i,NJ}). \quad (53)$$

At $z = 0$ the entrance $T = T_{in}$, $C_G = C_{Gin}$

$$(\varepsilon C_pC_t)_{1,j}\frac{T^{*}_{1,j}-T_{1,j}}{\Delta t}=k_{avg_{1,j}}\left(\frac{T_{2,j}-T_{in}}{\Delta z}\right)+k_{mid1,j}\left(\frac{T_{2,j}-T_{in}}{\Delta z}\right)-(C_pC_tv_z)_{1,j}\left(\frac{T_{2,j}-T_{in}}{\Delta z}\right)$$

$$-C_{p_{i,NJ}}\left(\frac{T_{i,NJ}}{R_{NJ}}\frac{R_{NJ}M_{ri,NJ}-R_{NJ-1}M_{ri,NJ-1}}{\Delta R}+M_{ri,NJ}\frac{T_{i,NJ+1}-T_{i,NJ-1}}{2\Delta R}\right)$$

$$-C_{p_{i,NJ}}\left(T^{*}_{i,NJ}\frac{M_{zi+1,NJ}-M_{zi-1NJ}}{2\Delta z}+M_{ri,NJ}\frac{T^{*}_{i+1,NJ}-T^{*}_{i-1,NJ}}{2\Delta z}\right)$$

$$+[k_{c1,j}A_{rBk1,j}\sum_{G}^{N_g}(C_{Gin}-C_{Gs1,j})C_{pG_{1,j}}+(h_m+h_c)_{1,j}](T_{s_{1,j}}-T_{in}) \quad (54)$$

At $z = Z$, (the exit) with $T = T_{out}$, $C_G = C_{Gout}$ one gets

$$(\varepsilon C_pC_t)_{Ni,j}\frac{T^{*}_{NI,j}-T_{NI,j}}{\Delta t}=k_{avg_{Ni,j}}\left(\frac{T_{NI,j}-T_{NI-1,j}}{\Delta z}\right)$$

$$-C_{p_{Ni,j}}\left(\frac{T_{NI,j}}{R_{NJ}}\frac{R_{j+1}M_{rNI,j+1}-R_{J-1}M_{rNi,j-1}}{2\Delta R}+M_{rNi,j}\frac{T_{NI,j+1}-T_{Ni,j-1}}{2\Delta R}\right)$$

$$-C_{p_{Ni,j}}\left(T^{*}_{Ni,j}\frac{M_{zNI,j}-M_{zNI-1,j}}{\Delta z}+M_{rNI,j}\frac{T^{*}_{NI,j}-T^{*}_{NI-1,j}}{\Delta z}\right)$$

$$+k_{mid\,NI,j}\left(\frac{T_{NI,j}-T_{NI-1,j}}{\Delta z}\right)-(C_pC_tv_z)_{NI,j}\left(\frac{T_{NI,j}-T_{NI-1,j}}{\Delta z}\right)$$

$$+[k_{ci,NJ}A_{rBki,NJ}\sum_{G}^{N_g}(C_{Gi,NJ}-C_{Gsi,NJ})C_{pG_{i,NJ}}+(h_m+h_c)_{i,NJ}](T_{si,NJ}-T_{i,NJ}) \quad (55)$$

The thermal conductivities used in the equation above are defined as

$$k_{avg_{i,j}}=(k_{i-1,j,n-1}+k_{i,j-1,n-1})/2 \quad (56)$$

$$k_{mid\,i,j}=(k_{i-1,j,n}+k_{i,j-1,n})/2. \quad (57)$$

CHAPTER 5

MODEL VALIDATION

5.1 INTRODUCTION

The mathematical model developed in Chapter 3 and discretized in Chapter 4 in finite difference form was programmed in FORTRAN 77. A completely self-contained program was designed to calculate the transient equations of the pellet and reactor bed subject to the initial conditions and any perturbation in the desired variables. In order to apply it to any significant process one has to verify the model using various techniques and aspects of the model. In this work the following approaches have been used: 1) Validation of the pellet model, 2) Validation of the bed model, and 3) Validation based on mass balance. Finally, the stability of the methods used has to be checked. These points are discussed below.

5.2 VALIDATION OF THE PELLET MODEL

The formulation for the pellet has been solved and applied to various scenarios. The results are compared with the experimental data. Mainly the following are used for validation:

1) Nickel oxide reduction with hydrogen
2) Hematite reduction with hydrogen,
3) Reduction of mixture of nickel oxide and hematite with hydrogen,
4) Gasification of carbon with carbon dioxide,
5) Wood pyrolysis.

In this context the overall conversions, pellet temperatures and pressures are used for comparison purposes. Since these results (of 1 to 4 above) were presented before (Abba, 1995) few selected results are presented and discussed here.

Conversion versus time data for the reduction of nickel oxide - hematite mixture with hydrogen are presented in Figure 5.1. In the same figure the conversion data for each solid reactant is shown. The fit is excellent in general; although there is some agglomeration and swelling in the solid pellet.

The comparison of conversion versus time for wood pyrolysis is given in Figure 5.2. The discrepancy earlier is due to volatiles such as water in drying which are not included in the modeling studies. The fit between the experimental and model results is fairly good. Again for wood pyrolysis the transient temperature within the pellet is shown in Figure 5.3 with remarkable fit considering this very complicated process. The importance of transient assumption for the temperature in such a pellet of 1 mm thickness is clearly justified as apparent form this figure.

Finally, a comparison for carbon gasification is shown in Figure 5. 4. Again the fit between the experimental and model results is excellent.

5.3 VALIDATION OF THE BED MODEL

Upon validation of the pellet model for a large range of operating conditions and various systems the equations for the bed are tested as well as the solution techniques applied. Transient data for bed are not readily available with the necessary input parameters such as thermal and physical quantities and other necessary operating conditions. For this purpose only partial data are available where steady state values

are given for HDS. The data have been obtained using a test unit with 0.46 *m* height and 0.027 *m* diameter. The particulars are given next.

The initial temperature in the bed and the feed temperatures are 250 °C. The operating pressure is 2757 kPa (400 psig). H_2 flow rate is 3.33×10^{-5} m^3/s (2 l/min). Initial concentration of thiophene is 5000 ppm (parts per million). The steady state exit concentration is 5 ppm. The pore volume is given as 0.3 cm^3/g of catalyst.

The thiophene profiles predicted by the model and the two experimental steady state values are given in Figure 5.5. The experimental values are mixed cup values. The model, on the other hand, predicts concentrations in radial as well as axial directions as given. The model values plotted show the variation between the wall and the center after 5000 s of simulated reaction time. The experimental values fall right between the upper and lower limits at the top and bottom of the reactor. The fit, although for the entrance and exit of the bed, is excellent. . The model gave a conversion of 99.98% compared to experimental value of 99.90% for thiophene at steady state. The higher model prediction is due to the fact that only thiophene was considered as sulfur-carrying component, while in reality many other components that may reduce the conversion are present. Steady state average temperature was predicted within 0.5 %. This also indicates that the steady state is reached in the given time which is supported by the results given in Chapter 6.

There are two temperature profiles given in Figures 5.6 and 5.7. The experimental temperature profiles in the bed are given for various positions in axial direction for 5000 s in Figure 5.6. The fluctuations in the profiles is clear at the earlier stages of the process, later on steadying. In axial direction there is strong temperature gradients. The average temperatures along the central axis of the bed are compared between the

model predictions and the experimental measurements. The accuracy is within few degrees with most of them coinciding with the accuracy of the measuring device (around 0.5 °C).

5.4 VALIDATION BASED ON THE MASS BALANCE

The model validation can be performed by applying mass balance on individual components and overall mass. For a given component the feed rate is known. The component flow in the exit stream is obtained by integrating the exit concentrations in the outflowing stream over the cross section of the fixed bed reactor. Then a mass balance is performed as the difference between inlet and exit streams is what has been converted through reactions. Since calculation of amounts reacted takes a long time to carry out in the whole of the reactor considering the pellets everywhere, the number of moles of a species crossing through the external surface film of the pellets have been calculated. Thus the difference between the total number of moles in the feed and exit stream is compared with the number of moles entering through the interfacial surface area of pellets. The net amount: (In - out - transfer across film) is an indication of the mass balance. Since the changes in the void space concentrations are not included in this approach the net amount will be driven to zero at steady state. However unless a global steady state is reached the net amount may change sign in time, a phenomena spearheaded by the changes in the temperature, pressure, reaction rates, and initial concentrations present both in the bed and in the pellets. Plots of net amounts versus time are shown for thiophene, C-4 and H_2S in Figure 5.8. Similar plot for H_2 is shown in Figure 5.9. The steep decrease to zero is shown for all components. In some cases this is driven to negative values which is due to changes in the accumulation terms within the bed.

5.5 STABILITY OF THE SOLUTION TECHNIQUE

In methods involving implicit or Crank-Nicolson type techniques the finite differencing technique is fairly stable, almost unlimited step size in any temporal or spatial directions. This is especially true for situations where the differential equations are linear and interrelationship between various parameters is not severe. In cases involving heavy nonlinearity and interdependence of the partial differential equations, as is the case here with three levels of solution geometric spaces with m, mm and micron sizes, the stability becomes very important.

During this study because of iterations in alternating-direction-implicit method the explicitness in spatial direction has been reduced substantially. However in temporal direction since a forward approximation has been used, thus effectively a totally explicit direction, time is the only variable controlling the convergence of the solution.

Too small time steps lead to errors introduced via truncation. This causes vibrations, and therefore, meaningless results. Too large time steps produce divergence with huge fluctuations. It has been experienced that even a procedure involving the solution of all the equations simultaneously is not immune to these problems. Especially when the reaction rates are higher, even some of the "*always-positive*" quantities are driven to negative values. These could be concentrations, pressure, temperature, in reacting solids grain diameters, mole fractions, etc. Therefore, the study of stability is both complex and unavoidable for such complex problems. The behavior of one of the many variables is shown as a function of time step in Figure 5.10.

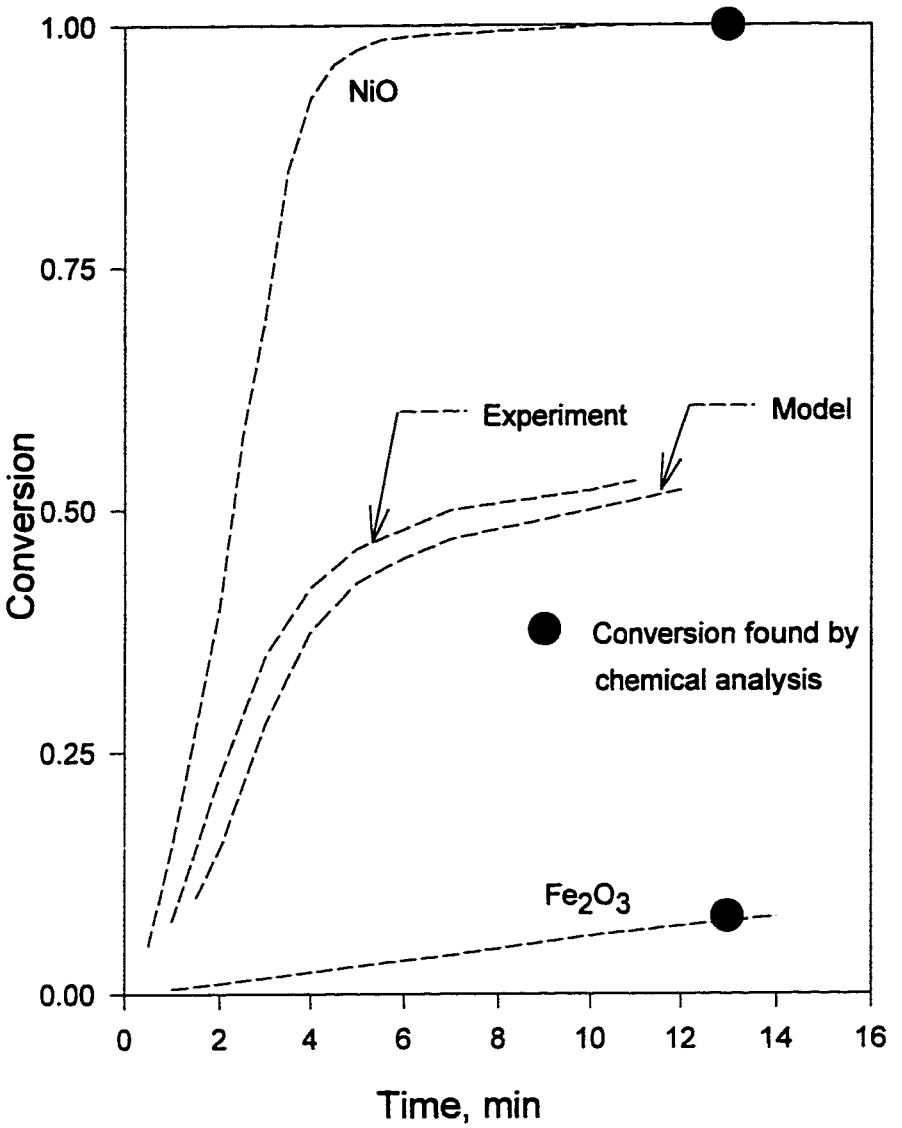

Figure 5.1 Conversion vs time for the reduction of hematite/nickel oxide with 1:1 ratio. $R_P = 0.0445$ cm (Szekely and Hastaoglu, 1976).

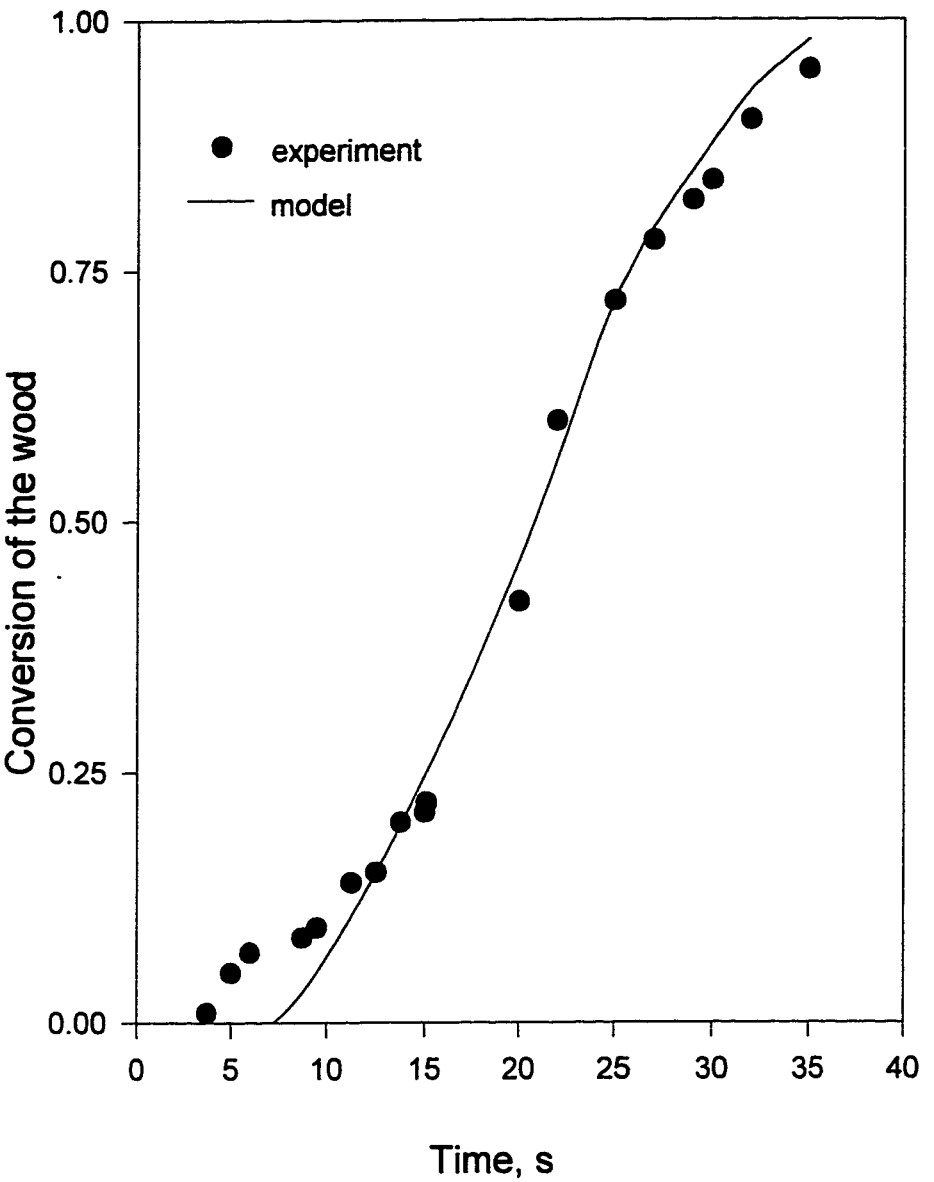

Figure 5.2 Transient conversion profile for wood pyrolysis at T_b = 528 °C (Hastaoglu and Berruti, 1989).

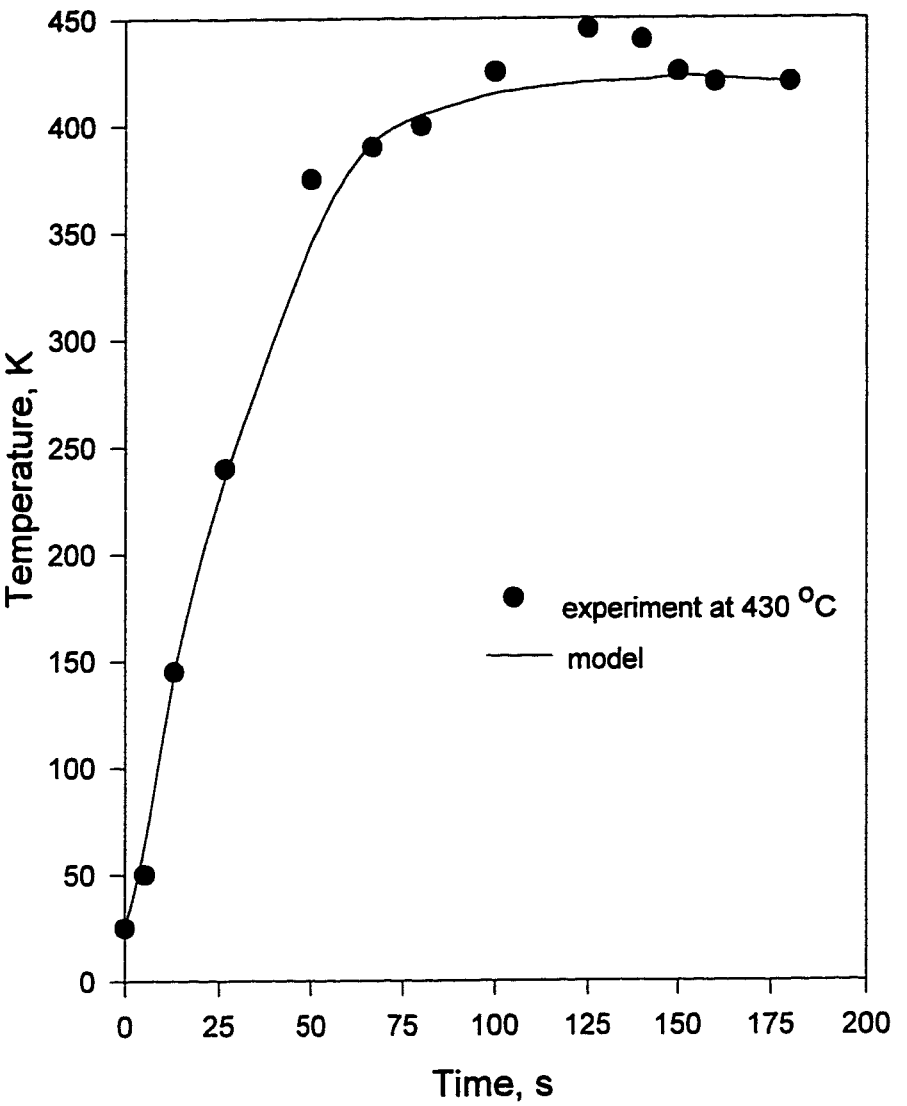

Figure 5.3 Temperature history at the pellet center with T_b=430 °C. (Hastaoglu and Berruti, 1989).

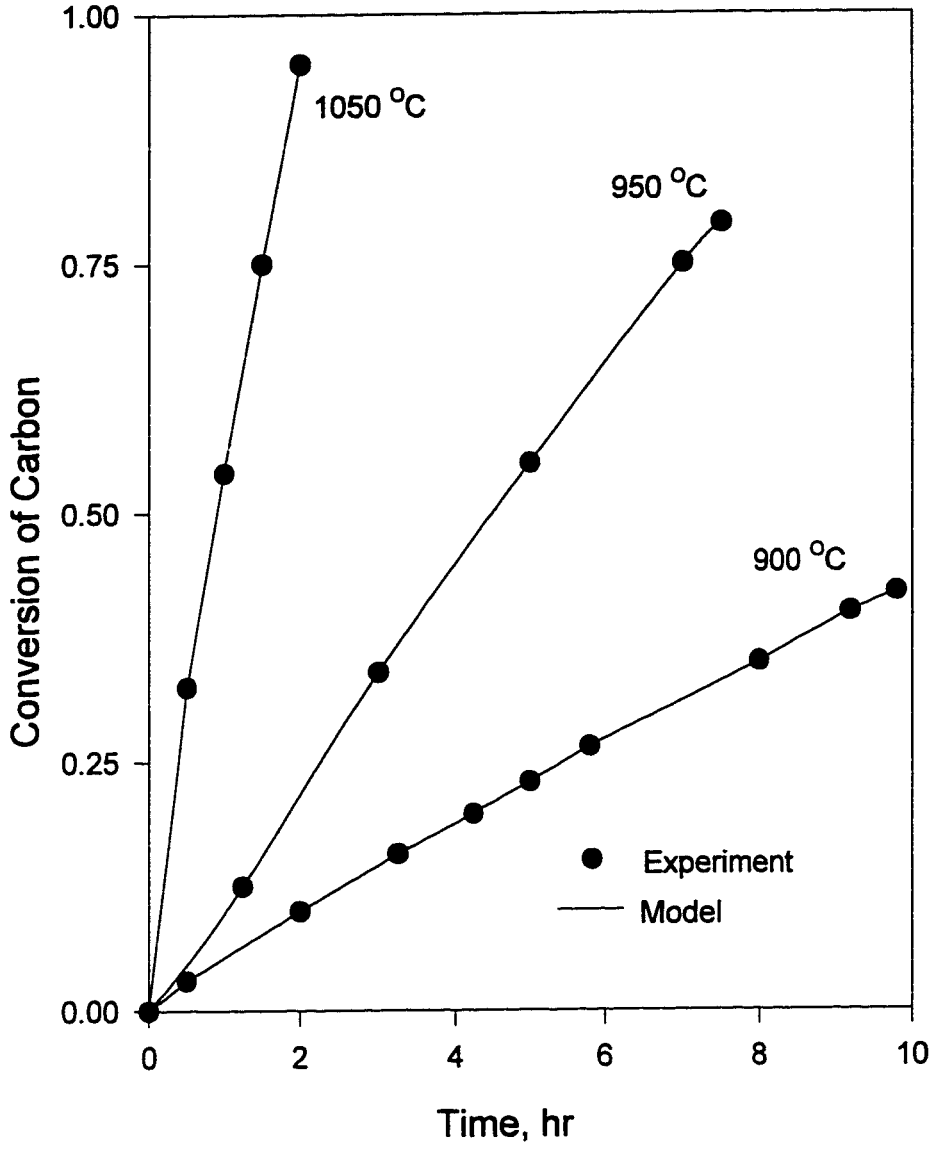

Figure 5.4 Transient conversion profile for noncatalytic carbon gasification (Hassam, 1987).

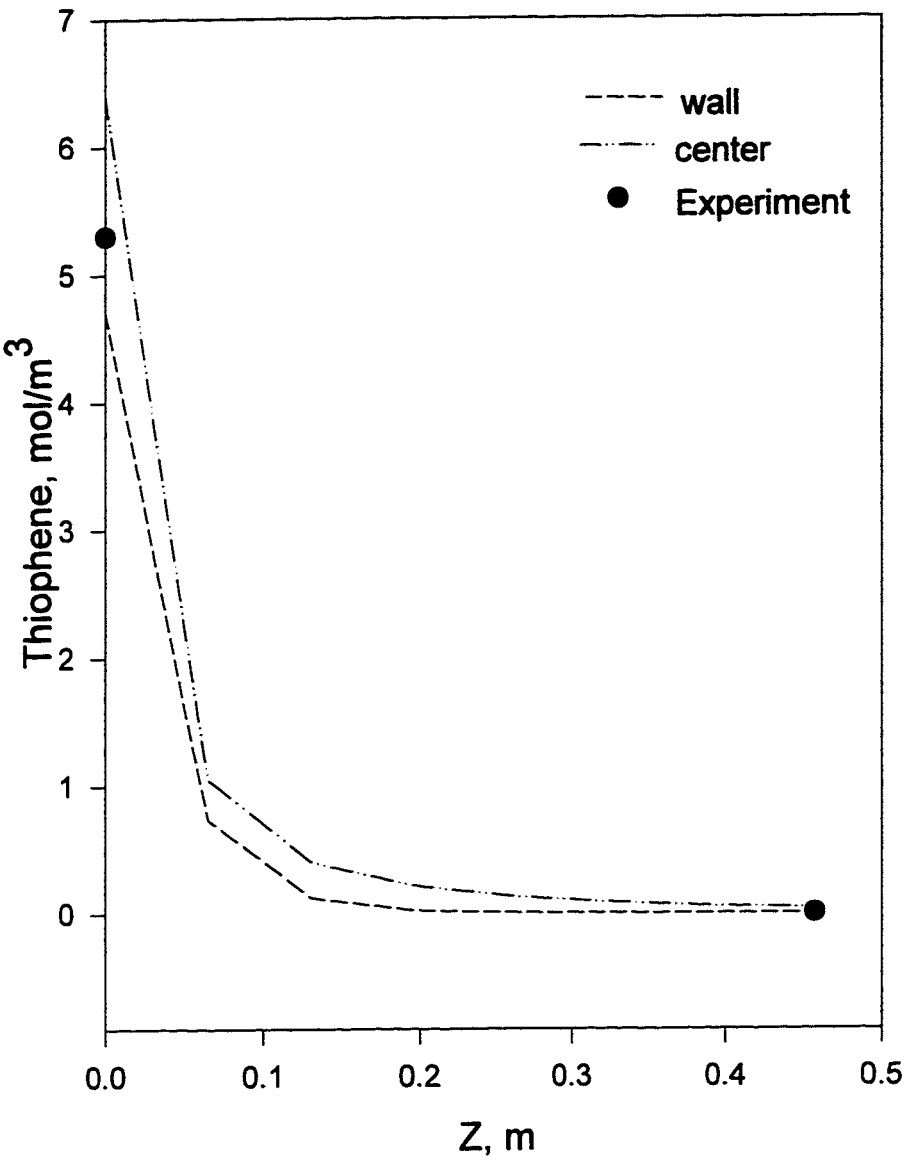

Figure 5.5. Thiophene concentrations in the reactor bed. Showing center and wall profiles. $T_b = 532.15$ K, $T_f = 532.15$ K, $T_{in} = 532.15$ K, $T_w = 500$ K.

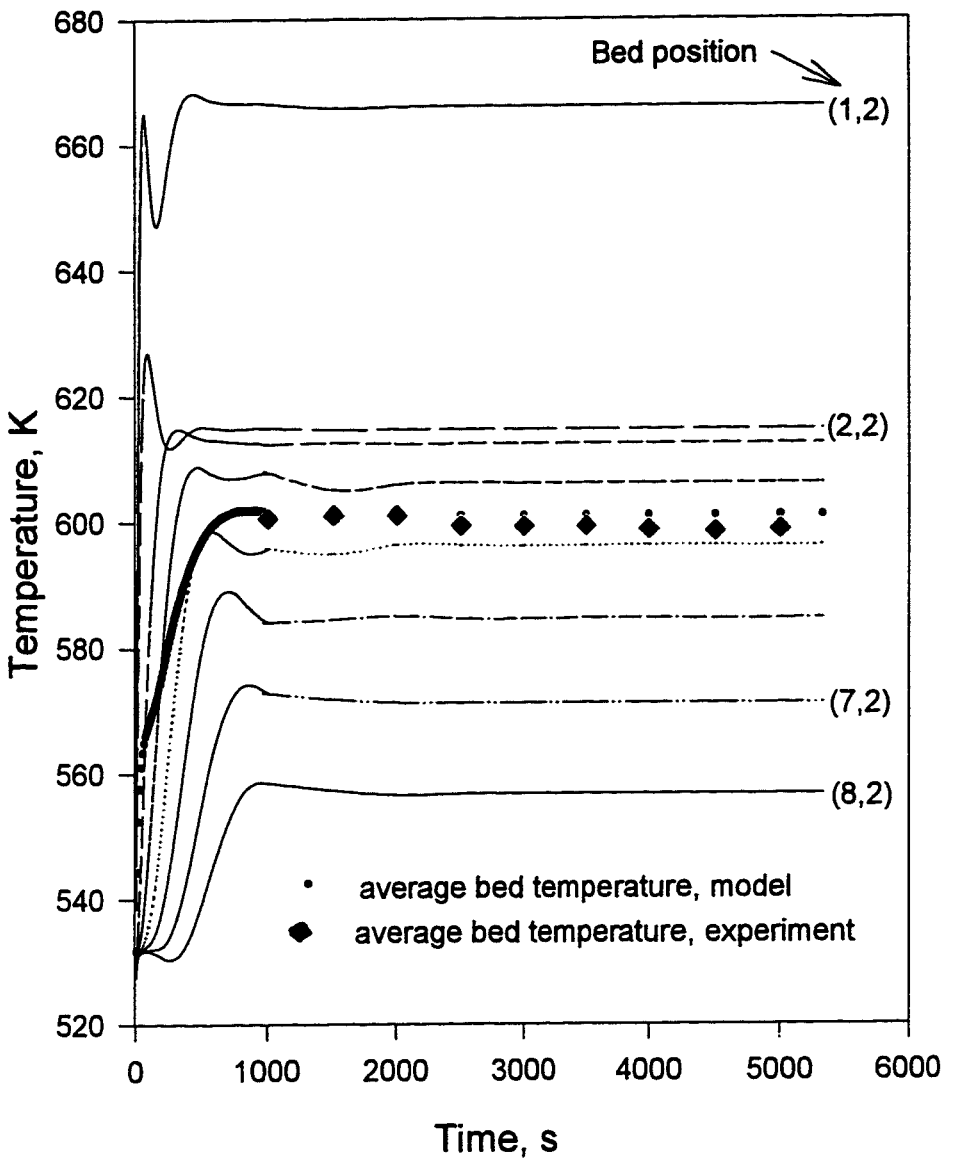

Figure 5.6. Temperature profile in the reactor bed. $T_b = 532.15$ K, $T_f = 532.15$ K, $T_{in} = 532.15$ K, $T_w = 500$ K.

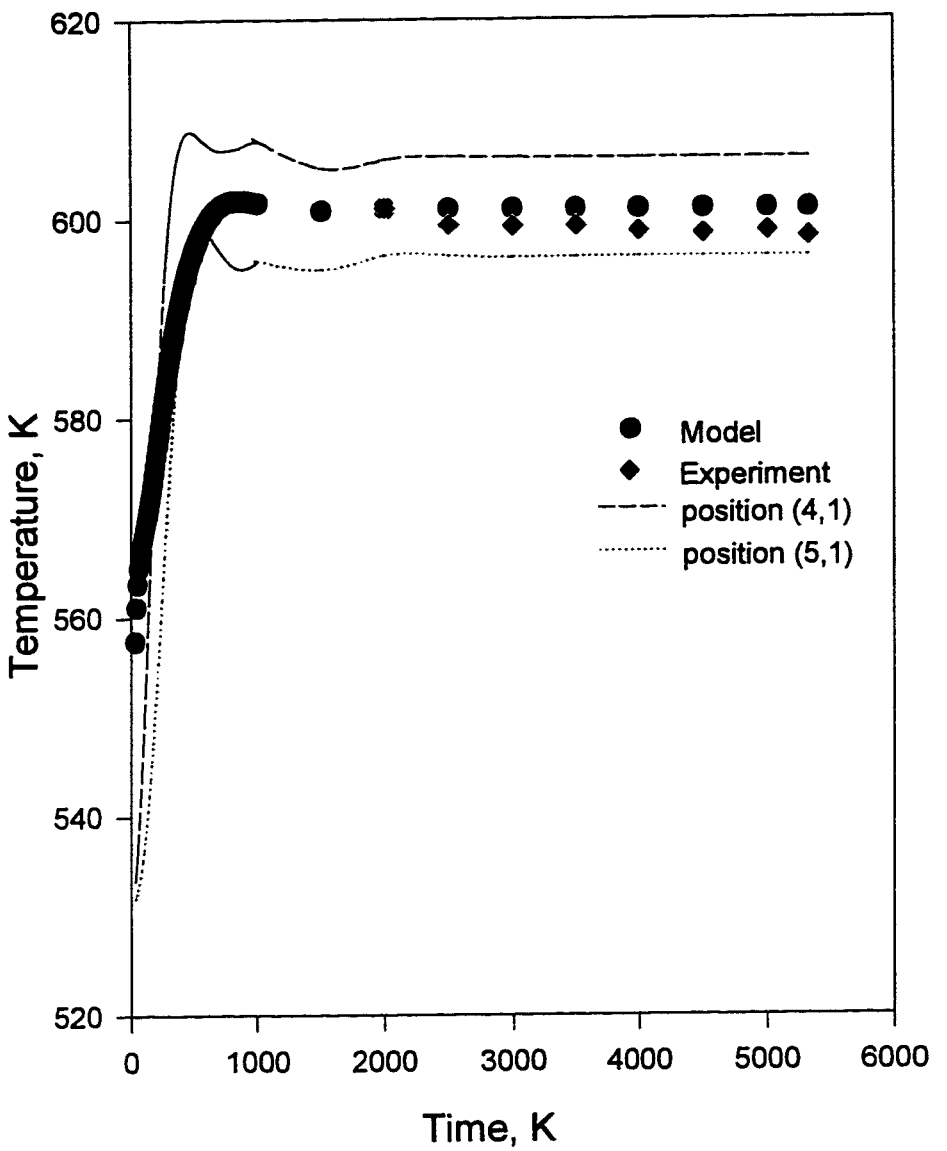

Figure 5.7. Temperature distributions in the reactor bed. Showing center and wall profiles. $T_b = 532.15$ K, $T_f = 532.15$ K, $T_{in} = 532.15$ K, $T_w = 500$ K.

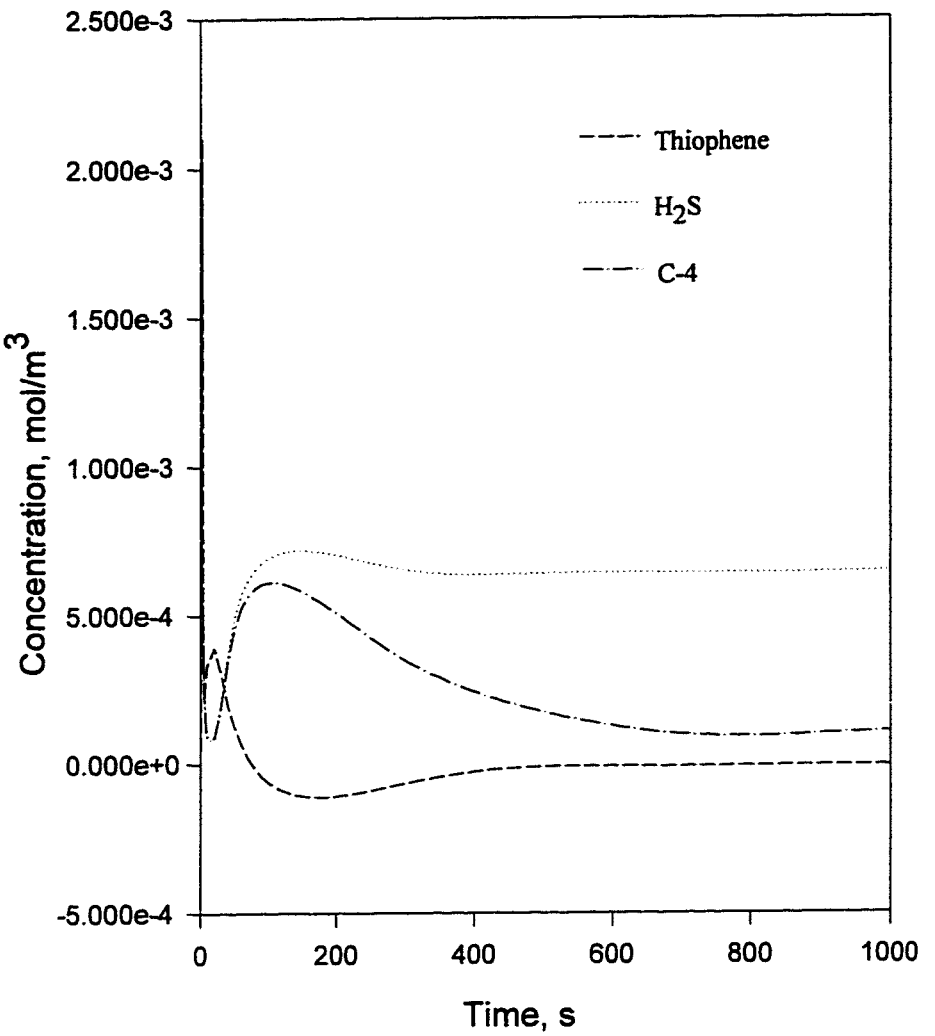

Figure 5.8. Net concentrations of the components in the reactor bed. P_b=5,066.25 kPa, T_{in}=600 K, T_b=700 K, T_f=700 K, T_w=700 K.

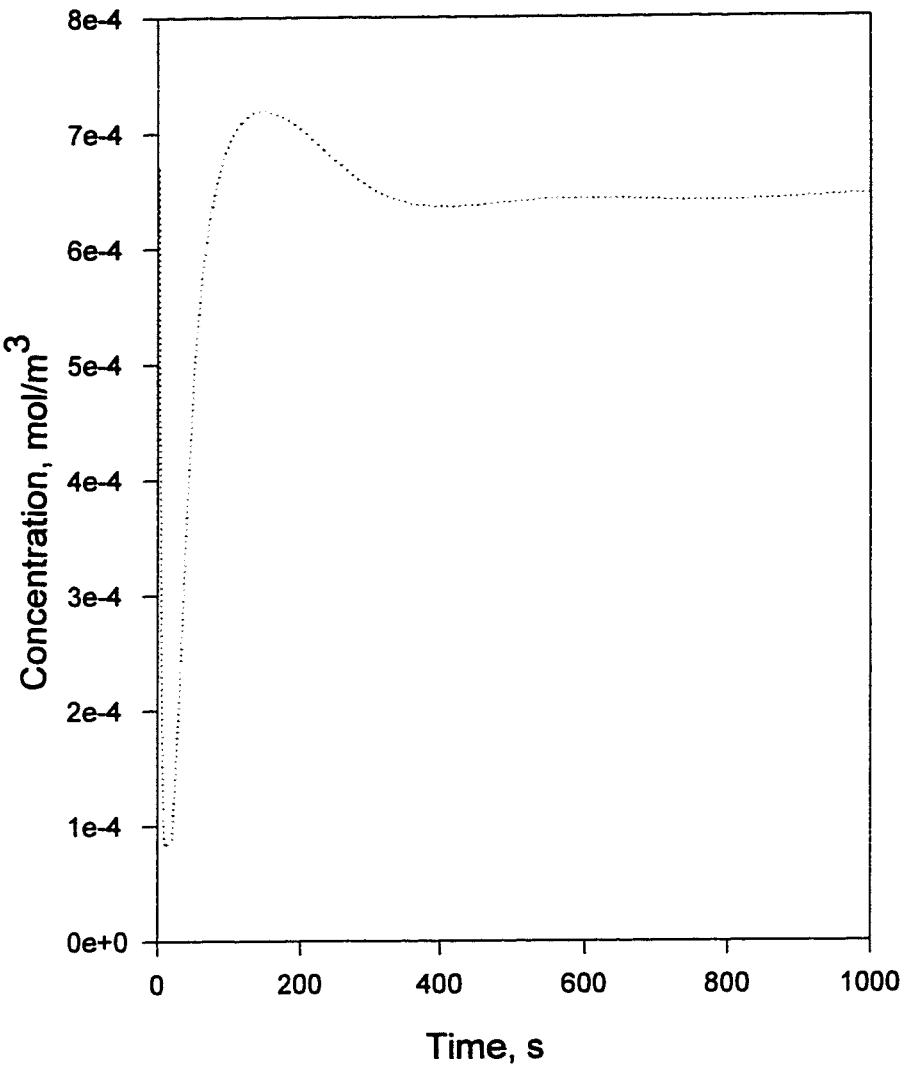

Figure 5.9. Net concentrations of hydrogen in the reactor bed.
P_b=5,066.25 kPa,T_{in}=600 K, T_b=700 K, T_f=700 K, T_w=700 K.

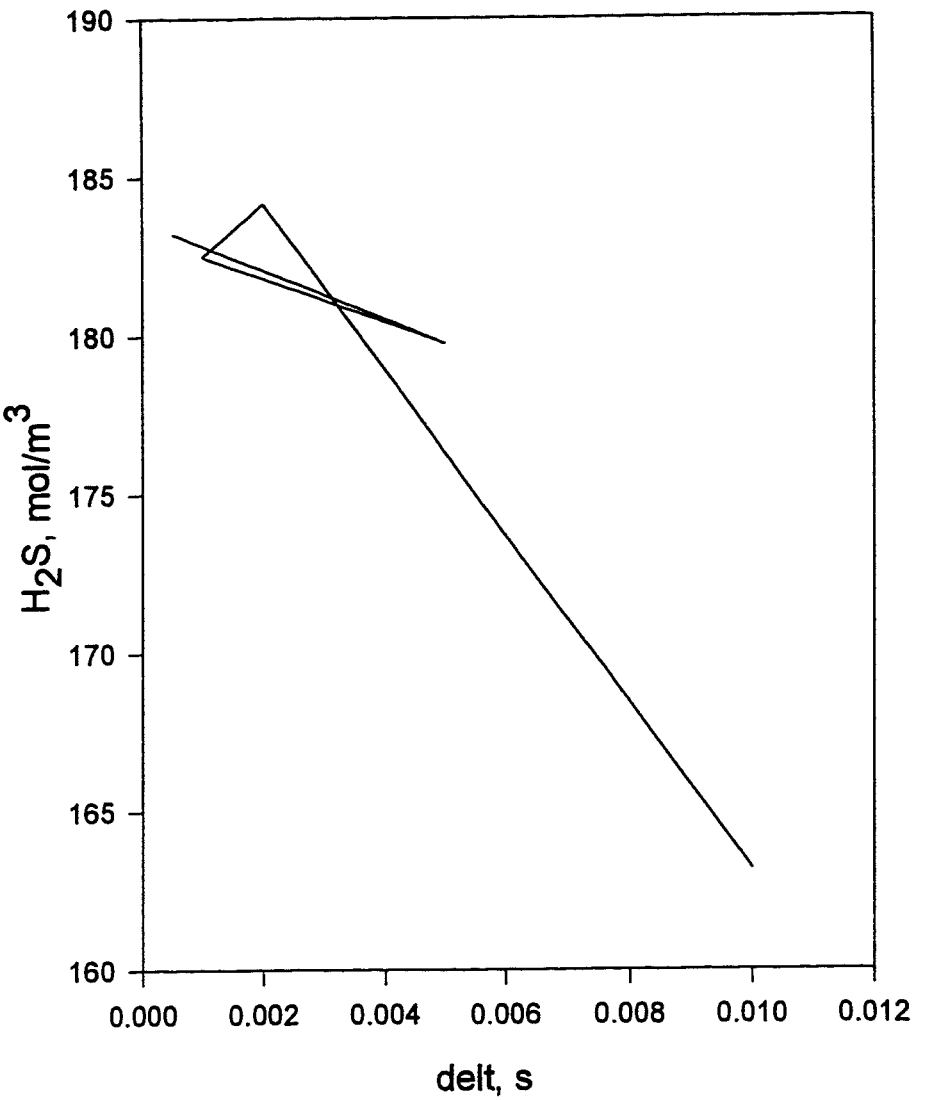

Figure 5.10 H_2S concentration vs time step, indicating the stability of the method.

CHAPTER 6

SIMULATION RESULTS AND DISCUSSIONS

6.1 INTRODUCTION

Although the system behavior in a fixed bed reactor can be studied in an unlimited number of ways, it is attempted here to give the salient features of the model and some interesting aspects are shown. The behavior of single pellets at various bed positions is studied showing the temperature and concentration profiles, and the effect of changes of input variables is demonstrated.

The second part of discussions centers around the behavior of the bed variables, namely, concentration and temperature profiles along the reactor bed and their temporal behavior are explained. In addition, responses of these variables to changes in the input variables are briefly described.

6.2 THE SYSTEM PARAMETERS

The model developed in Chapter 3 and discretized in Chapter 4 in finite difference form was programmed into a completely self-contained code which was designed to calculate the transient equations of the pellet and reactor bed. This model has been run for a reactor of 0.46 m height and 0.027 m diameter. It is filled with catalyst particles of 0.003 m diameter for naphtha hydrodesulfurization. The catalyst porosity is 0.566 and the bed porosity is 0.35. Other necessary parameters for the reactor are given in appendix C.

The model has been applied to desulfurization of thiophene in the following reaction:

$$\text{Thiophene} + 3H_2 \rightarrow C_4 + H_2S. \quad (1)$$

Although there may be many other reactions taking place in a hydrodesulfurization reaction only the reaction above has been selected to reduce the solution or CPU time. Therefore, there are four gas components in the system and all variables are calculated based on such a multicomponent system. Catalyst degeneration or deposition of solids and impurities at the active sites are not included during these runs. The structural changes in the catalyst particles and the bed are bypassed although the model includes these aspects.

Solid-solid reactions and diffusion on the solid surfaces are ignored and cracking reactions are not considered. Catalyst decay, agglomoration, pore closure, and catalyst rupture can be incorporated if desired.

The system has uniform temperature, pressure and concentration profiles at the beginning. In general, initially there are two gases in the pellets and the voidage of the bed. Then inlet stream with different concentrations and temperature is introduced. The pressure in the bed is 5,066.25 kPa (50 atmospheres) unless otherwise indicated. The initial mole fractions in the pellet and the bed as well as the feed are $y_A = 0.05$, $y_2 = 0.95$ where y_A is mole fraction of thiophene and y_2 is that of hydrogen. Some selected runs are carried out with $y_A = 0.2$. The walls are set to desired temperatures.

Under the conditions described above the pellets and the bed are studied in terms of concentrations, temperature and any other system variable. The general grid points in the reactor are shown in Figure 6.0

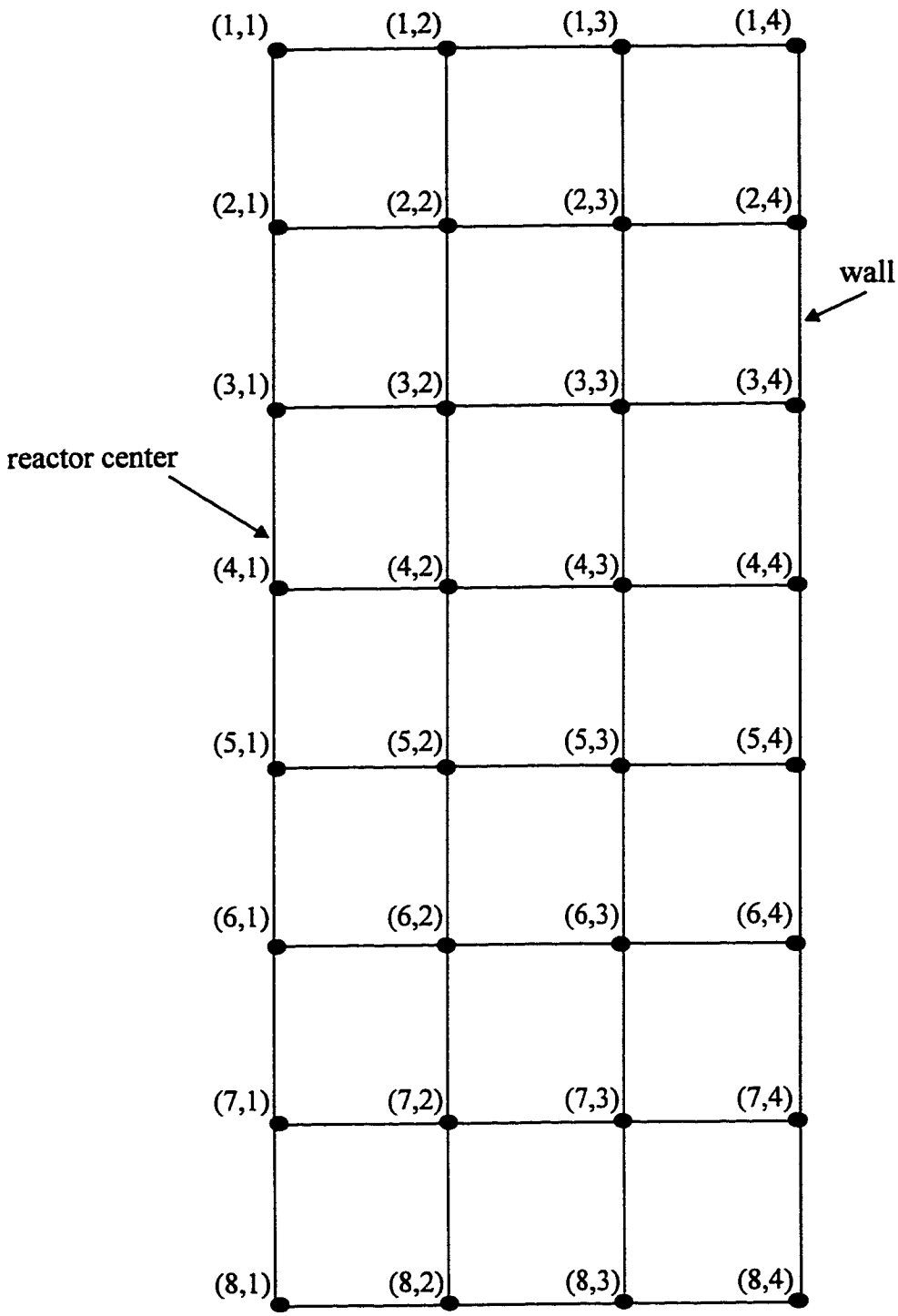

Figure 6.0. General arrangement of grid points for the reactor (half due to symmetry)

6.3 PELLET BEHAVIOR

6.3.1 Temperature

The transient behavior of the pellet temperature is shown in Figures 6.1 - 6.10. The transient surface and center temperatures of a pellet at a bed location (z, R) = (i, j) = (1,2) for two seconds are shown in Figure 6.1. Initially, T_b = 700 K, T_f = 700 K, T_{in} = 600 K, T_w = 700 K. The pellet at 700 K is at the top of the column, closest to the feed which is at 600 K. The temperature rises due to the heat of reaction. Clearly even a pellet of such small size (0.003 m) contains a considerable temperature gradient. The surface temperature rises more due to the fact that reactants are more readily available at the surface compared to the center. On the other hand, when the initial bed - pellet - gas temperatures are reduced to 600 K, the rise of temperature is more tamed as shown in Figure 6.2. The difference between the center and surface temperatures also is quite smaller due to slower rate of reaction.

The temperatures for the first 30 seconds are shown in Figure 6.3 for the same conditions as Figure 6.2. The rise of temperature is steady, even picking up due to increased rate of reaction at the beginning.

The temperatures in a pellet at bed position (2,2) are shown in Figure 6.4 for two seconds with T_b = 800 K, T_f = 800 K, T_{in} = 600 K, T_w = 900 K. Due to increased temperatures in the pellet the concentrations are considerably lower compared to beds with 700 K. The surface temperature is lower than the center in contrast with Figure 6.1. There are opposing effects due to reaction (T increases), due to higher initial temperature (T increases) and lower initial concentration (rate and

temperatures decrease) in addition to opposing forces in the feed (low temperature, high concentration). At this location in the bed the reactants already have reacted to some extent leading to lower rates at position (2,2) compared to position (1,2) in Figure (6.1). In other words, the pellet surface at (1,2) is exposed to higher concentrations of reactants, thus, enhanced surface reaction and higher temperature compared to the center. But the pellet at (2,2), down the reactor, is exposed to lower reactant concentrations and lower surface temperatures.

Temperatures at pellet center are shown in Figures 6.5 and 6.6 at two different bed locations of (1,2) and (2,2) respectively with conditions of T_b = 700 K, T_f = 700 K, T_{in} = 600 K, T_w = 700 K. At the top of the reactor at (1,2) in Figure 6.5 the reactants in the pellet center are sort of used up and now it relies on the their transport from the outside as indicated by the maximum temperature and a decreasing behavior later on towards 120 s of reaction time. However, the temperature in a pellet at position (2,2) keeps on increasing further as shown in Figure 6.6. In this case although the reaction is slower due to lower reactant concentration it has the benefit of receiving warmer fluid from above (not the feed which is at 600 K). As expected the temperature is considerably higher than that at position (1,2). The effect of changing the bed temperatures from 700 to 800 K and the wall temperature from 700 to 900 K (concentrations change as well) can be seen by comparing Figures 6.6 and 6.7. Although the concentrations in case of Figure 6.7 are lower, the rates are considerably higher, and hence higher temperatures at the pellet center.

The temperatures for prolonged times are shown in Figures 6.8 - 6.10. With the conditions same as Figure 6.6 the temperature in the pellet indicates a minimum at around 275 s and then it increases slightly as shown in Figure 6.8. This is due to

the reduction in the reactant concentrations in the bed initially, however, new reactants reach the pellet interior from above, thus stabilizing the reaction rate and the temperatures. It should be noted that the maximum in Figure 6.8 is lower then the maximum in Figure 6.6 which is merely due to printing frequency in the program to save storage. Similar behavior with a maximum and then a local minimum can be observed at longer times in Figure 6.9 which has the same conditions as with Figure 6.7.

The temperature in a pellet at (1,2) in Figure 6.10 with T_b = 600 K, T_f = 600 K, T_{in}= 600 K, T_w = 700 K indicates a maximum which is higher than that in Figure 6.8 but lower than the one in Figure 6.9. This is due to increase in initial and inlet concentrations to the grid point (it is exposed to the feed). A similar trend of maximum and a slight dip just before stabilized values is observed in temperature.

6.3.2 Concentration

The pellet and the bed contain four gaseous components at any given time after the beginning. The concentrations of the reactants and products in the pellet are studied next.

The thiophene concentrations in the pellet at various locations in the bed are shown in Figures 6.11 - 6.16. with T_b = 700 K, T_f = 700 K, T_{in} = 600 K, T_w = 700K. The initial thiophene concentration is zero. The system contains initially H_2 and H_2S in the molar ratio of 5/95. The bed position is progressively downward in the column from (1,2) to (6,2) which is the cylindrical surface next to the main axes of the bed. The parameter in the figures is the radial position in the pellet.

The thiophene concentration at the top position exhibits a maxima within the pellet in time. This is due to the penetration of thiophene from the surface inward and in the mean time reacting along the travel path. Once temperature starts rising the reaction rates become higher, thus, depleting the reactant in the pellet as will be seen later on. H_2 exhibits a drop in concentration at earlier times because it is already there from the beginning. The concentration of thiophene within the pellet goes down towards the center. It decreases swiftly to zero at the pellet center. These profiles become flatter and less pronounced down the reactor due to reaction as evidenced from Figures 6.12 to 6.16. For instance, in Figure 6.14 at position (4,2) thiophene concentration flattens at a much lower value. Within the same duration, the concentrations in the lower part of the reactor, at (6,2), as an example, can achieve much smaller rises inside the pellet as shown in Figure 6.16.

For similar conditions as Figures 6.11 - 6.16 but with an initial thiophene/H_2 mole fractions of 0.20/0.80, the thiophene concentrations within the pellet decrease sharply due to increase induced by the effect of initial concentration in the reaction rates as shown in Figure 6.17. The fact that the feed contains much less thiophene reaching the position (1,2) does not help it either.

Similar profiles as in Figures 6.11-6.16 for one of the products (H_2S) are given in Figures 6.18 and 6.19 at two positions in the bed: (1,2) and (6,2). The conditions are: T_b = 600 K, T_f = 600 K, T_{in} = 600 K, T_w = 700 K. The thiophene/H_2 ratio is 0.05/0.95. The product concentration in the pellet goes up suddenly in time. Due to absence of flux at the center it stabilizes at a certain value. At other locations, however, it exhibits maxima and drops to a certain level causing local minima and then stabilizes in time. This is due to the faster reaction at the beginning because of larger amounts of reactants present, and then slowing down considerably because

of reliance on the transport of reactants from outside. The increase after a certain time is due to increased reaction rates caused by temperature increases in the system. Higher temperatures are as a result of heat of reaction. A study of Figure 6.19 indicates sustained H_2S concentration in the pellet at bed location (6,2). This is due to the fact that reaction caused by the initial abundance of reactants is, sort of, abated but the product is built up within the pellets because the bulk H_2S concentration is high caused by the supply from grids above in the bed. Thus, the product has difficulty in escaping from the pellet interior having the flux determined by the concentration differences between the pellet surface and bulk concentrations.

The hydrogen concentrations in the pellet at location (2,2) in the bed are shown in Figure 6.20 with T_b = 800 K, T_f = 800 K, T_{in} = 600 K, T_w = 900 K. The initial mole fractions of thiophene and H_2 are 0.05 and 0.95 respectively. The concentrations decrease swiftly with clear difference between pellet surface and center. The surface concentrations are higher due to fresh supply of H_2.

In order to present the situation from a different perspective, the variations in thiophene concentrations at pellet surfaces down the reactor are shown in Figures 6.21 and 6.22. Figure 6.21 has the conditions T_b = 700 K, T_f = 700 K, T_{in} = 600 K, T_w = 700 K which are similar to the conditions in Figure 6.11. There is a distinctive maximum in transient values which is highest at the top of the reactor and progressively decreasing down the reactor. This shift in the maxima is similar to the bed temperature profiles to be shown later in Figure 6.31. At higher temperatures of T_b = 800 K, T_f = 800 K, T_{in} = 600 K, T_w = 900 K the maxima are exhibited at lower concentration values in Figure 6.22. Similar shift in maxima down the reactor is apparent in this figure.

The hydrogen concentrations in the pellet at various locations in the bed are shown in Figures 6.23 - 6.25 with T_b = 800, T_f = 800, T_{in} = 600, T_w = 900 K. In Figure 6.23 the pellet surface concentrations deplete due to reactions, thus, depleting the thiophene then rising due to feed content. The downward trend later on is due to increased rates induced by rises in the temperatures. Down the reactor, however, the hydrogen content of the inlet to each grid point is much less than that of the top, thus stabilizing at much lower values of H_2 concentrations. The interesting phenomena here are that there are maxima in the pellet surface concentrations.

The H_2 concentrations halfway in the pellet are shown in Figure 6.24. Again similar maxima are present as in Figure 6.23 but with lower H_2 concentrations. Pellet center concentrations at bed positions (1,2) and (6,2) are shown in Figure 6.25. These concentrations are considerably lower than the previous values with no maxima present. This is due to the absence of fluxes at the center as mentioned before.

The concentrations of various components in the pellet are shown in Figures 6.26-6.30. The pellet center concentrations are shown in Figure 6.26 at (1,2) with T_b = 700 K, T_f = 700 K, T_{in} = 600 K, T_w = 900 K, thiophene mole fraction = 0.05. The thiophene and H_2 concentrations decrease with time due to reaction and H_2S increases stabilizing later on. There is no maxima exhibited because of lack of flux. When the bed and wall temperatures are increased to 700 K and 900 K respectively the pellet center concentrations stabilize at lower values for thiophene and H_2 in Figure 6.27. This is due to effect of temperature on concentration calculations. H_2S, on the other hand, maintains higher values although temperature decreases its concentration but the reaction causes it to increase. For the prevailing temperatures are higher with T_b = 800 K, T_f = 800 K, T_{in} = 600 K, T_w = 900 K the

changes in the concentrations are sudden and the stabilized values are attained much earlier as evidenced in Figure 6.28. However note that this figure is for position (2,2).

At position (3,2) with T_b = 700 K, T_f = 700 K, T_{in} = 600 K, T_w = 900 K pellet center and r/R_p = 0.75 concentration profiles are shown in Figures 6.29 and 6.30 respectively. The center concentrations do not exhibit any maxima or minima as before. However off center position in Figure 6.30 shows maxima for products and the previously mentioned down and up behavior for hydrogen. This is due to consumption of the initial thiophene present in the pellet. Later on the rates are enhanced as well as transport properties due to temperature rise, thus, a reduction in H_2 concentration at later stages.

6.4 BED BEHAVIOR

The behavior of bed variables is discussed in this section. Temperature profiles in time and along the axial directions are shown and in the radial direction the profiles are found to exhibit major variations in contrast to most of the previously exercised assumptions. This aspect is studied in detail. Next, the concentration profiles are given which are also found to have quite interesting behaviors. Finally, in this section the system response to sudden changes in the boundary conditions is shown.

6.4.1 Temperature

The transient temperature profiles in the reactor bed are shown in Figure 6.31. Profiles at 8 different locations in the bed are presented. The conditions are T_b =

700 K, T_f = 700 K, T_{in} = 600 K, T_w = 700 K, y_A = 0.05, y_2 = 0.95. As observed, there is a temperature maxima or hot spot in the bed. The maxima emerges at progressively delayed times along the reactor indicating the sweep of the initial conditions with sharper behavior at the entrance of the bed (1,2) where there is much higher reaction due to continues supply of material from the outside. Later the temperature profiles continuous with fairly smooth distribution in z-direction.

The development of maxima in temperature profile is shown in Figures 6.32-6.34 with T_b = 700 K, T_f = 700 K, T_{in} = 600 K, T_w = 700 K, y_A = 0.2, y_2 = 0.8. Due to higher initial thiophene concentration in the pellets and the bed there is enhanced reaction at the beginning and then there is a sudden drop in temperature due to decreased thiophene concentrations. The progress of the profiles from 10 s to 90 s are demonstrated in these figures. Also the maximum increases in temperature in time due to reactions should be noted.

With higher wall temperature and lower initial thiophene concentration the temperature behavior is shown in Figures 6.35 - 6.40 with T_b = 700 K, T_f =700 K, T_{in} = 600 K, T_w = 900 K, y_A = 0.05, y_2 = 0.95. The gradual development of profiles in the axial direction are shown in these figures as time progresses. After 30 s there are maxima in the bed which change in R-direction as observed in Figure 6.35. The importance of including the radial direction in the formulation is clearly demonstrated in this group of figures as the difference from the wall to the bed axis

is quite pronounced. This behavior and the progress of maxima to positions lower in the bed in 120 s are shown in Figure 6.36. After 250 s the profiles assume different distributions along the axial and radial directions due to reactions and

effect of wall temperature on the system as given in Figure 6.37. They seem to stabilize down the reactor. Later on with the contribution due to heat of reaction and the wall temperature the profiles are at higher values and assume increasing trends over and above the wall temperatures near the wall (See Figure 6.38). Similar increasing trends are clear in Figures 6.39 and 6.40. Again the radial direction exhibits large temperature gradients.

The importance of employing heat transfer coefficients near the wall is demonstrated in Figures 6.41 - 6.43. In these figures the bed position near the wall is assumed to have the wall temperature, thus ignoring the convective heat transfer coefficient between the wall and the bed. Thus near the wall, temperatures are not allowed to go above that of the wall which is in contrast to the previous behaviors in Figures 6.37 - 6.40 where temperatures higher than that of the wall are exhibited. This is quite an interesting behavior. Ignoring the wall heat transfer coefficient has caused problems in the running of the program as with the fixed wall temperature, the effect of heat of reaction and fluxes, etc. are suppressed. However, though lower than wall, similar temperature trends in development of profiles are observed near the central position: initially sudden reaction with lowering in profiles down the reactor, later on assuming increasing trends. Again the importance of radial direction is clear.

6.4.2 Concentration

The bed contains four gaseous components at any given time after the beginning. The concentrations of the reactants and products in the bed are studied in this section. Figures 6.44 to 6.46 show the concentration profiles of thiophene in the reactor bed. The conditions are T_b = 700 K, T_f = 700 K, T_{in} = 600 K, T_w = 900 K,

and thiophene mole fraction of 0.05 with the remainder hydrogen. The profiles are at central axial positions in the bed for 30, 60 and 300 s. The thiophene concentration goes down rapidly in the bed in z-direction approaching zero value. The top concentrations, however, progressively go down and later on, they stabilize. This is due high rate of reaction at the inlet of the reactor and low concentration of thiophene feed to the reactor.

The hydrogen concentrations are shown in Figures 6.47 - 6.53 at similar conditions but at times of 30, 60, 90, 200, 300, 400, and 500 s respectively. In the first two of these figures the profiles exhibit maxima. This can be explained as following. In the bed originally the concentration is lower due to higher temperatures. Later on the incoming fluid with lower temperature and thus higher concentrations is introduced. Since thiophene has decreased to close to zero values as shown previously the reaction is much slower and thus causing a rise in H_2 concentration in the bed. Further down the bed the temperatures are higher which cause lower H_2 concentrations. Again, the effect of radial direction is clearly indicated in Figures 6.47 and 6.48.

Due to effect of wall temperature H_2 profiles exhibit large variations in R-direction as shown in Figures 6.49 - 6.53. The effects of initial concentrations in the pellets and the bed as well as that of wall temperature are absorbed by the bed, thus, leading to smoother distributions, again with variations in R-direction but stabilized values in z-direction. As the effect of wall temperature takes on, the concentrations in z-direction near the wall ($r/R_B = 0.67$) decrease down the reactor. This is mainly due to effect of temperature on concentrations.

The concentration distributions of H_2S, which is one of the products are shown in Figures 6.54 - 6.58 at times of 30, 60, 120, 300, and 400 s which have the same conditions as the group of Figures 6.49 - 6.53. Initially there are maxima exhibited in these concentrations due to reaction of thiophene and lower temperatures up the reactor. Later on these concentrations stabilize. At later times as H_2 concentration goes down the concentration of the product, H_2S, goes up due to reaction at higher temperatures. However higher temperatures work in other direction, reducing the concentrations. The effect of radial direction with combined influences due to temperature and reaction factors is clearly apparent from Figures 6.56 - 6.58 where even a crossover is observed between the profiles in different radial positions which indicates the contrasting effects of reaction and temperature on the product concentrations.

For conditions of T_b = 700 K, T_f = 700 K, T_{in} = 600 K, T_w = 900 K, y_A = 0.2, y_2 = 0.8 the transient concentrations of all components at position (1,2) are shown in Figure 6.59. For thiophene a dip and a maximum before stabilizing later on are due to higher initial concentration in the bed and the pellets. Other components exhibit more tamed behavior. For the same conditions a three dimensional graph in Figure 6.60 shows the temperature profile. Here the maxima changes in time along the z-direction, as suggested by the two dimensional plot shown earlier.

6.4.3 Parametric studies

In this section the effect of changing one of the input parameters after a certain length of time from the start is studied. The conditions for the base case are T_b = 700 K, T_f = 700 K, T_{in} = 700 K, T_w = 700 K, y_A = 0.05, y_2 = 0.95. After 30 s T_{in} is changed to 600 K and the variation of thiophene concentration at position (1,2) is

shown in Figure 6.61. When the temperature is lowered the concentration increases and stabilizes at its final value at that position. This is due to decreased reaction rates and effect of temperature on concentration. The response time is approximately 300 s. A similar behavior in H_2S concentration is shown in Figure 6.62 which decreases due to less reaction and temperature effect on concentration. Again there is a similar but slightly longer response time. For a shorter time 60 s in Figure 6.62. The effect of changes causing fluctuation is shown in Figure 6.63.

The effect of lowering the inlet temperature to 600 from 700 K is shown in Figure 6.64 at position (1,2) at the top of the reactor for 600 s. Clearly with lower inlet temperature the values are lower due to less reaction and lower temperature. There is also a maximum exhibited for each inlet temperature case. The higher inlet temperature has the maximum at later times due to lowered concentrations, and thus, the effect of heat of reaction which is less with decreased reaction rates. Near the wall a similar trend is observed without a maximum as in Figure 6.65. This is due to effect of wall temperature via convective heat transfer from the wall. The temperatures are already high and the concentrations low. Thus they attain stabilized values without maxima.

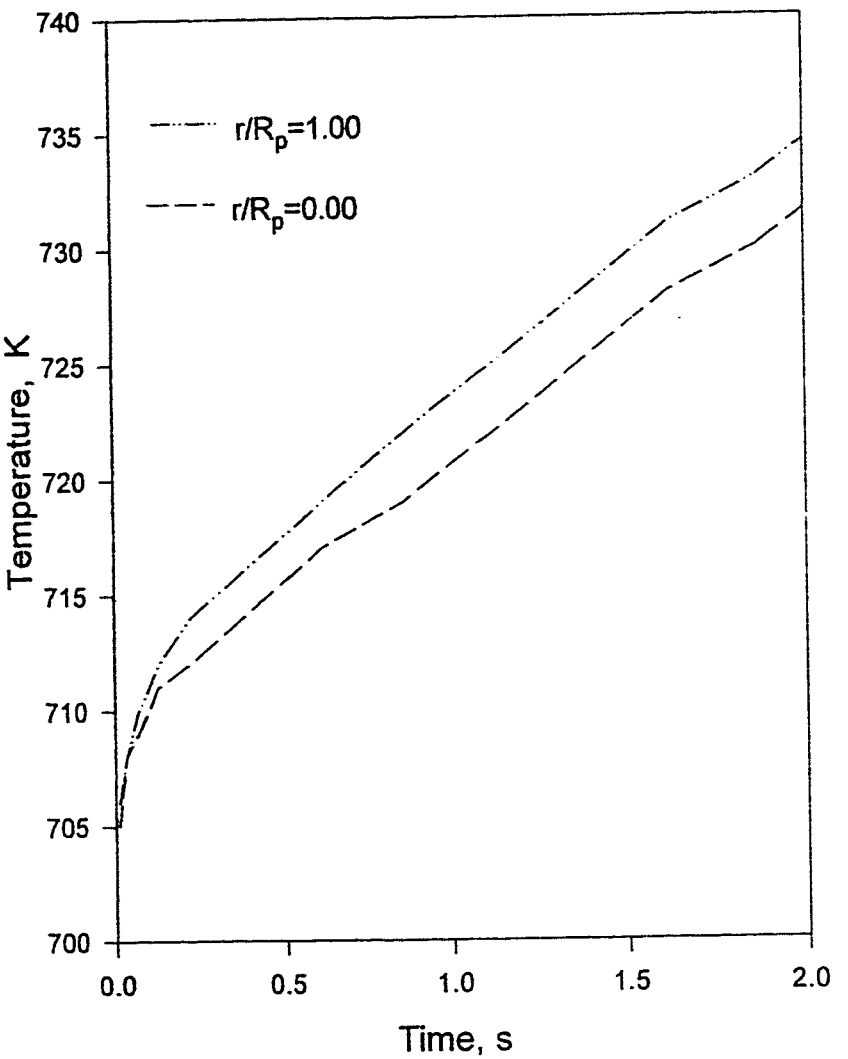

Figure 6.1. Temperature profiles in a pellet at two radial locations at position (1,2). P_b = 5,066.25 kPa, T_b = 700, T_f = 700 K, T_{in} = 600 K, T_w = 700 K.

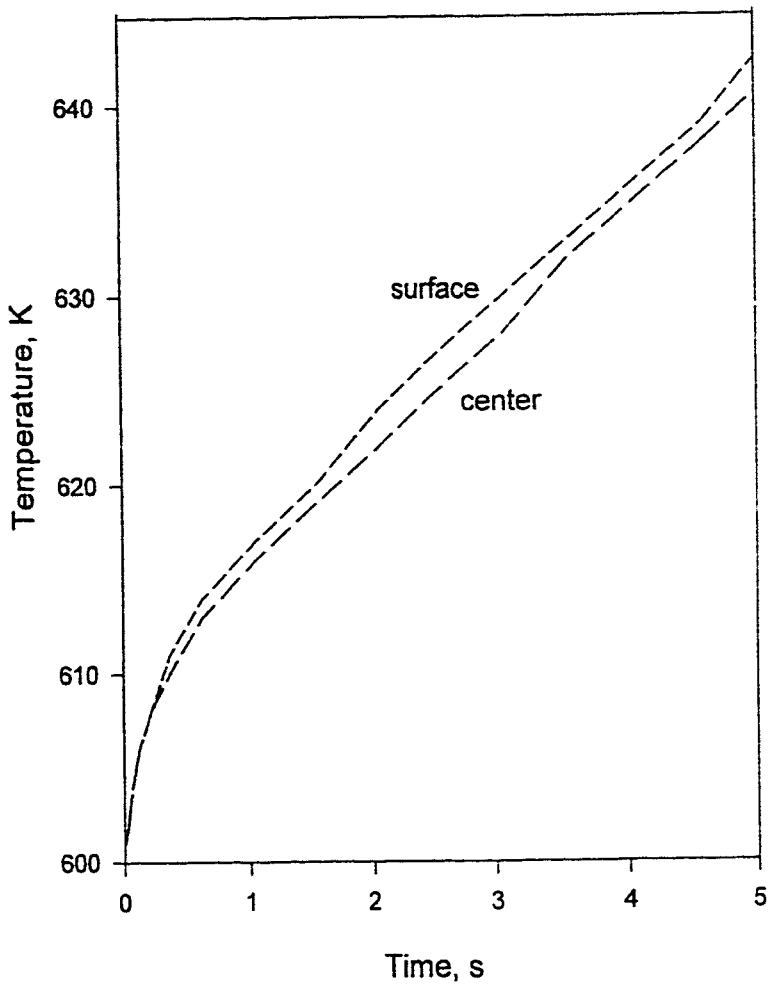

Figure 6.2. Temperature profiles at pellet center and surface at (1,2). P_b = 5,066.25 kPa, T_b = 600 K, T_f = 600 K, T_{in} = 600, T_w = 700.

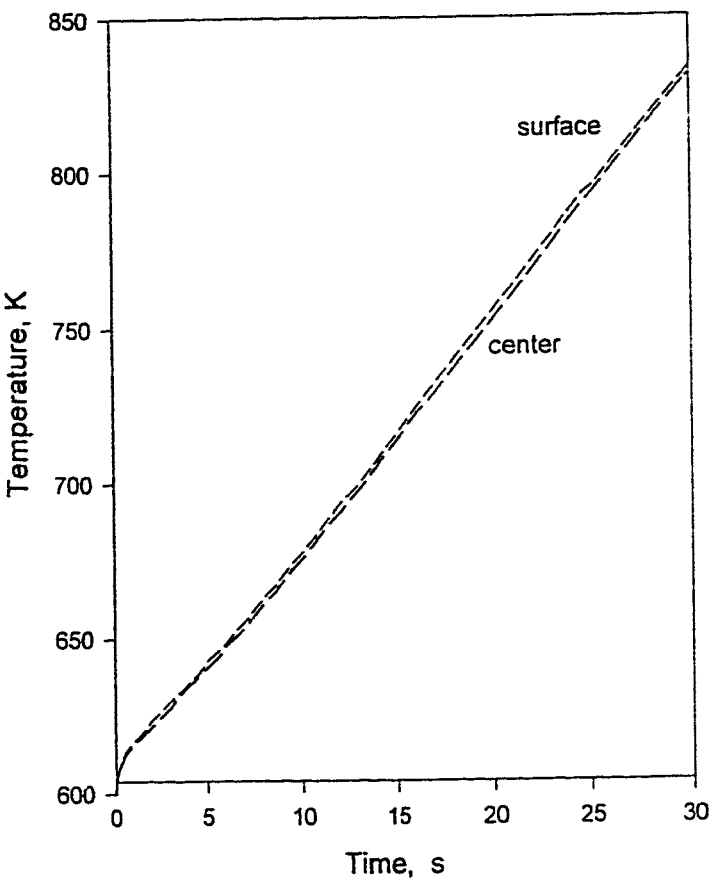

Figure 6.3. Temperature profiles in a pellet at position (1,2) and two pellet radial positions. $P_b = 5066.25$ kPa, $T_b = 600$ K, $T_f = 600$ K, $T_{in} = 600$ K, $T_w = 700$ K.

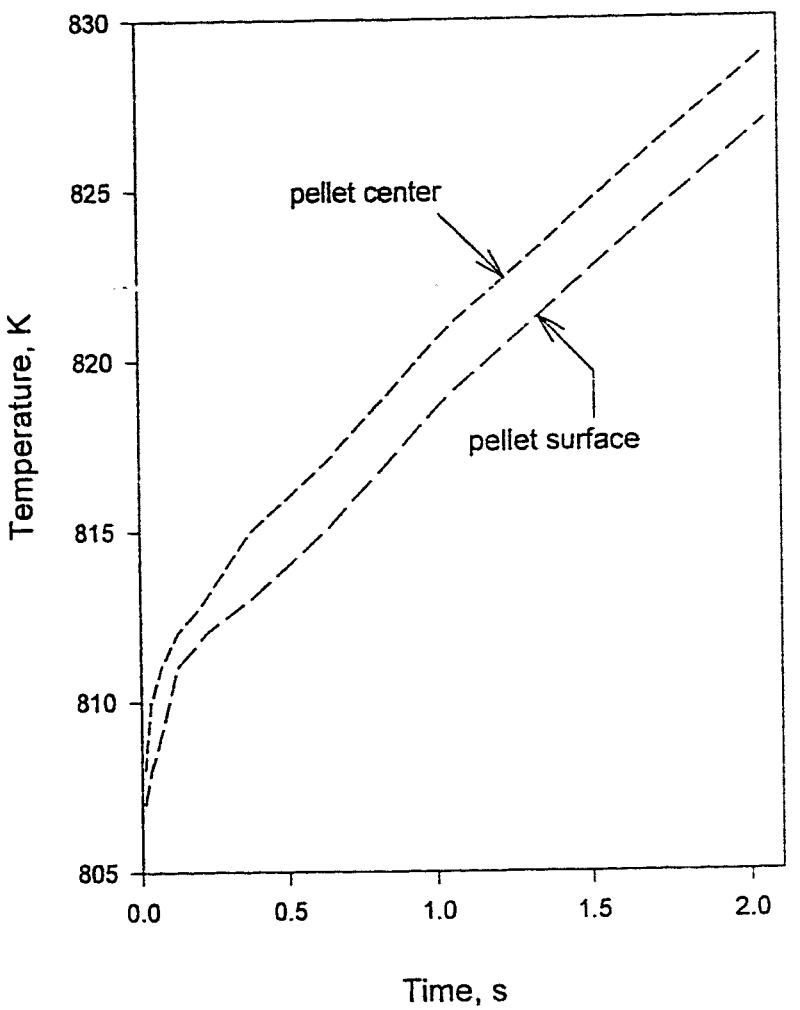

Figure 6.4. Temperature profiles at pellet center and surface at (2,2). $P_b = 5{,}066.25$ kPa, $T_b = 800$ K, $T_f = 800$ K, $T_{in} = 600$, $T_w = 900$.

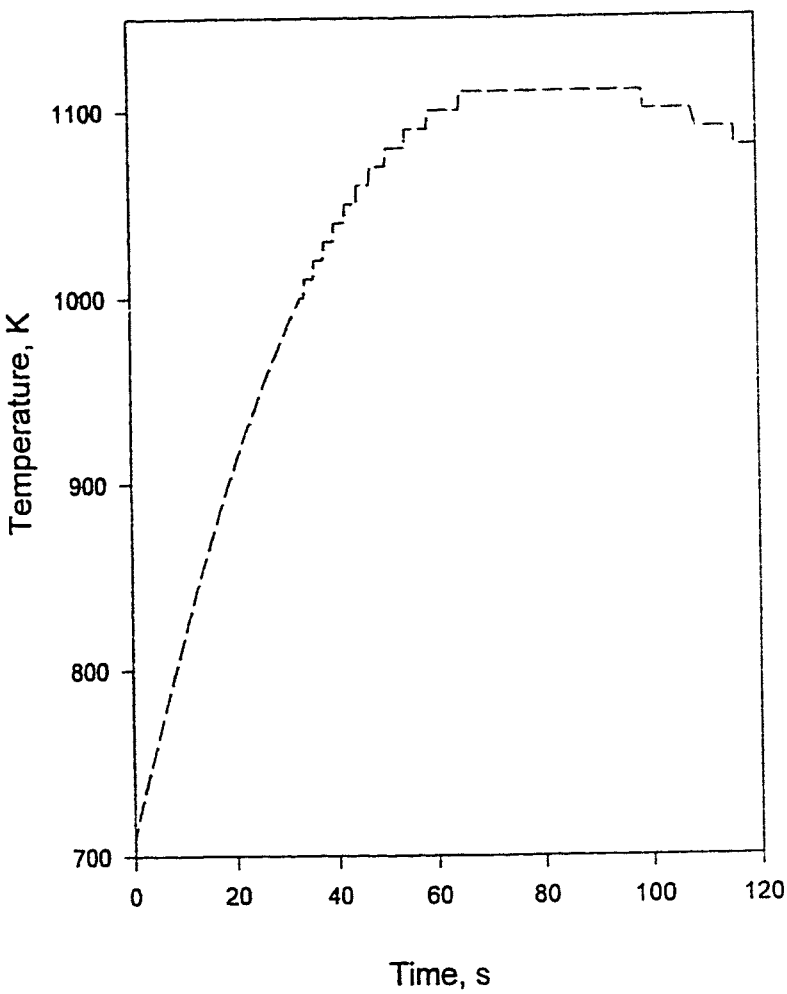

Figure 6.5. Temperature profile at pellet center at (1,2).
$P_b = 5{,}066.25$ kPa, $T_b = 700$ K, $T_f = 700$ K,
$T_{in} = 600$, $T_w = 700$.

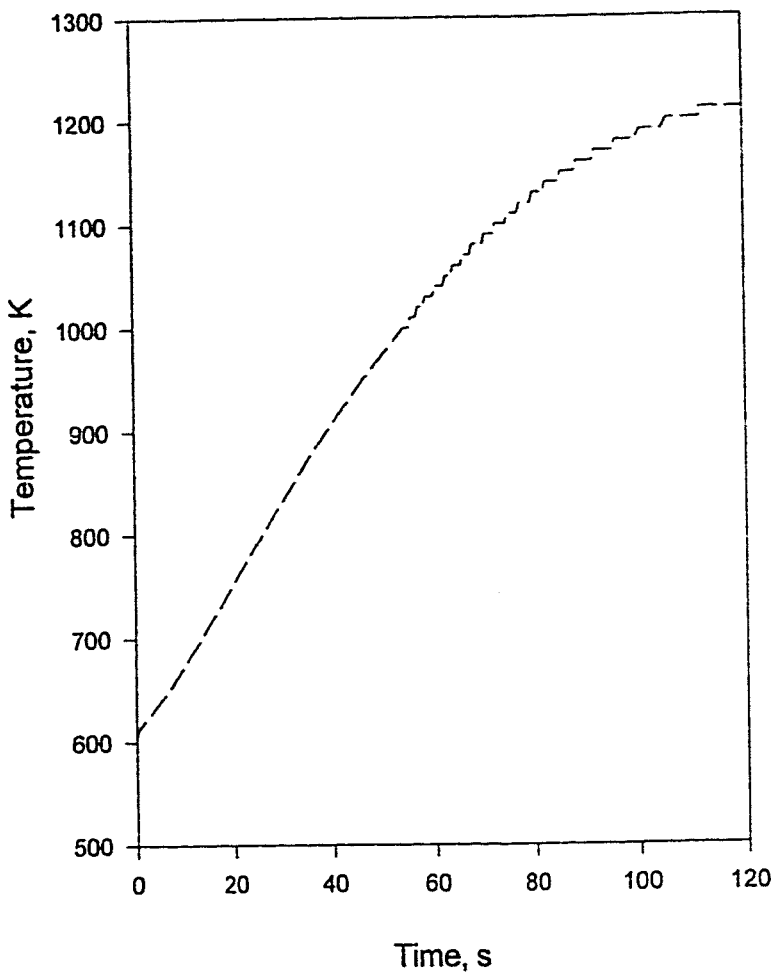

Figure 6.6. Temperature profile at pellet center at (2,2).
$P_b = 5{,}066.25$ kPa, $T_b = 700$ K, $T_f = 700$ K,
$T_{in} = 600$, $T_w = 700$.

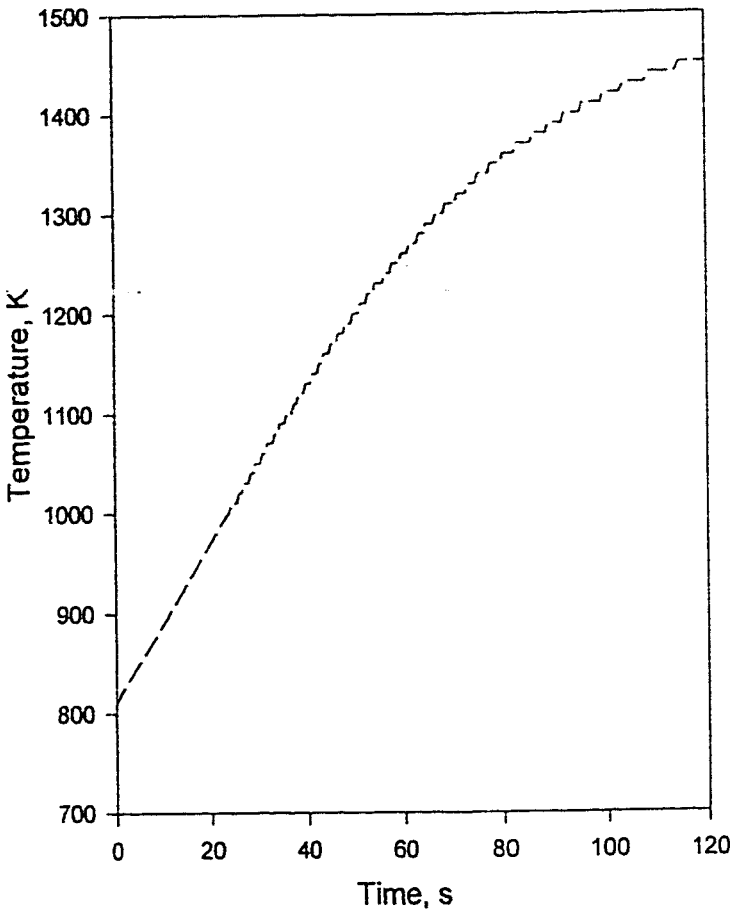

Figure 6.7. Temperature profile at pellet center at (2,2).
$P_b = 5{,}066.25$ kPa, $T_b = 800$ K, $T_f = 800$ K,
$T_{in} = 600$, $T_w = 900$.

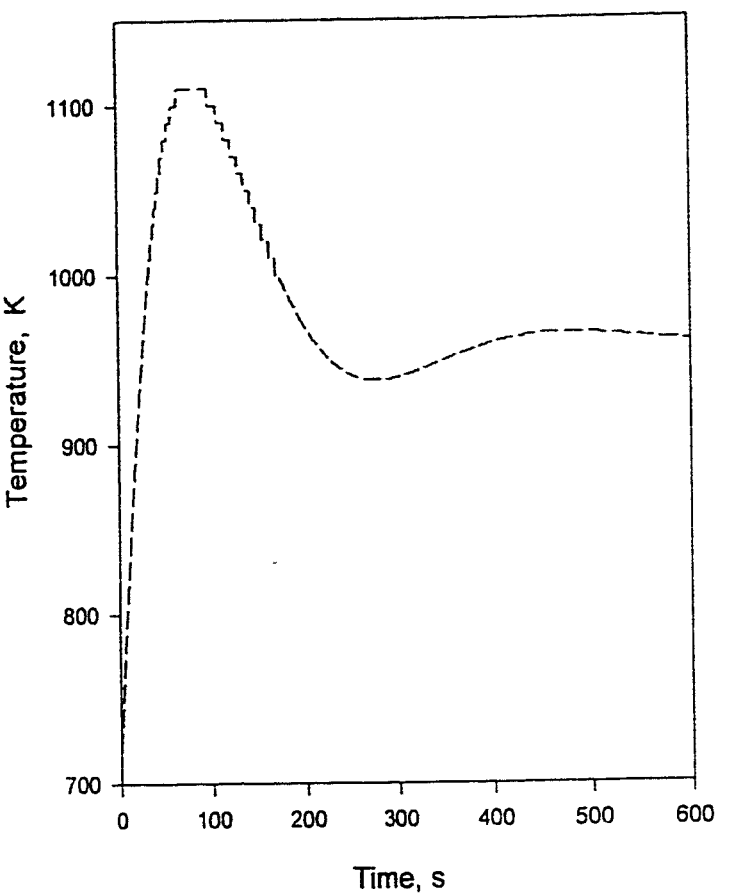

Figure 6.8. Temperature profile at pellet center, reactor position (2,2).
$P_b = 5{,}066.25$ kPa, $T_b = 700$ K, $T_f = 700$ K, $T_{in} = 600$,
$T_w = 700$.

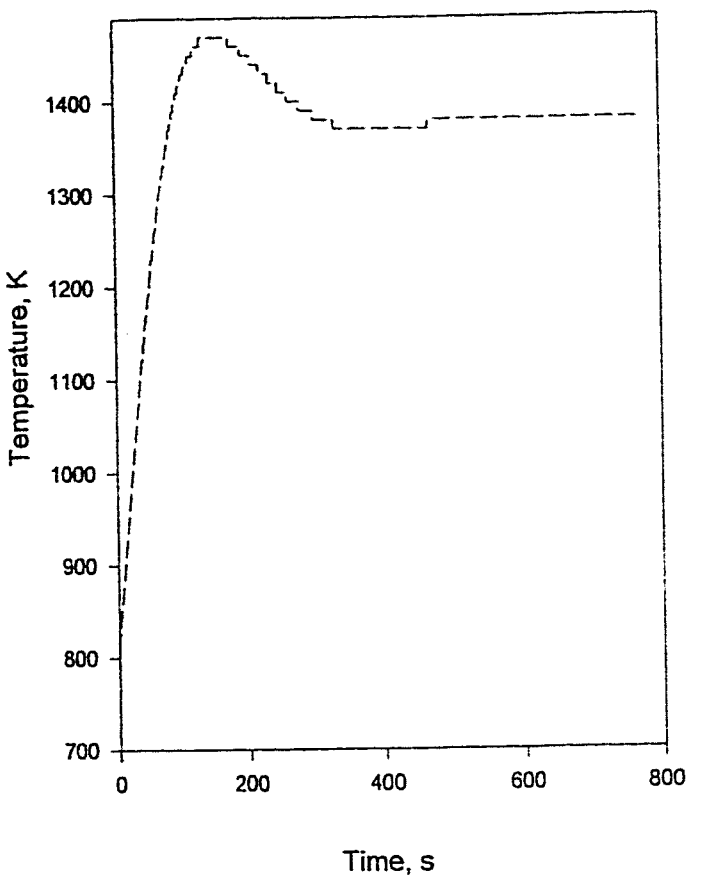

Figure 6.9. Temperature profile in a pellet center at position (2,2).
$P_b = 5{,}066.25$ kPa, $T_b = 800$ K, $T_f = 800$ K, $T_{in} = 600$ K,
$T_w = 900$ K.

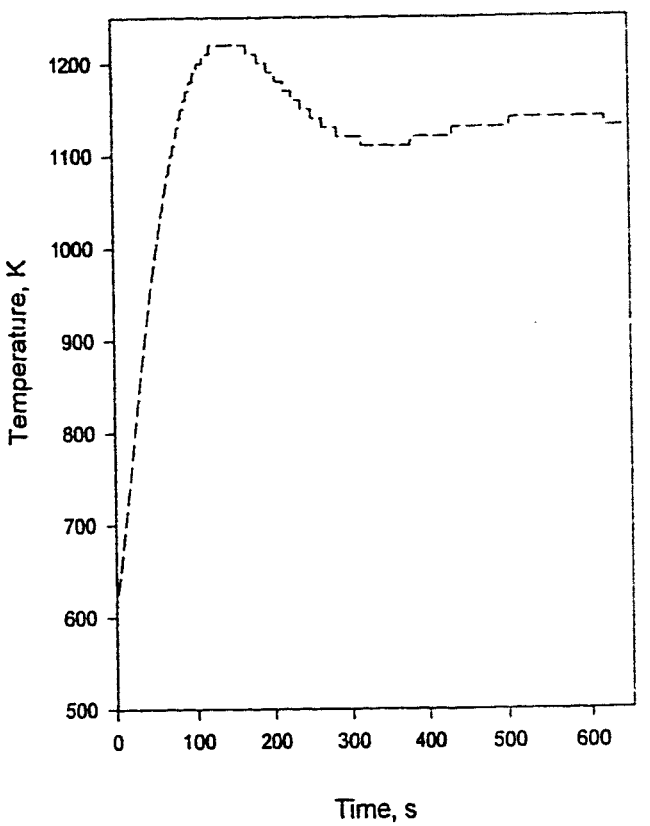

Figure 6.10. Temperature profile at pellet center at position (1,2).
$P_b = 5{,}066.25$ kPa, $T_b = 600$ K, $T_f = 600$ K,
$T_{in} = 600$ K, $T_w = 700$ K.

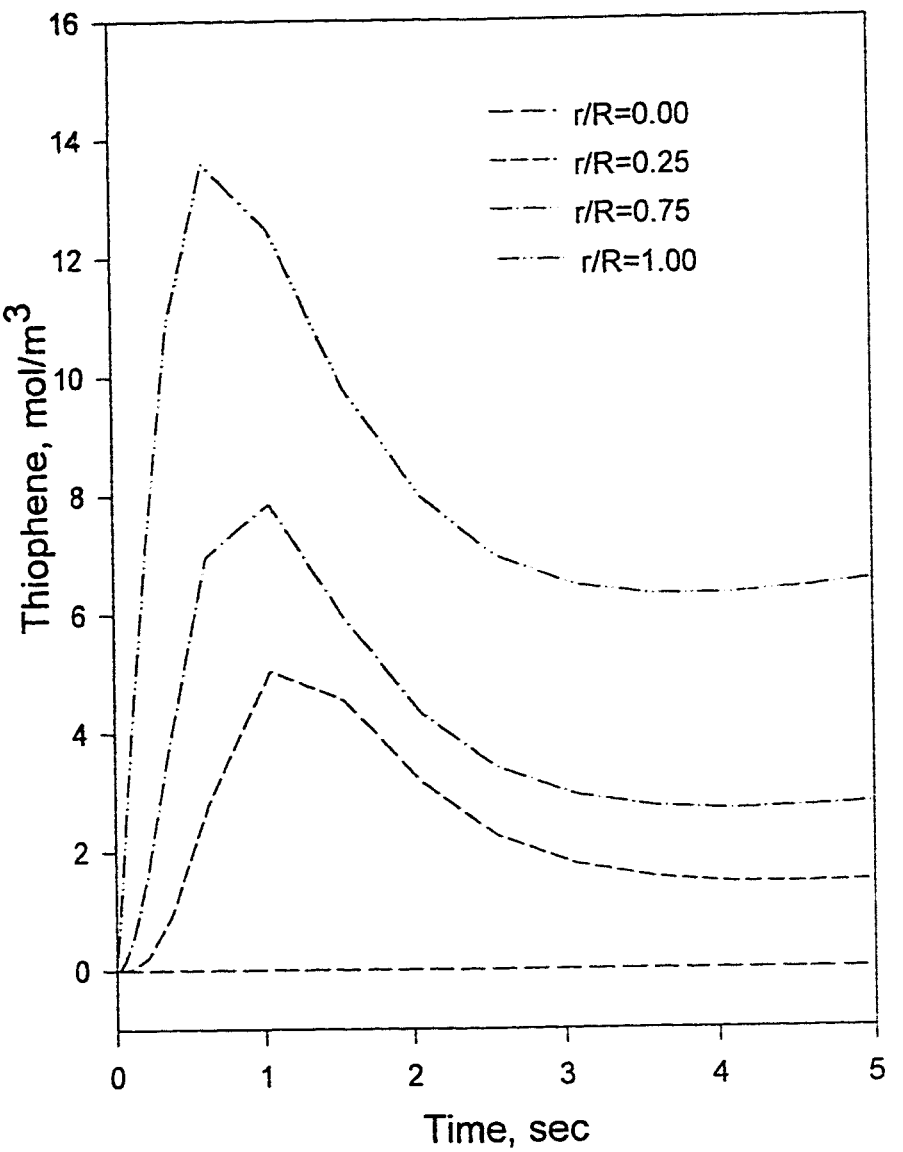

Figure 6.11 Transient thophene concnetration in pellet at reactor position (1,2). P_b = 5,066.25 kPa, T_b = 700 K and T_{in} = 600 K.

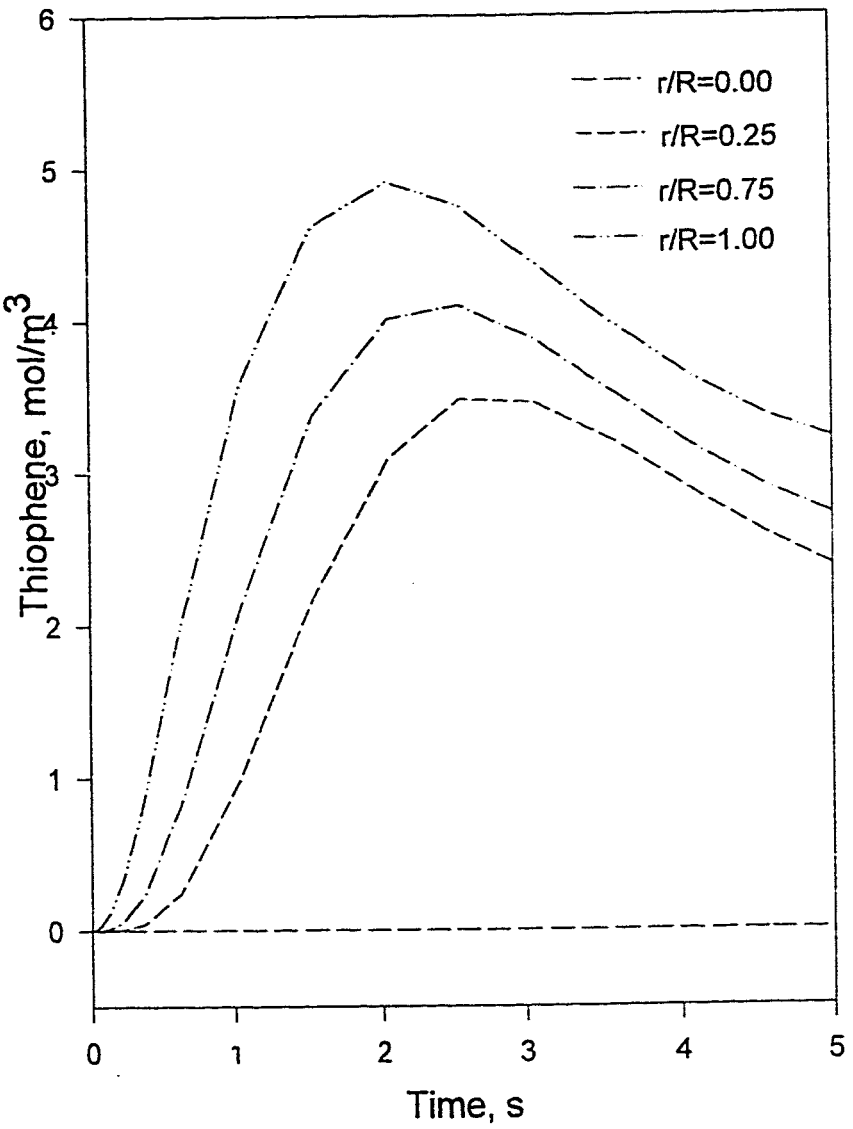

Figure 6.12 Transient thophene concnetration in pellet at reactor position (2,2). P_b = 5,066.25 kPa, T_b = 700 K and T_{in} = 600 K.

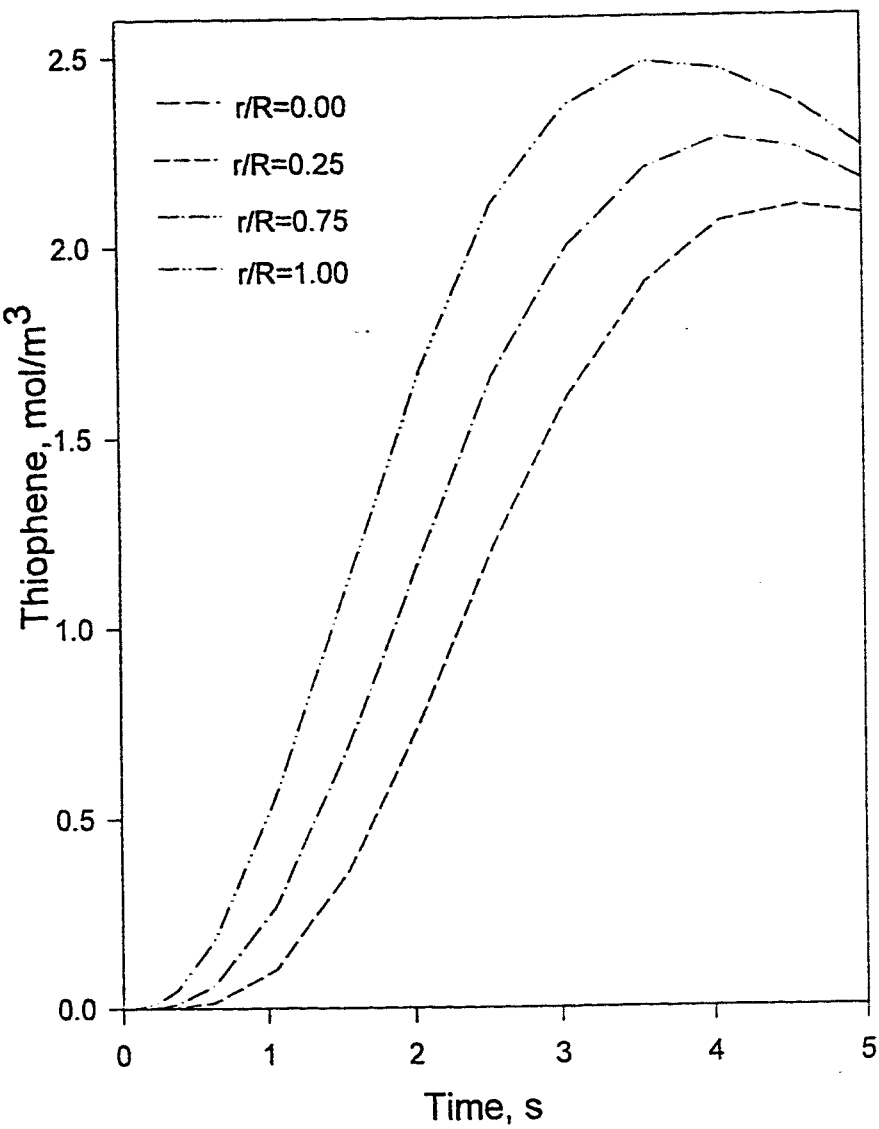

Figure 6.13 Transient thophene concnetration in pellet at reactor position (3,2). P_b = 5,066.25 kPa, T_b = 700 K and T_{in} = 600 K.

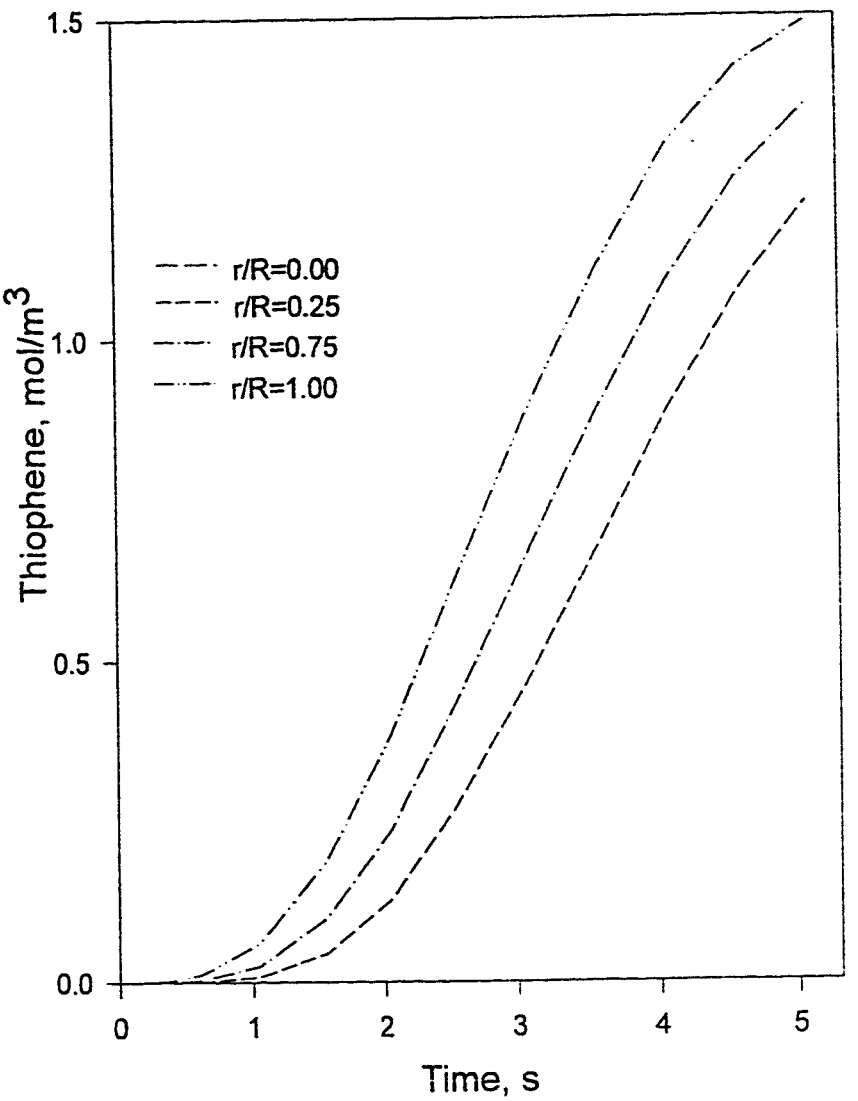

Figure 6.14 Transient thophene concnetration in pellet at reactor position (4,2). $P_b = 5{,}066.25$ kPa, $T_b = 700$ K and $T_{in} = 600$ K.

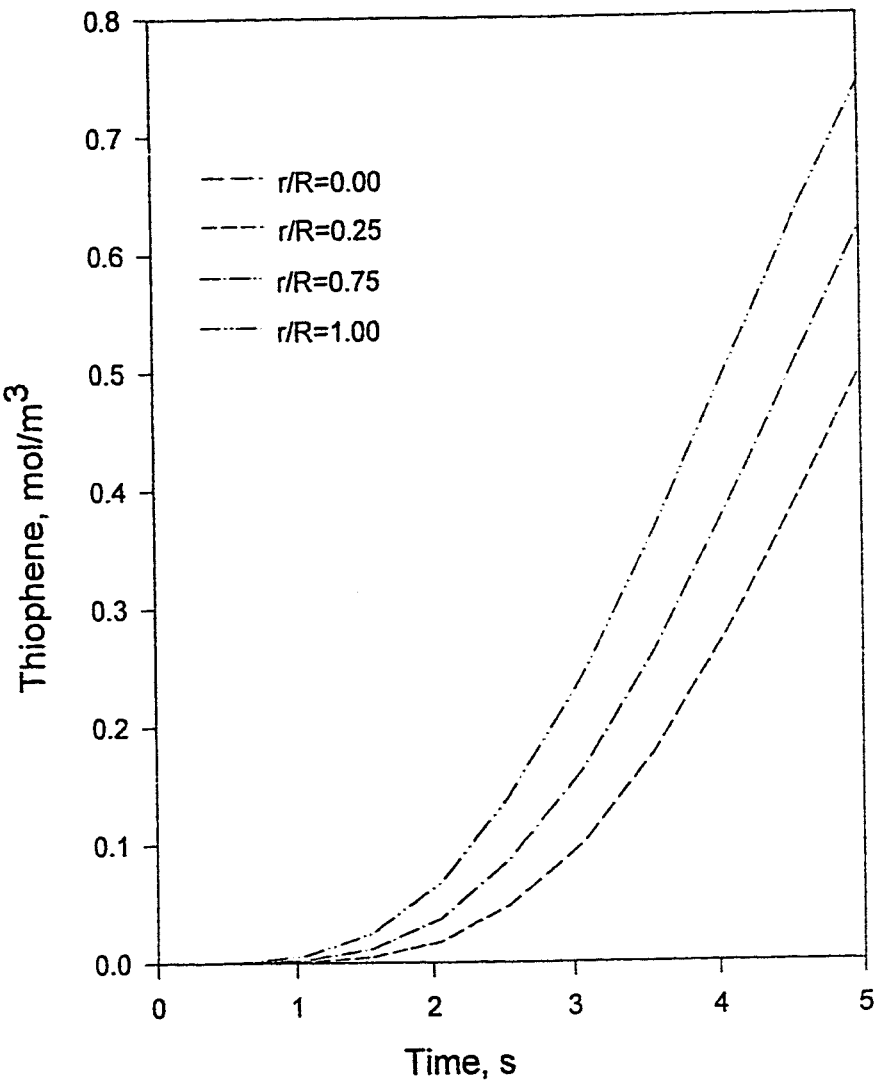

Figure 6.15 Transient thophene concnetration in pellet at reactor position (5,2). $P_b = 5{,}066.25$ kPa, $T_b = 700$ K and $T_{in} = 600$ K.

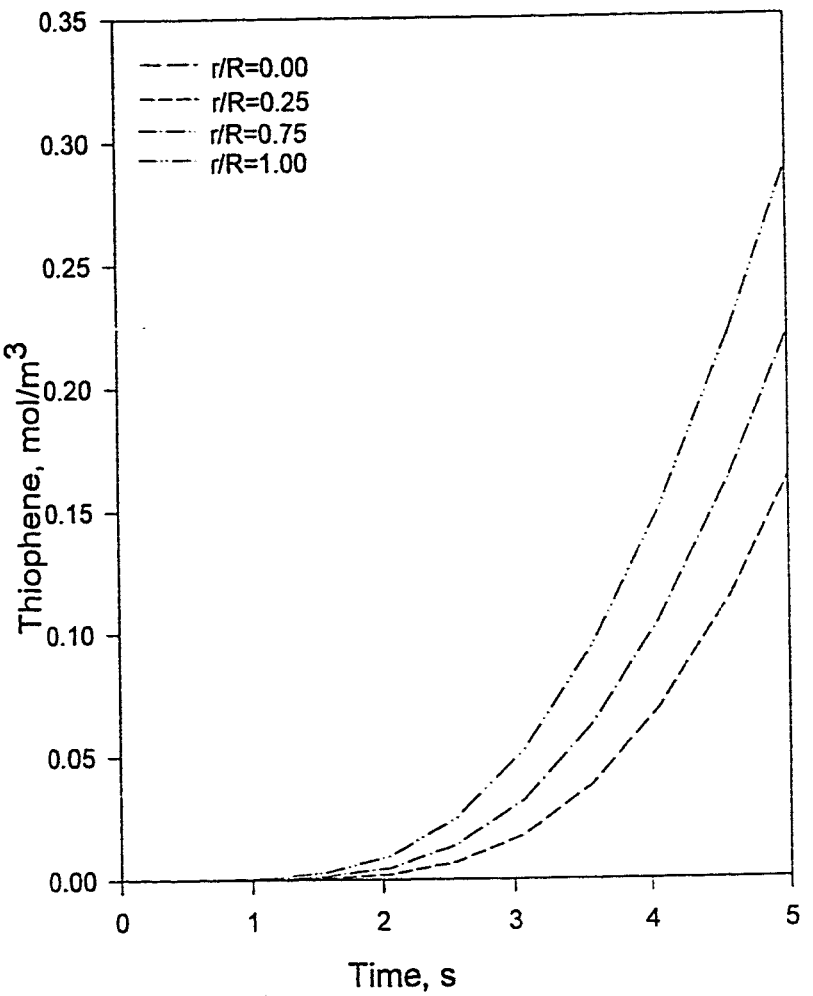

Figure 6.16 Transient thophene concnetration in pellet at reactor position (6,2). P_b = 5,066.25 kPa, T_b = 700 K and T_{in} = 600 K.

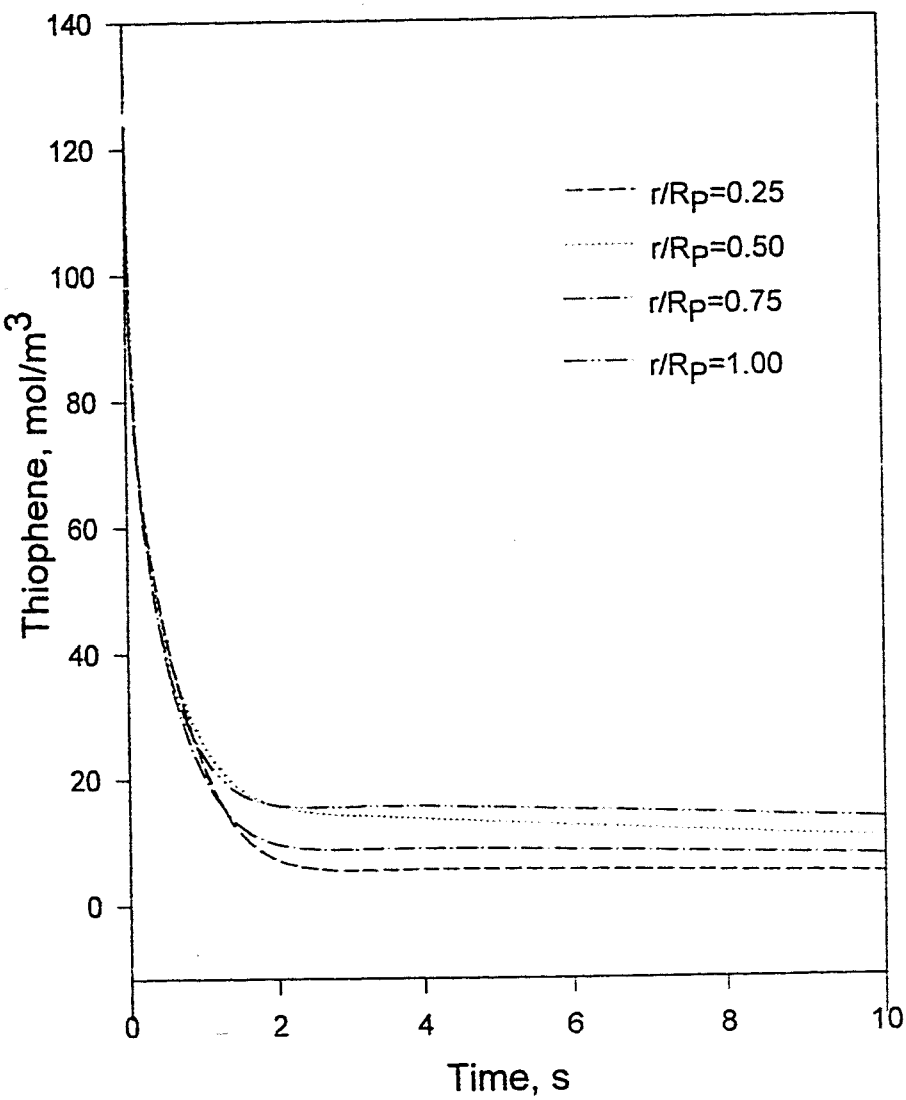

Figure 6.17. Transient thiophene concentration in a pellet at position (1,2).
P_b=5,066.25 kPa, T_b=700 K, T_{in}=600 K, T_w=900 K, T_f=700 K.

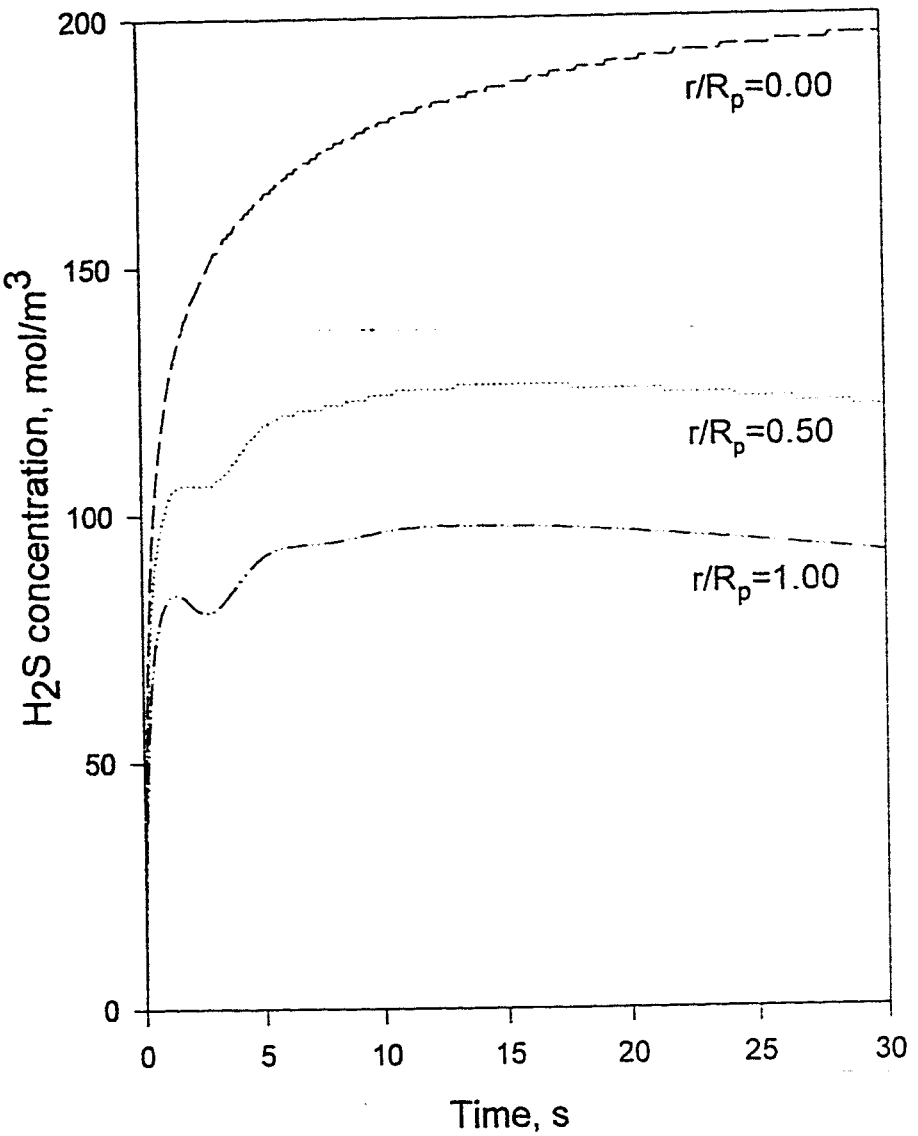

Figure 6.18 Transient H_2S concentration in a pellet at different pellet radial positions and bed position (1,2). $T_b = 600$ K, $T_f = 600$ K, $T_{in} = 600$ K and $T_w = 700$ K.

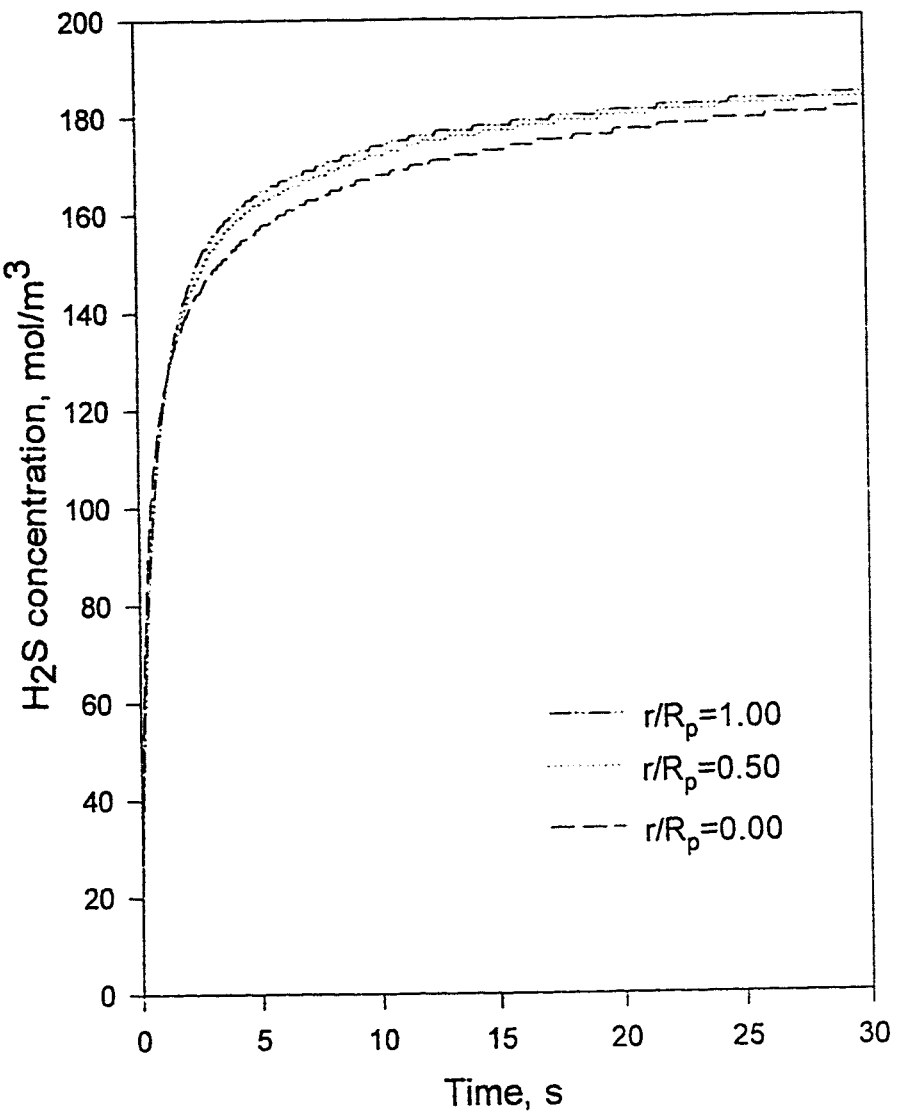

Figure 6.19 Transient H_2S concentration in a pellet at different pellet radial positions and bed position (6,2). T_b = 600 K, T_f = 600 K, T_{in} = 600 K and T_w = 700 K.

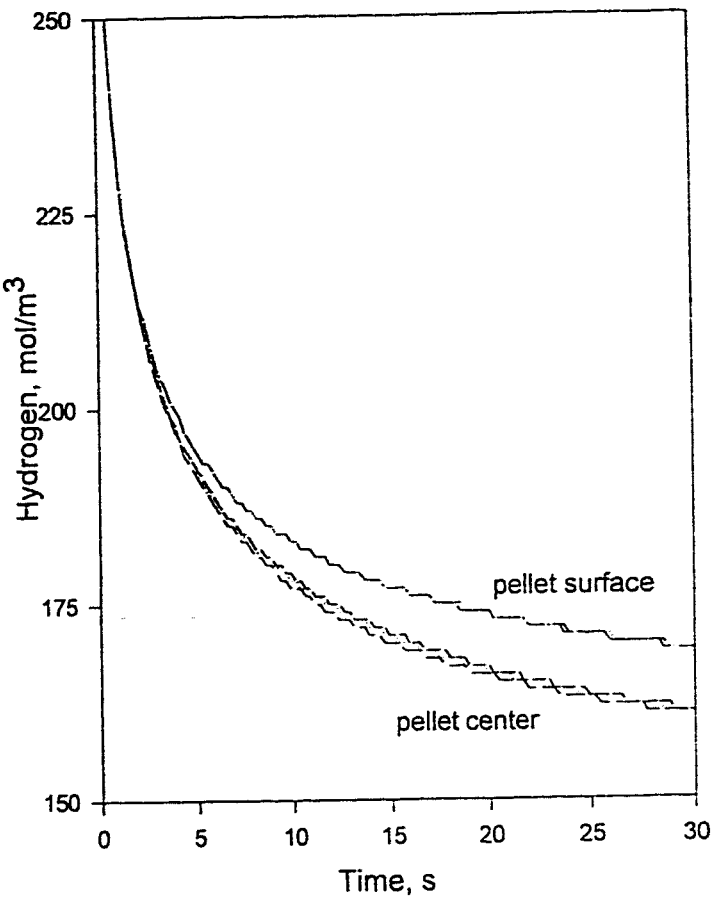

Figure 6.20. Hydrogen concentrations in a pellet at different radial positions and bed position (2,2). $P_b = 5{,}066.25$ kPa, $T_b = 800$ K, $T_f = 800$ K, $T_{in} = 600$ K, $T_w = 900$ K.

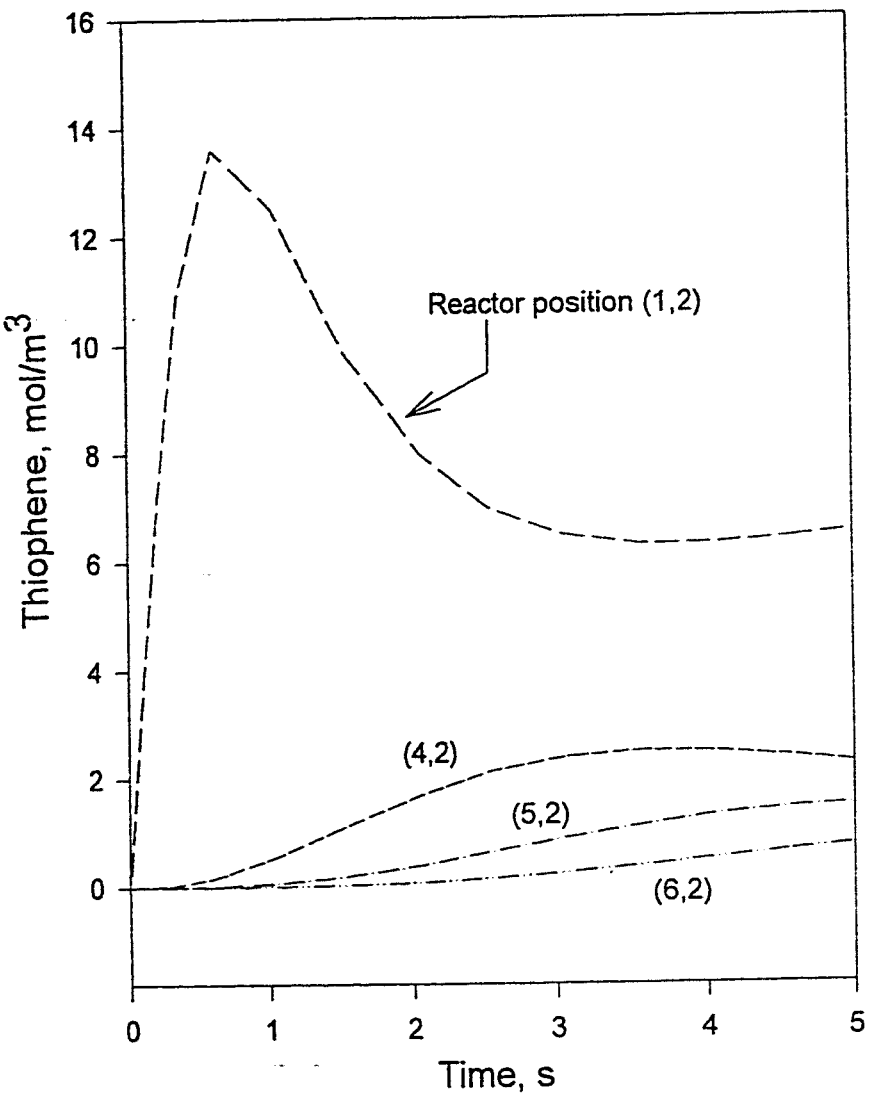

Figure 6.21. Thiophene concentration in pellets. T_w= 700
P_b = 5,066.25 kPa, T_b = 700 K, T_{in} = 600 K.
Parameter (1,2) indicates position (i,j) in the bed.

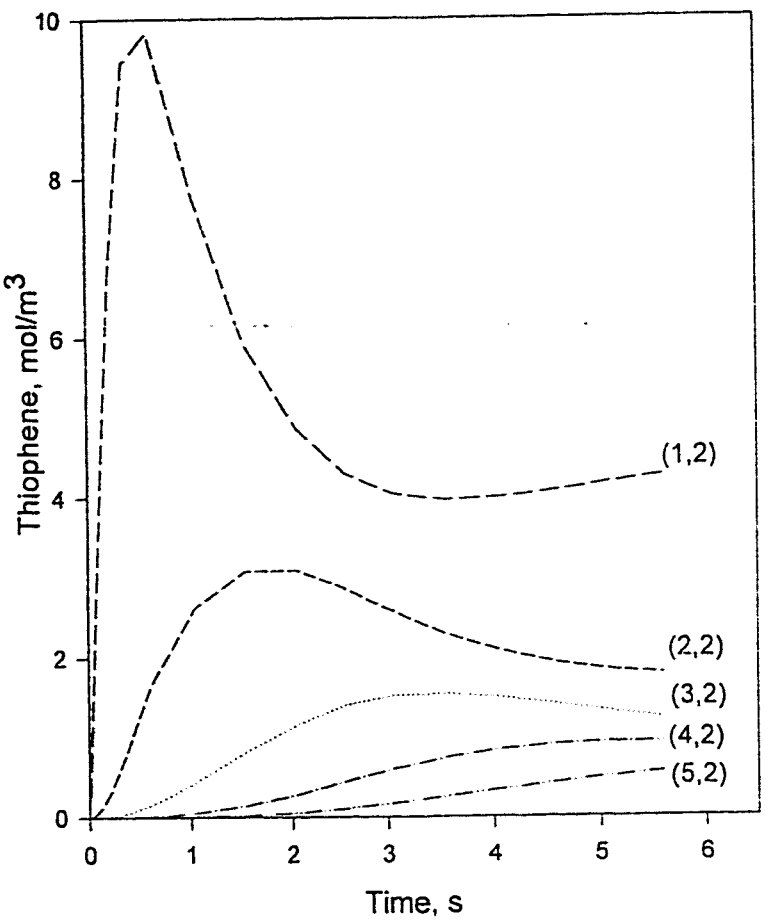

Figure 6.22. Transient thiophene concentration in pellets. P_b = 5,066.25 kPa, T_b = 800 K, T_f = 800 K, T_{in} = 600 K, T_w = 900. Parameter (1,2) indicates position (i,j) in the bed.

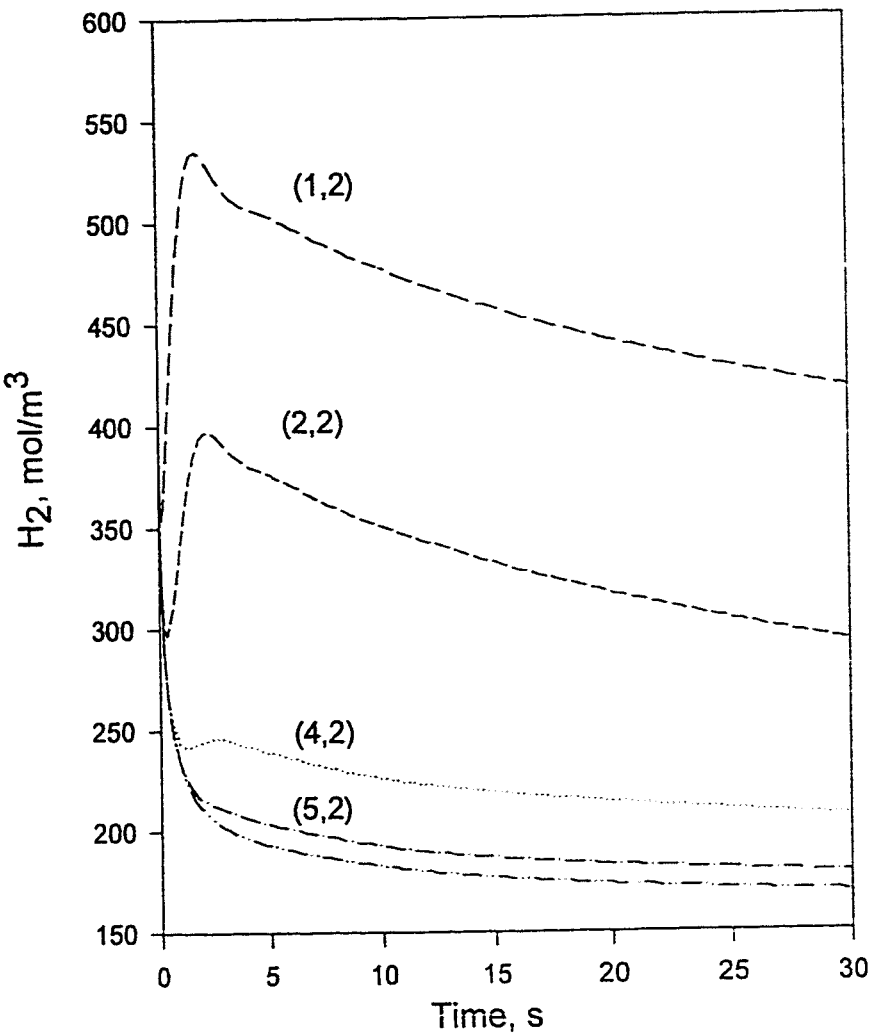

Figure 6.23. Hydrogen concentrations in pellets at $r/R_p = 1.0$ and different bed locations. $P_b = 5{,}066.25$ kPa, $T_b = 800$ K, $T_f = 800$ K, $T_{in} = 600$ K, $T_w = 900$ K.

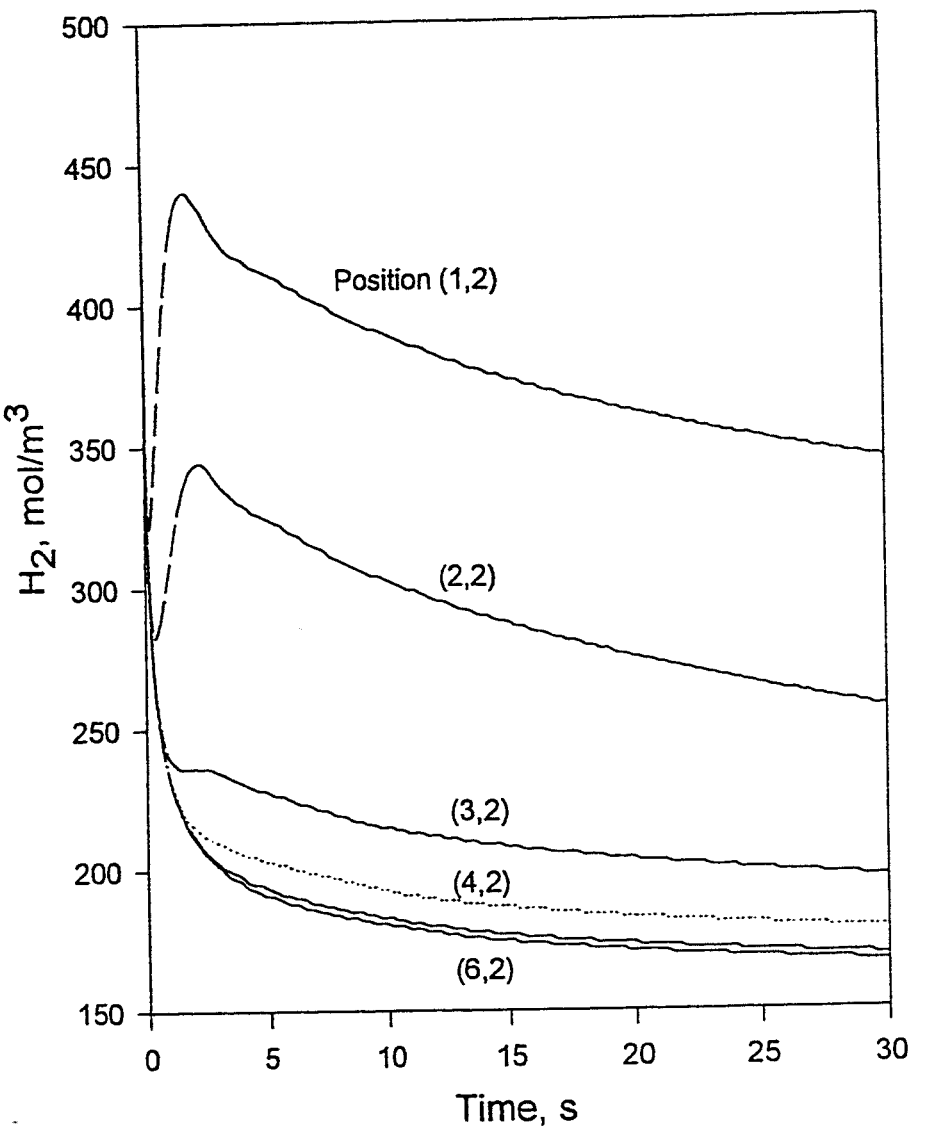

Figure 6.24. Hydrogen concentrations in pellets at $r/R_p = 0.5$ and different bed locations. $P_b = 5{,}066.25$ kPa, $T_b = 800$ K, $T_f = 800$ K, $T_{in} = 600$ K, $T_w = 900$ K.

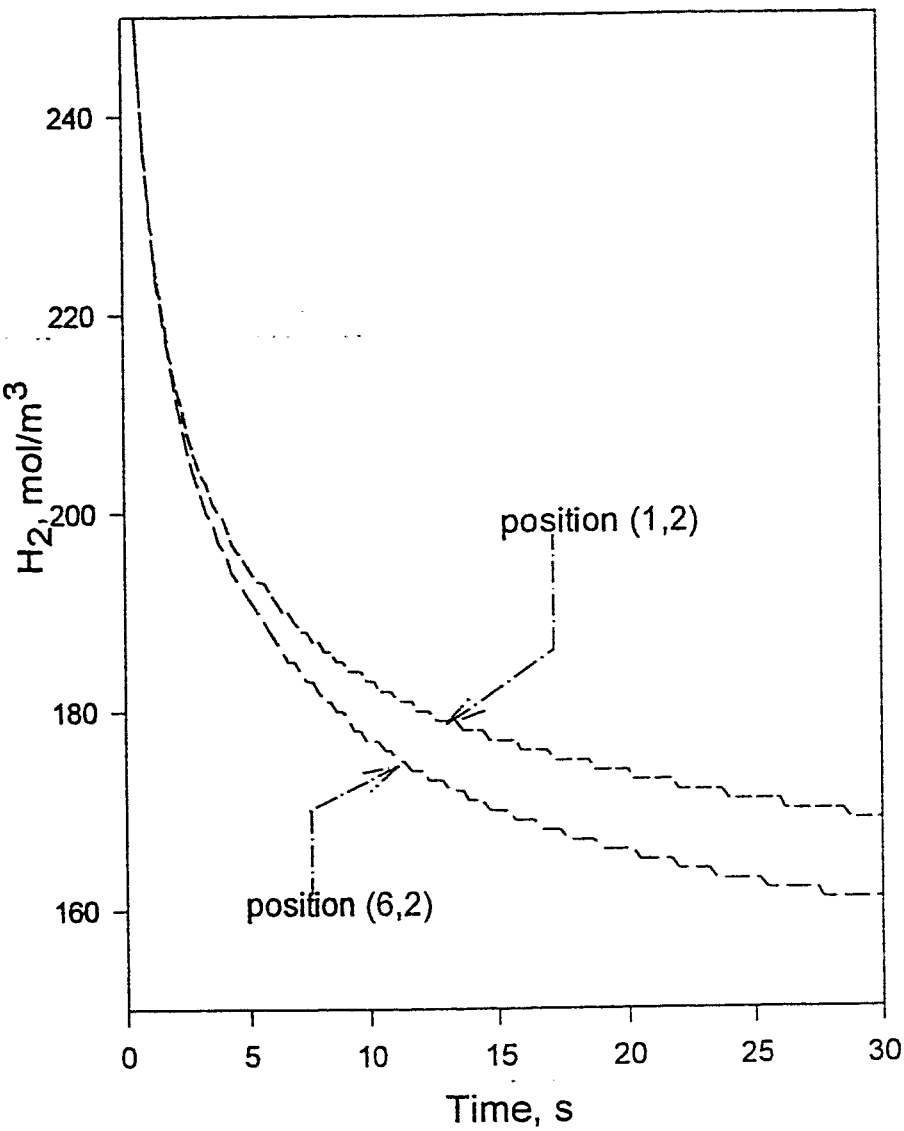

Figure 6.25. Hydrogen concentrations at pellet centers at bed positions (1,2) and (6,2). P_b = 5,066.25 kPa, T_b = 800 K, T_f = 800 K, T_{in} = 600 K, T_w = 900 K.

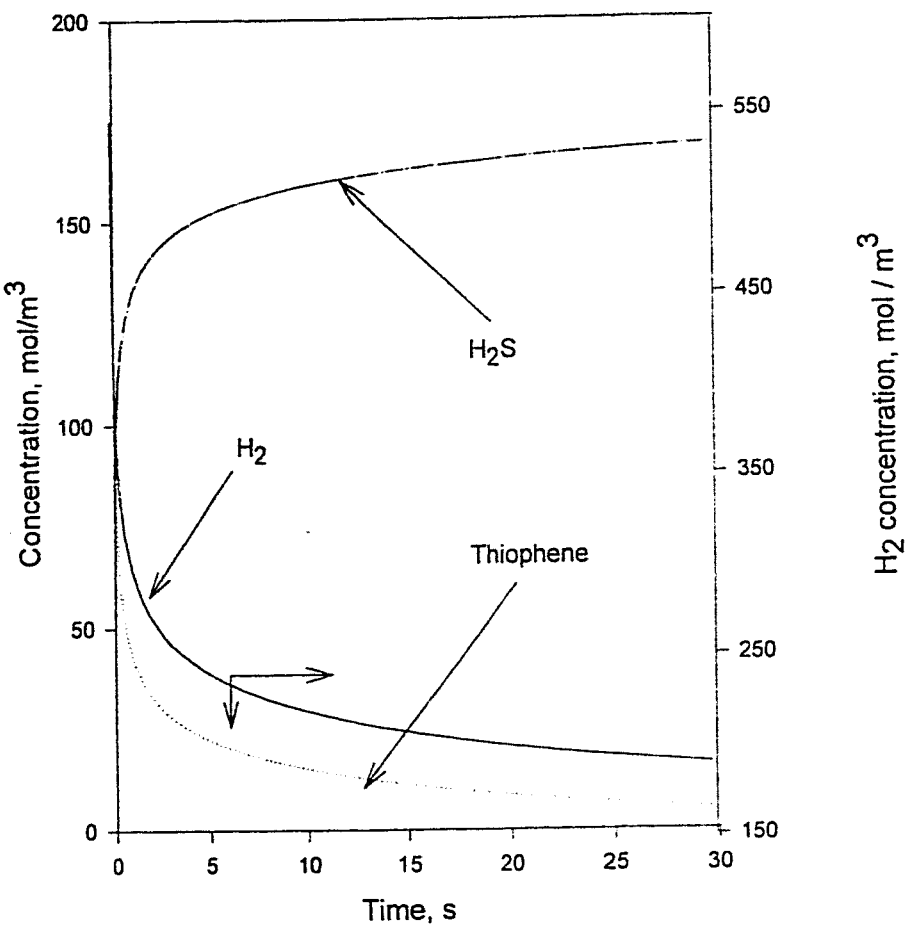

Figure 6.26. Transient thiophene concentration in a pellet at position (1,2). P_b=5,066.25 kPa, T_b=700 K, T_{in} = 600 K, T_w=900 K, and T_f=700 K r/R_p=0.00.

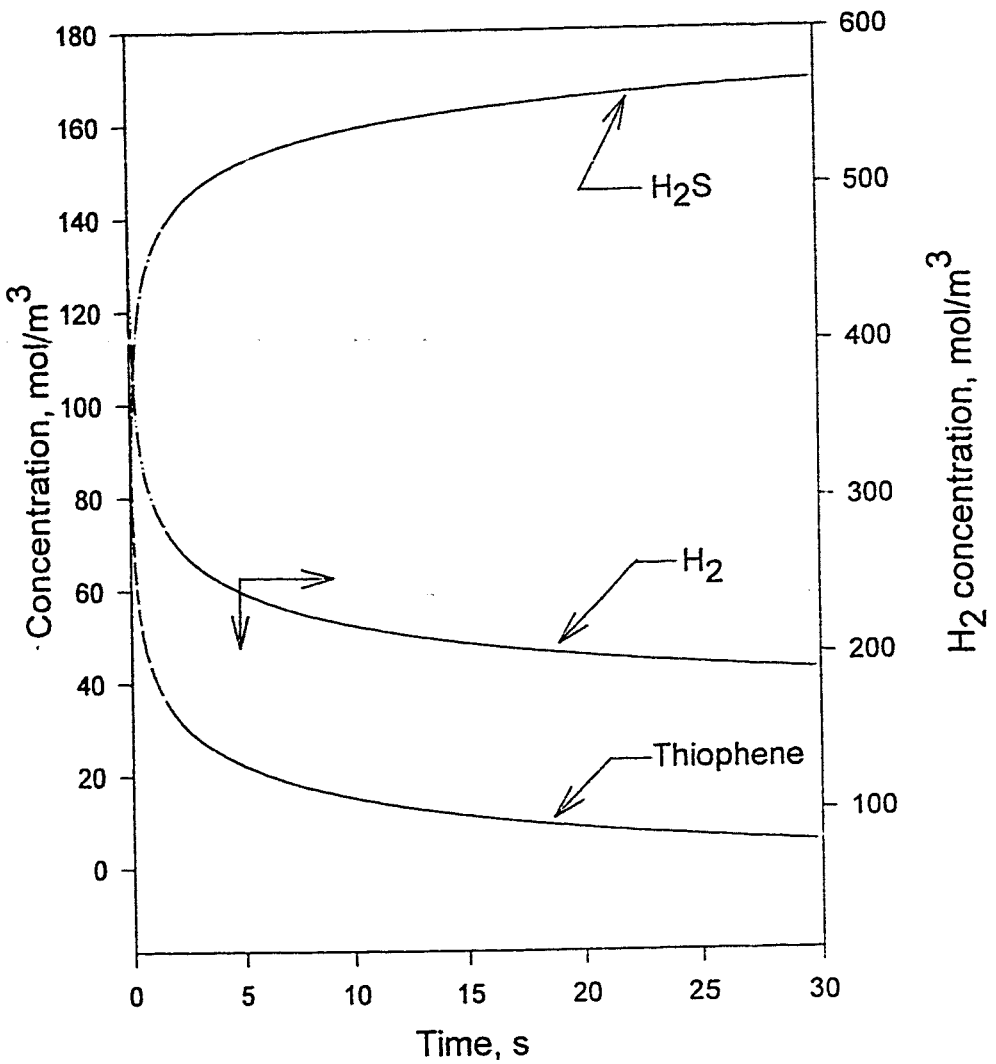

Figure 6.27. Transient pellet concentration at position (1,2).
P_b = 5,066.25 kPa, T_b = 600 K, T_f = 600 K T_{in} = 600 K,
T_w = 700 K.

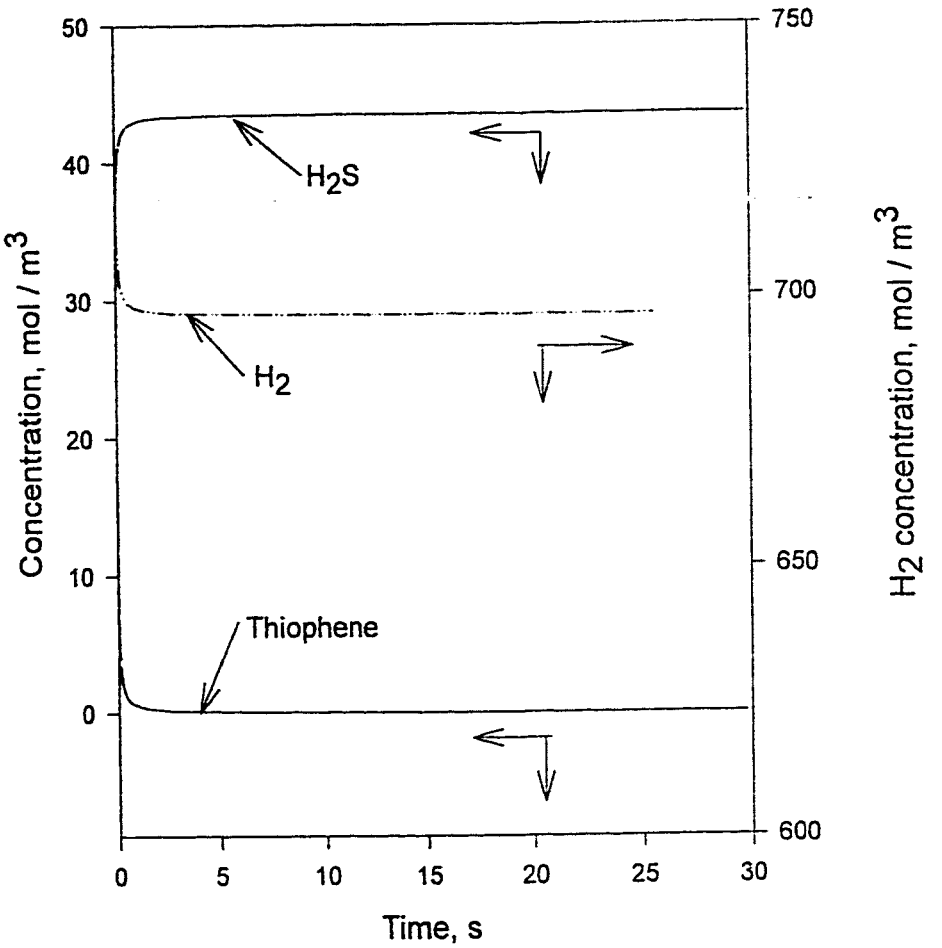

Figure 6.28. Concentrations in a pellet center at (2,2).
$P_b = 5{,}066.25$ kPa, $T_b = 800$ K, $T_f = 800$ K, $T_w = 900$ K.
Initial mole fraction of thiophene = 0.05.

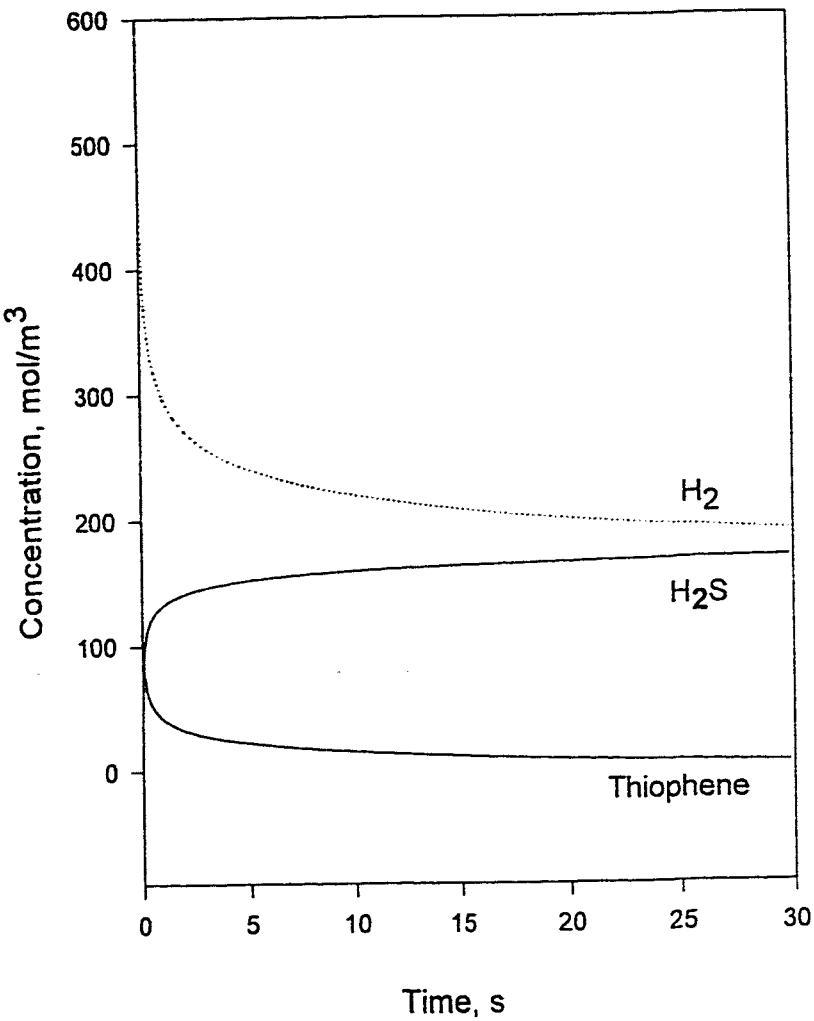

Figure 6.29. Transient concentrations at pellet center at (3,2).
P_b = 5,066.25 kPa, T_b = 700 K, T_f = 700 K, T_w = 900 K.

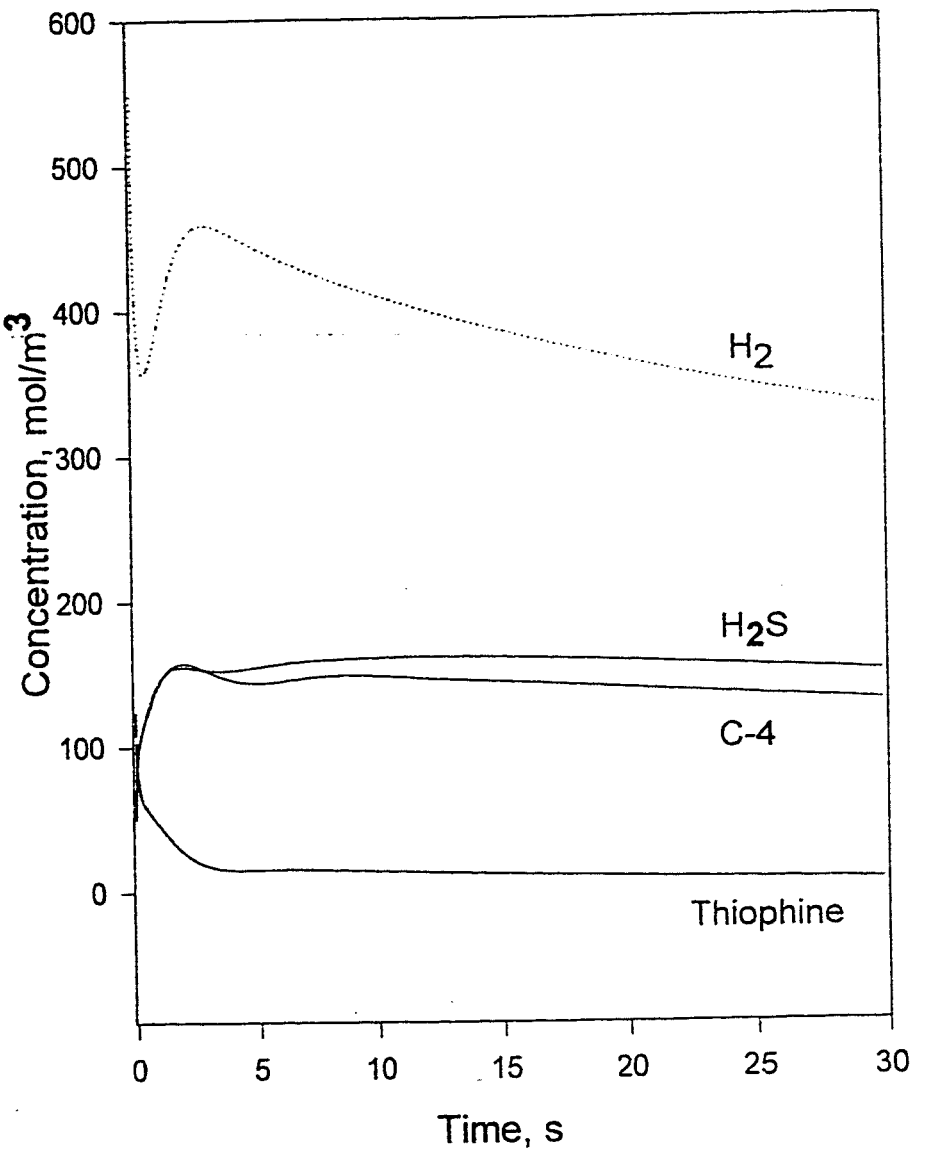

Figure 6.30. Transient concentrations in pellet at $r/R_p = 0.75$ and (3,2). $P_b = 5{,}066.25$ kPa, $T_b = 700$ K, $T_f = 700$ K, $T_w = 900$ K.

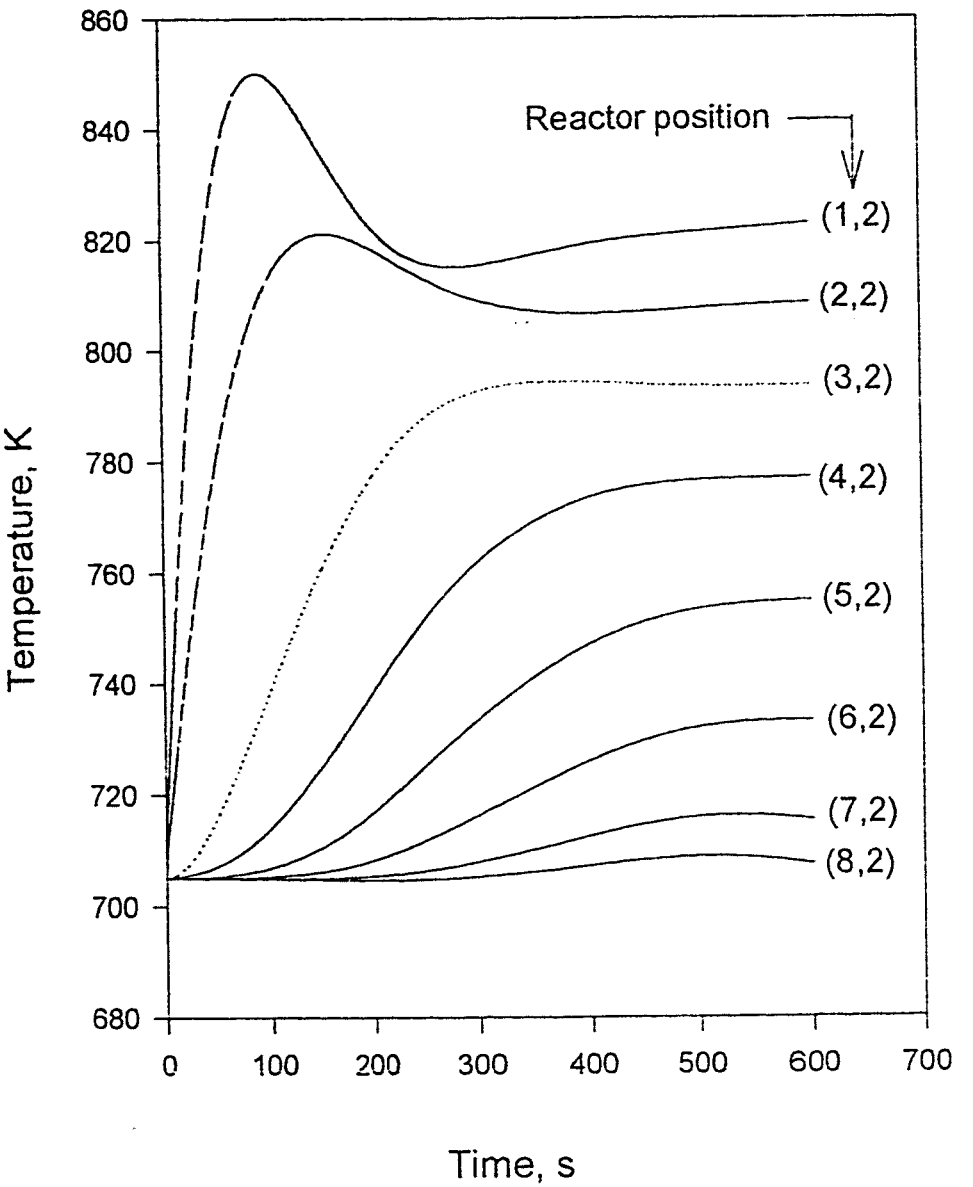

Figure 6.31. Temperature profiles at different positions in the reactor bed. $P_b = 5{,}066.25$ kPa, $T_b = 700$K , $T_f = 700$ K $T_{in} = 700$ K, $T_w = 700$ K.

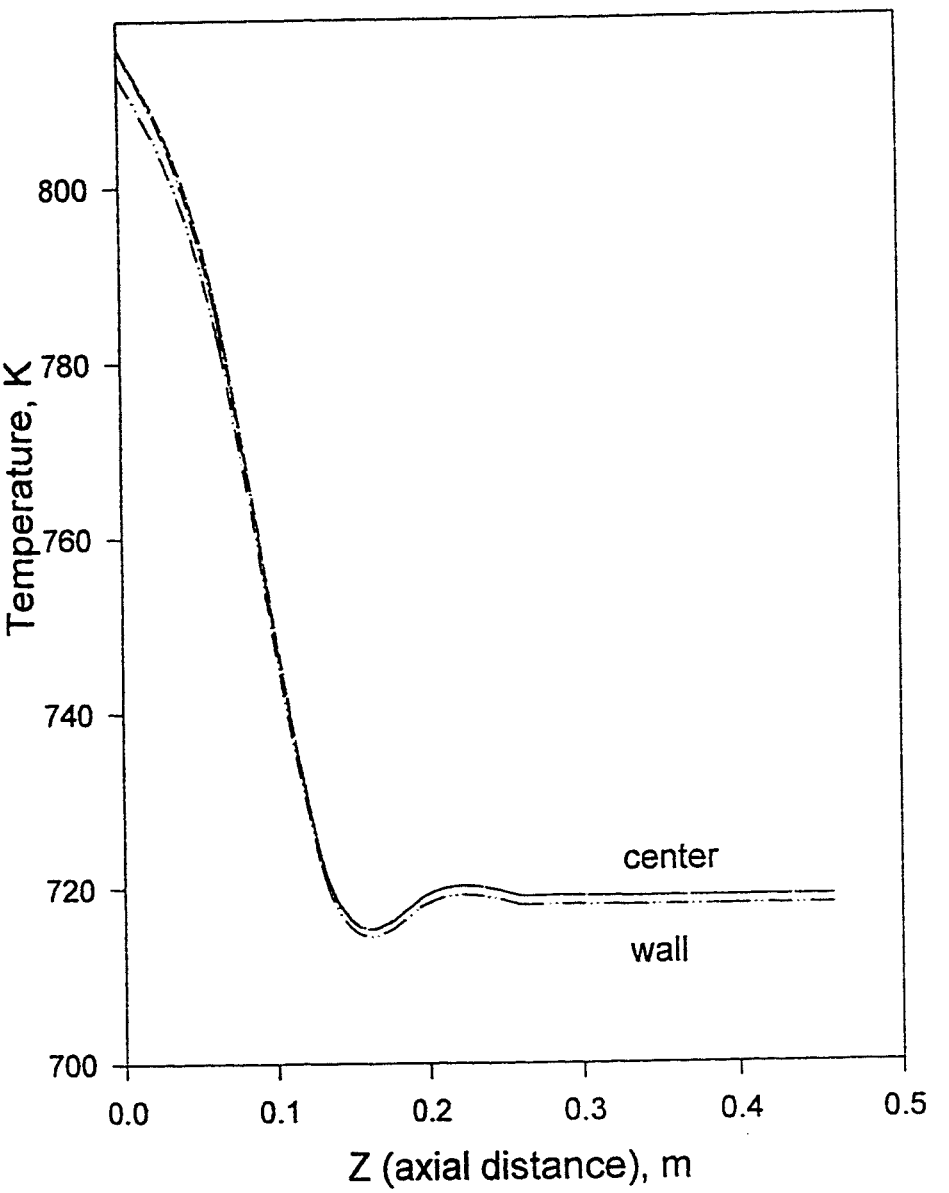

Figure 6.32. Temperature profile in the reactor. Time = 10 s, y_A=0.2, P_b=5,066.25 kPa, T_{in}=600 K, T_b=700 K, T_f=700 K, T_w=700 K.

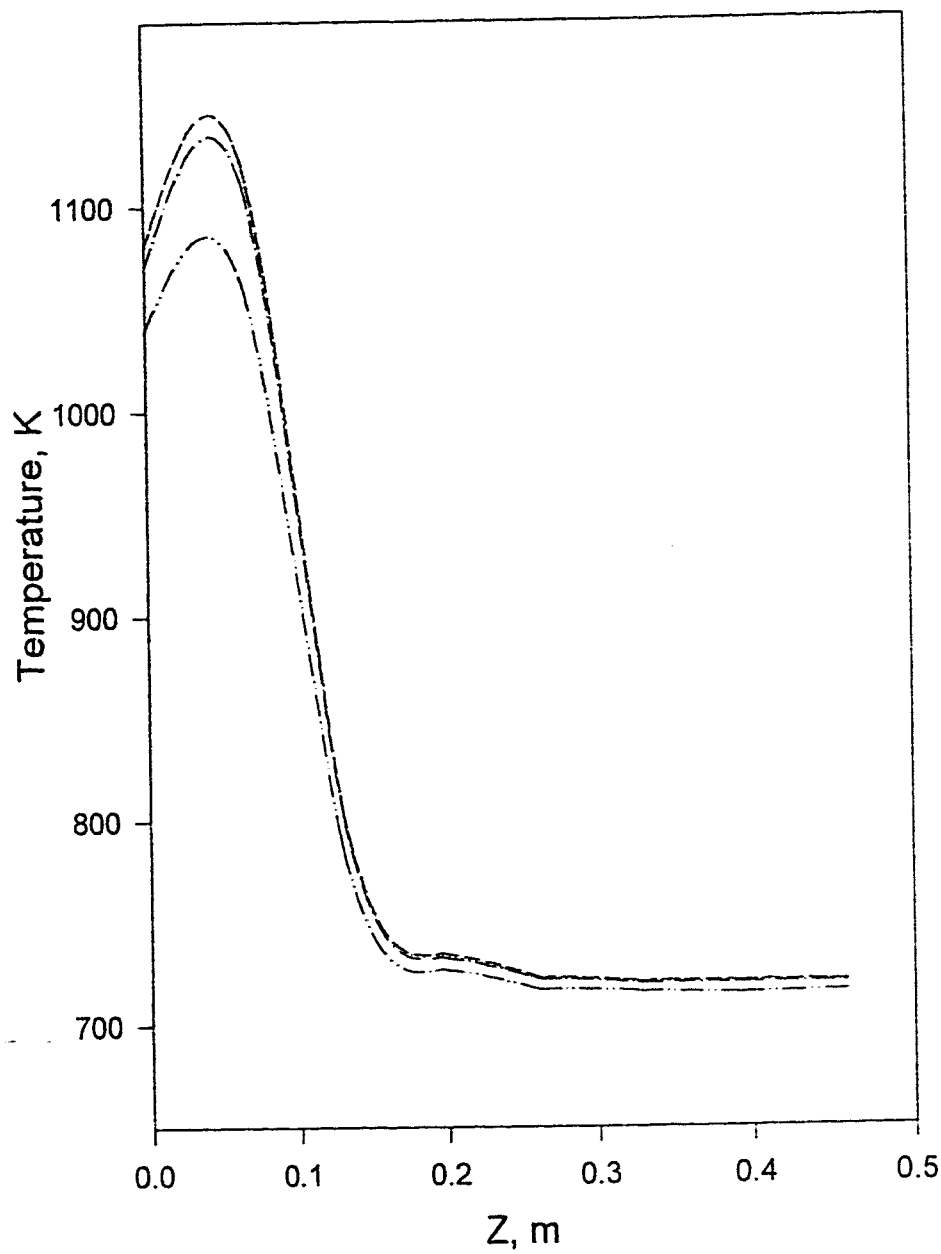

Figure 6.33. Temperature profile in the reactor. Time = 60 s, y_A=0.2
P_b=5,066.25 kPa, T_{in}=600 K, T_b=700 K, T_f=700 K, T_w=700 K.

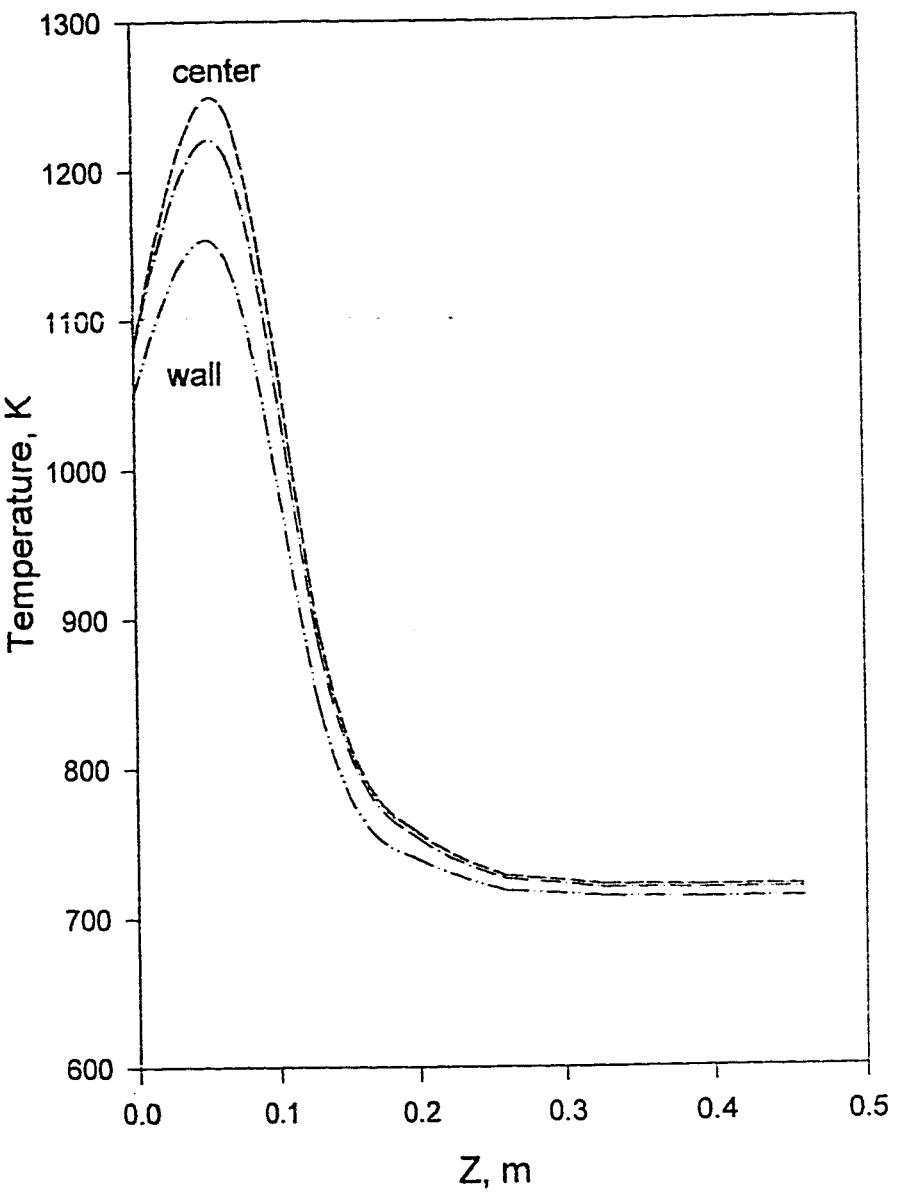

Figure 6.34. Temperature profile in the reactor. Time = 90 s, y_A=0.2
P_b=5,066.25 kPa, T_{in}=600 K, T_b=700 K, T_f=700 K, T_w=700 K.

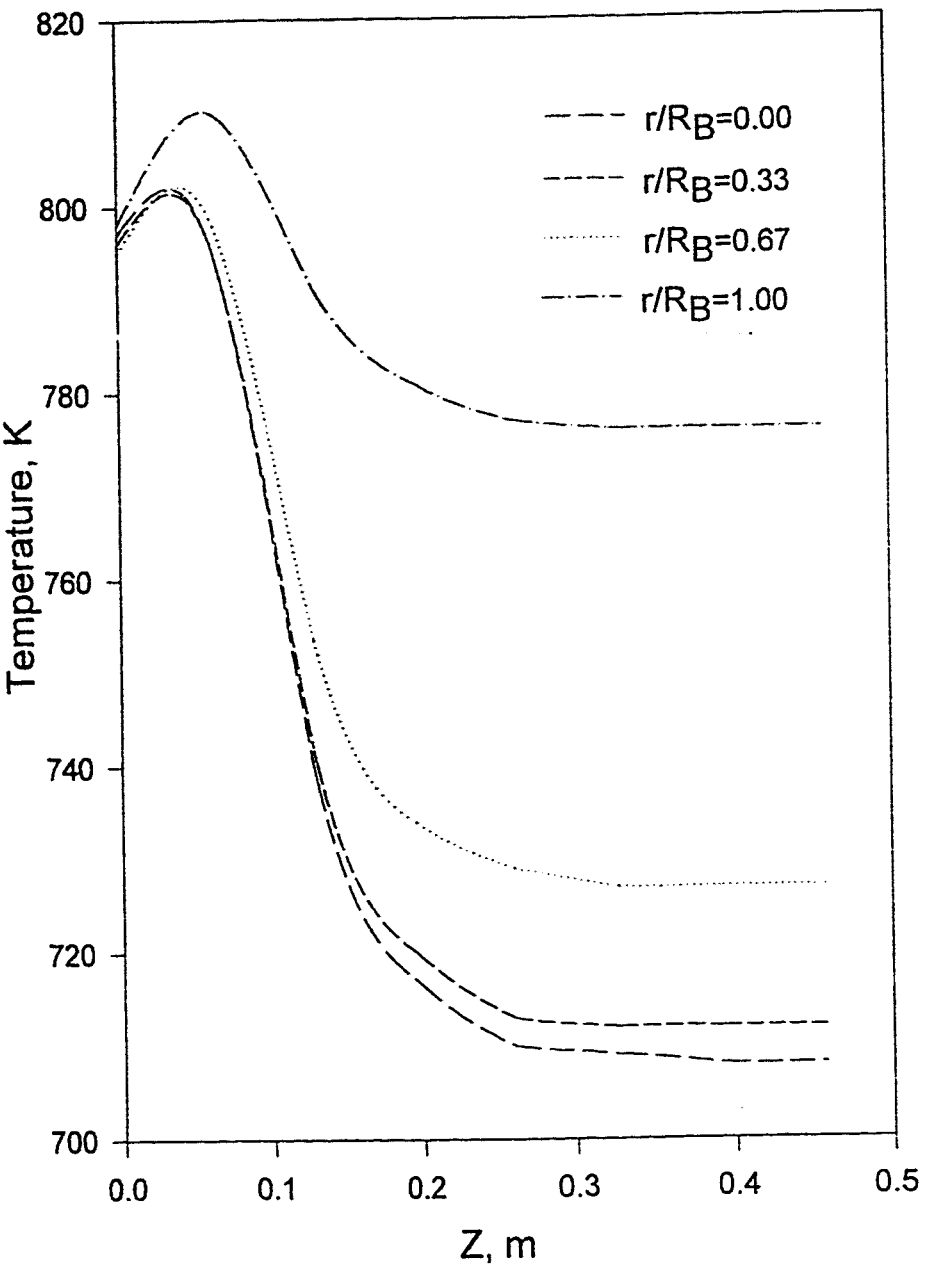

Figure 6.35. Temperature profile in the reactor. Time = 30 s,
P_b=5,066.25 kPa, T_{in}=600 K, T_b=700 K, T_f=700 K, T_w=900 K.

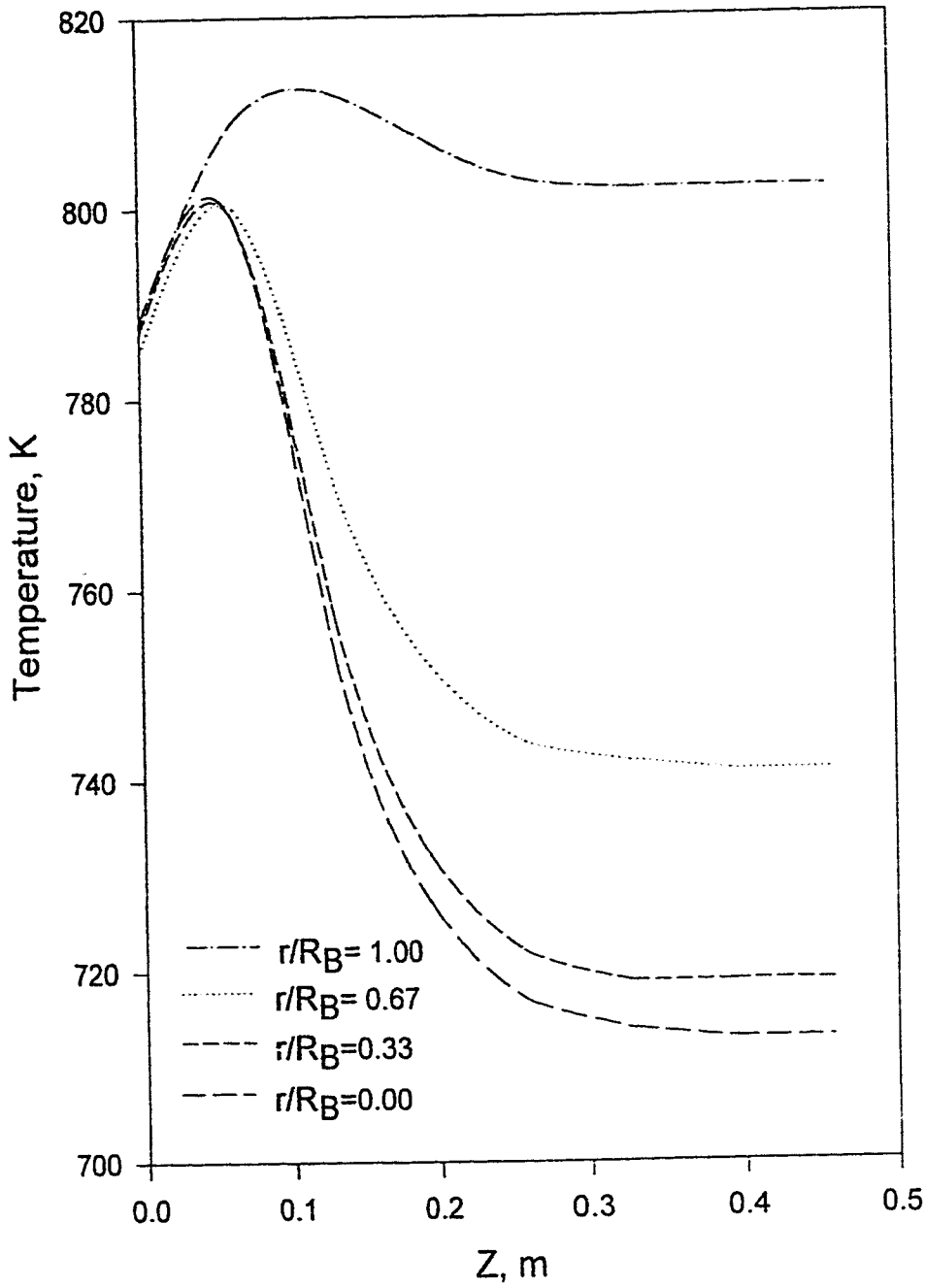

Figure 6.36. Temperature profile in the reactor. Time = 120 s,
P_b=5,066.25 kPa, T_{in}=600 K, T_b=700 K, T_f=700 K, T_w=900 K.

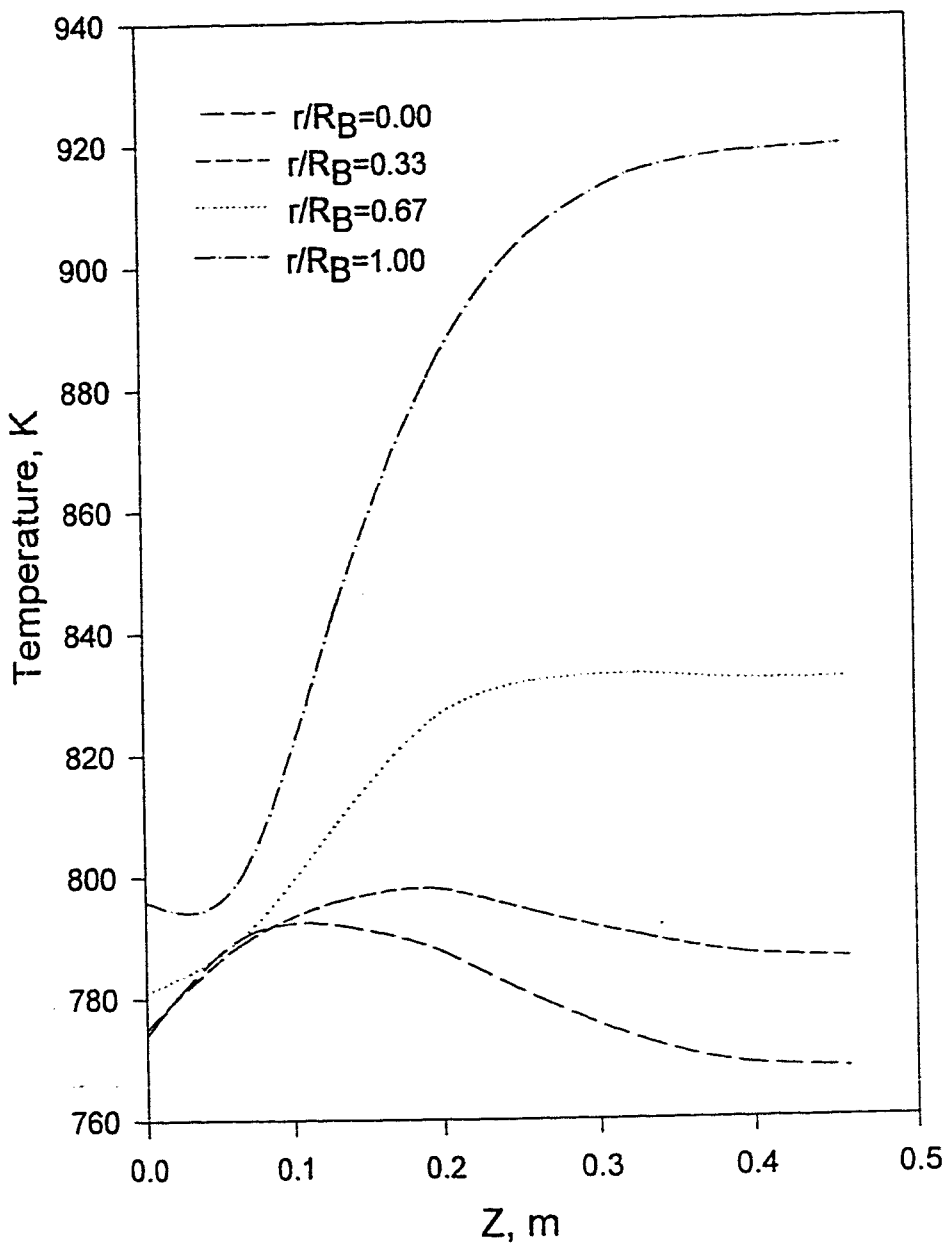

Figure 6.37. Temperature profile in the reactor. Time = 250 s,
P_b=5,066.25 kPa, T_{in}=600 K, T_b=700 K, T_f=700 K, T_w=900 K.

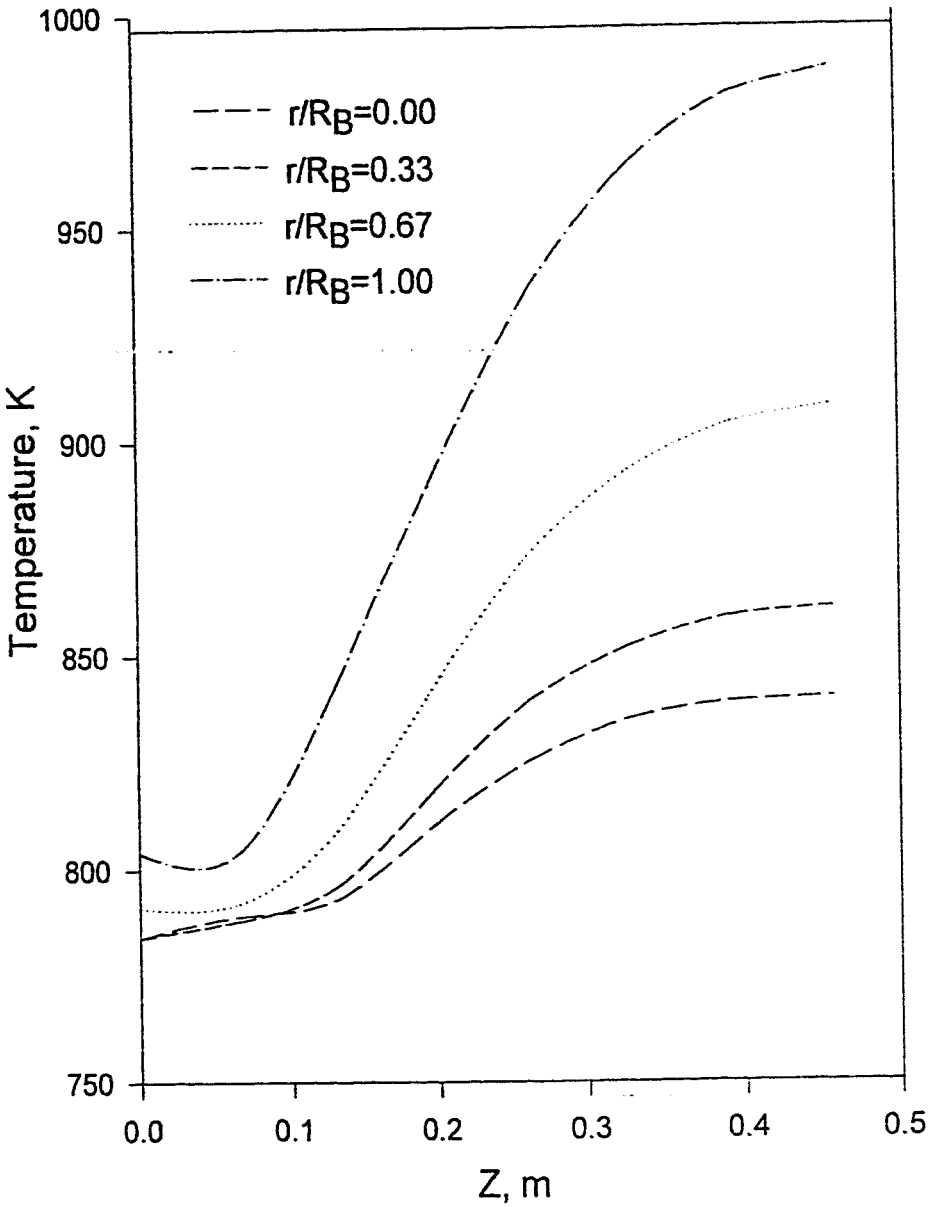

Figure 6.38. Temperature profile in the reactor. Time = 350 s,
P_b=5,066.25 kPa, T_{in}=600 K, T_b=700 K, T_f=700 K, T_w=900 K.

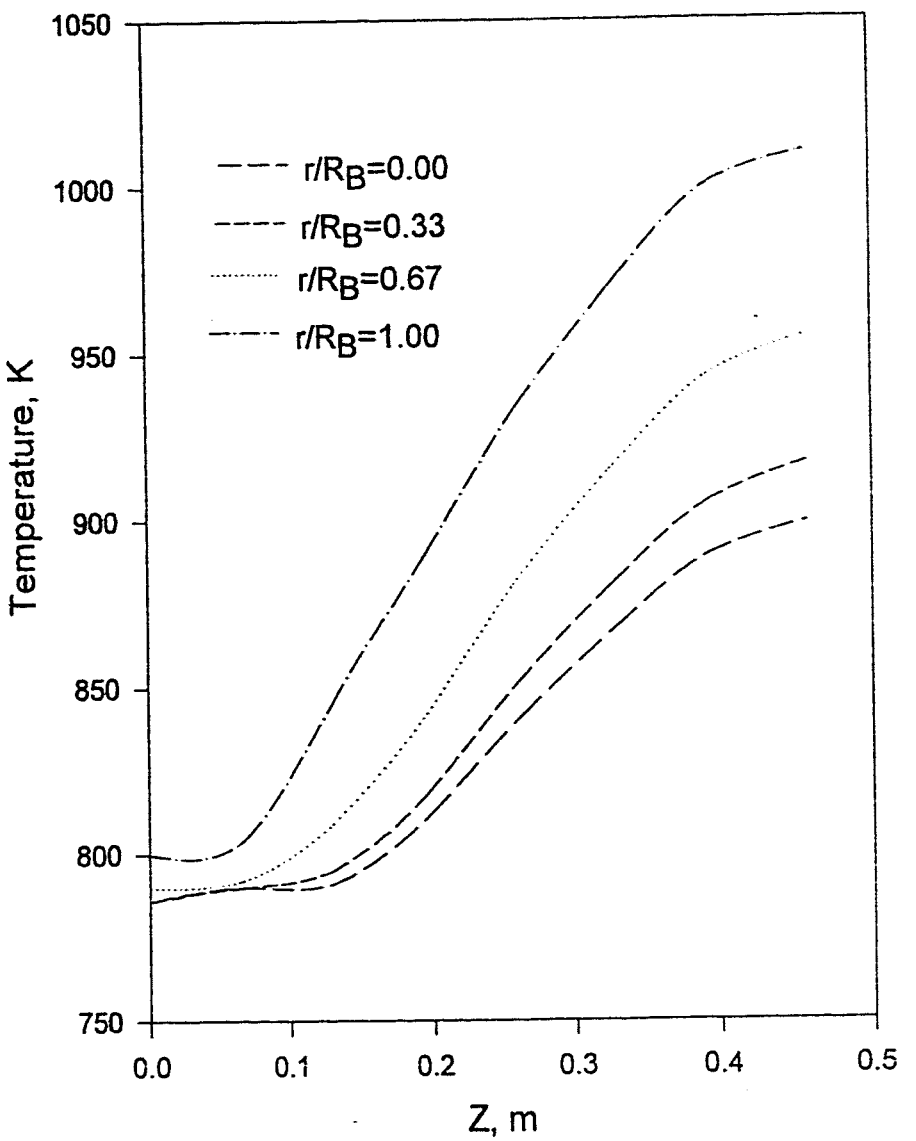

Figure 6.39. Temperature profile in the reactor. Time = 500 s,
P_b=5,066.25 kPa, T_{in}=600 K, T_b=700 K, T_f=700 K, T_w=900 K.

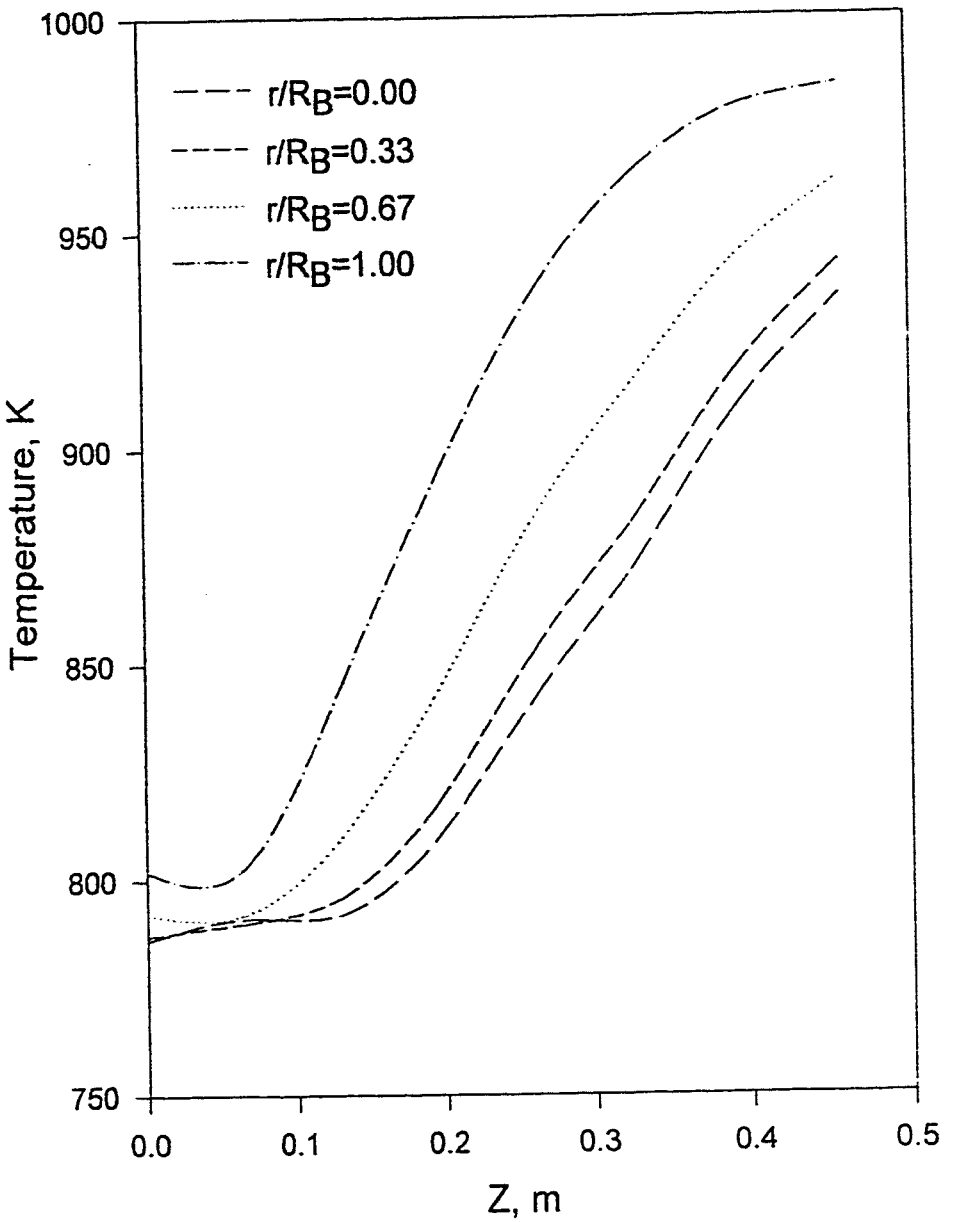

Figure 6.40. Temperature profile in the reactor. Time = 700 s,
P_b=5,066.25 kPa, T_{in}=600 K, T_b=700 K, T_f=700 K, T_w=900 K.

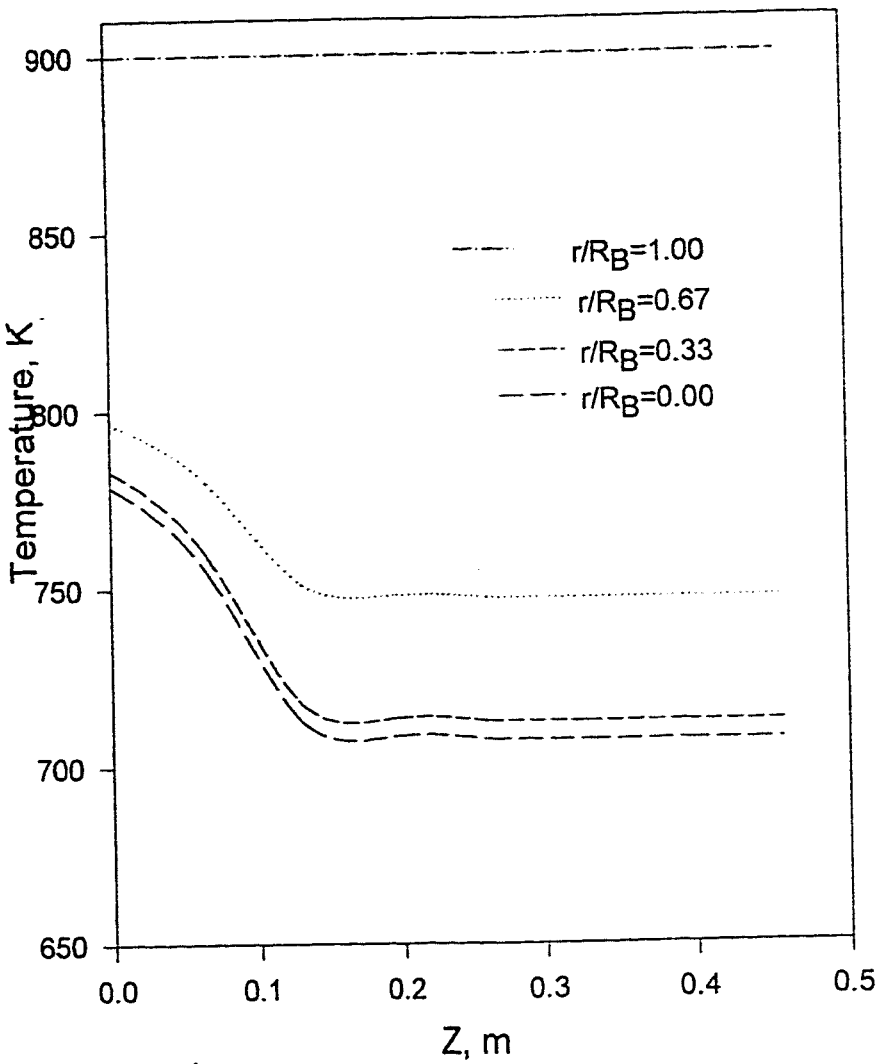

Figure 6.41. Temperature profile in the reactor. Time = 30 s,
P_b=5,066.25 kPa, T_{in}=600 K, T_b=700 K, T_f=700 K, T_w=700 K.

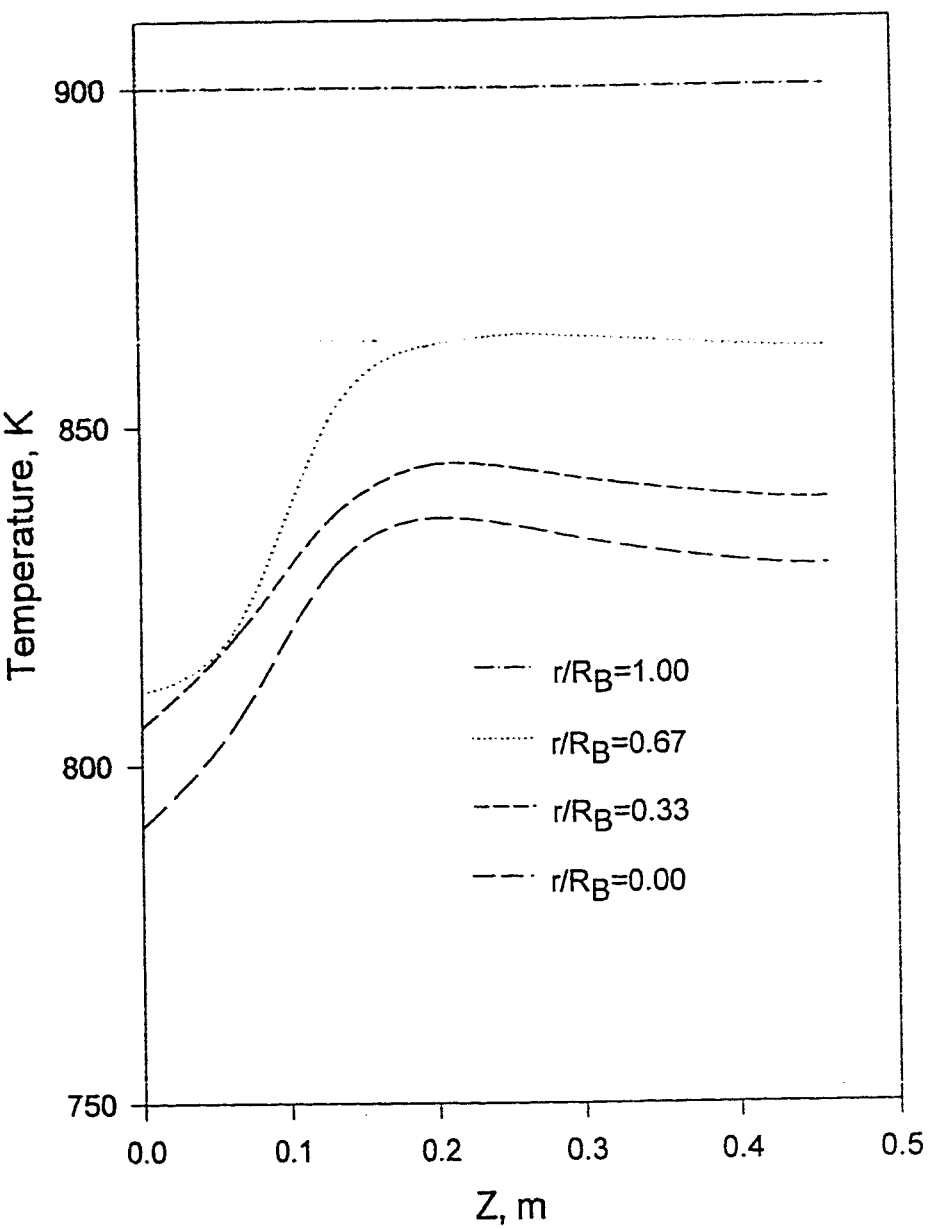

Figure 6.42. Temperature profile in the reactor. Time = 300 s,
P_b=5,066.25 kPa, T_{in}=600 K, T_b=700 K, T_f=700 K, T_w=700 K.

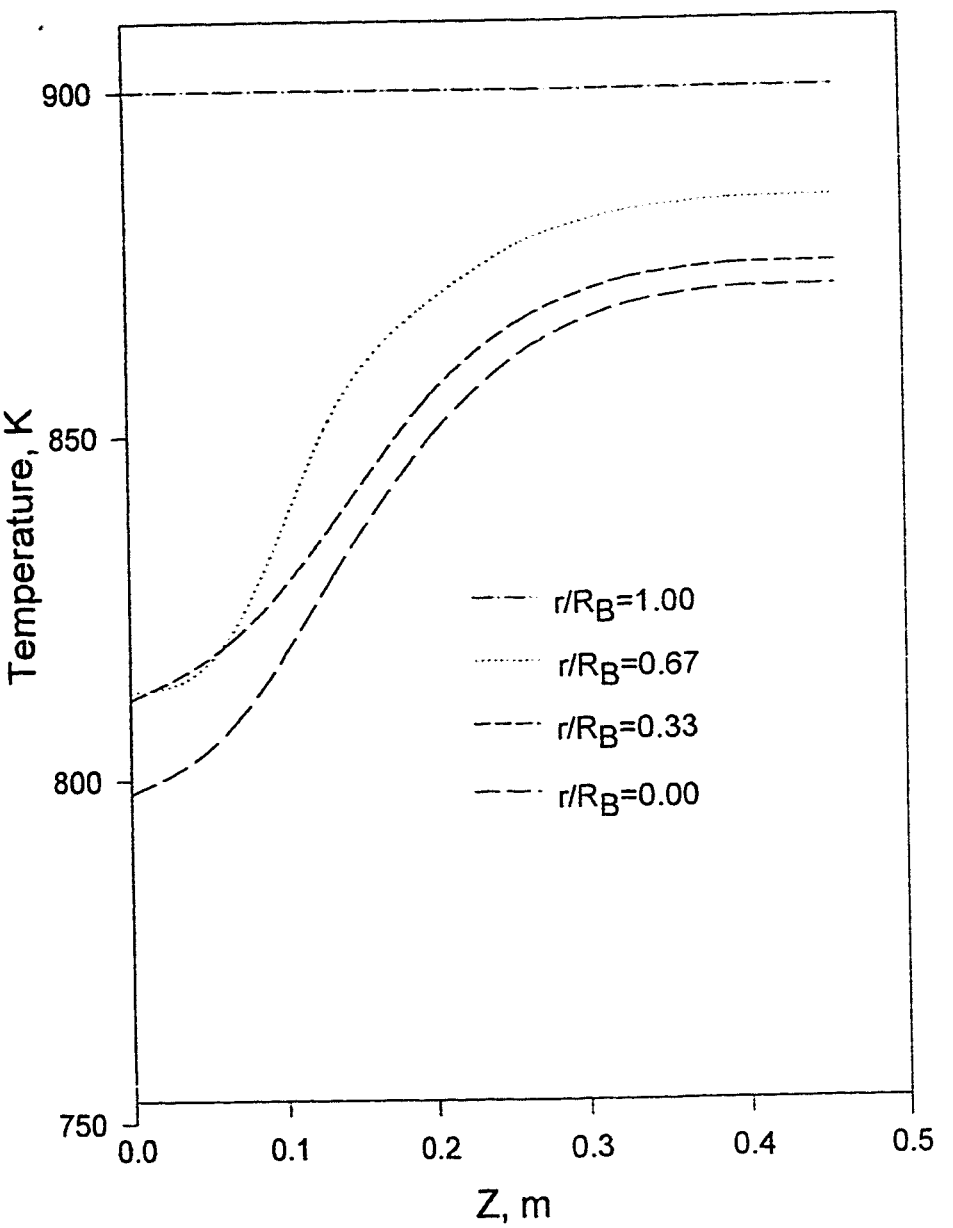

Figure 6.43. Temperature profile in the reactor. Time = 500 s,
P_b=5,066.25 kPa, T_{in}=600 K, T_b=700 K, T_f=700 K, T_w=700 K.

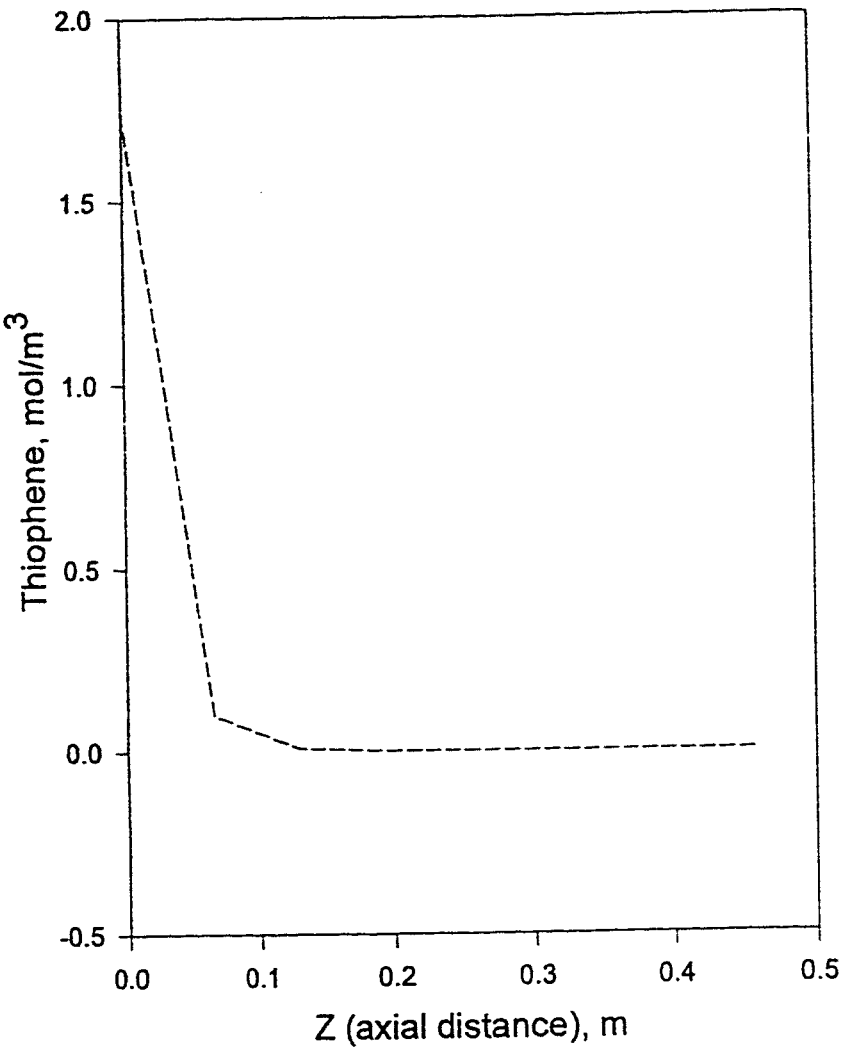

Figure 6.44. Thiophene profile at reactor bed centre. Time=30 s. P_b=5,066.25 kPa,T_{in}=600 K, T_b=700 K, T_f=700 K, T_w=900 K, y_A =0.05.

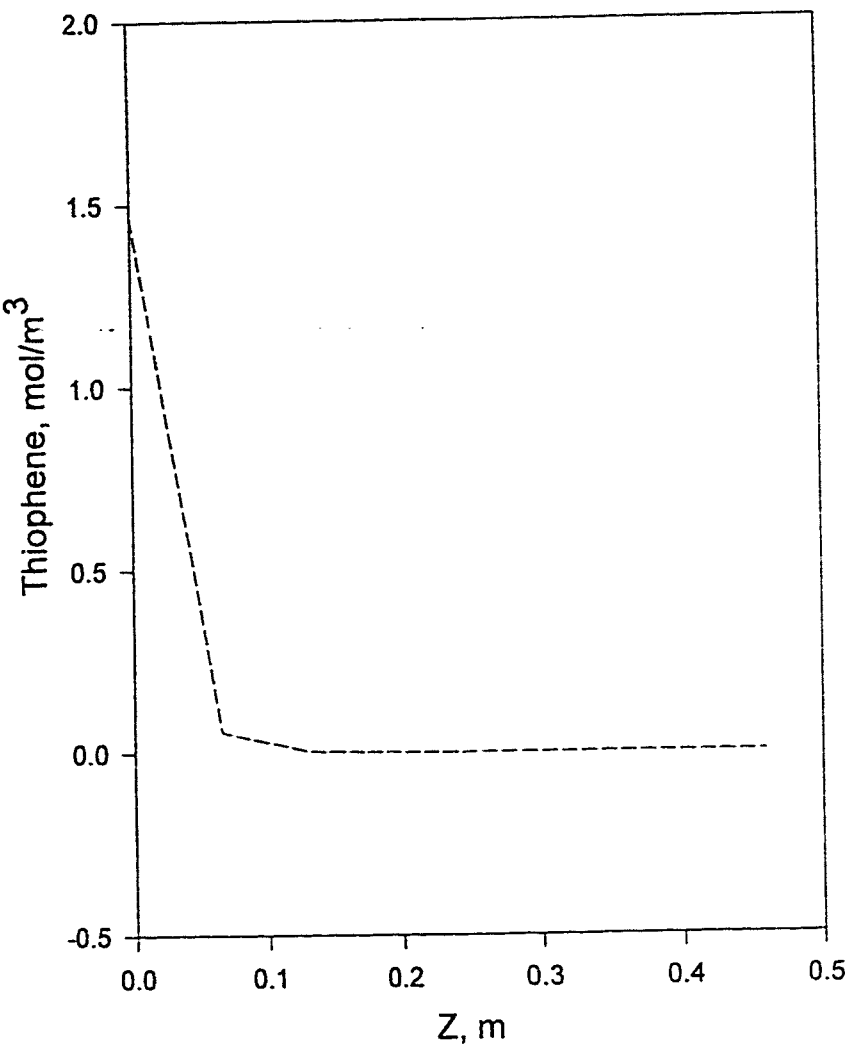

Figure 6.45. Thiophene profile at reactor bed centre. Time = 60 s. P_b=5,066.25 kPa,T_{in}=600 K, T_b=700 K, T_f=700 K, T_w=900 K. y_A =0.05.

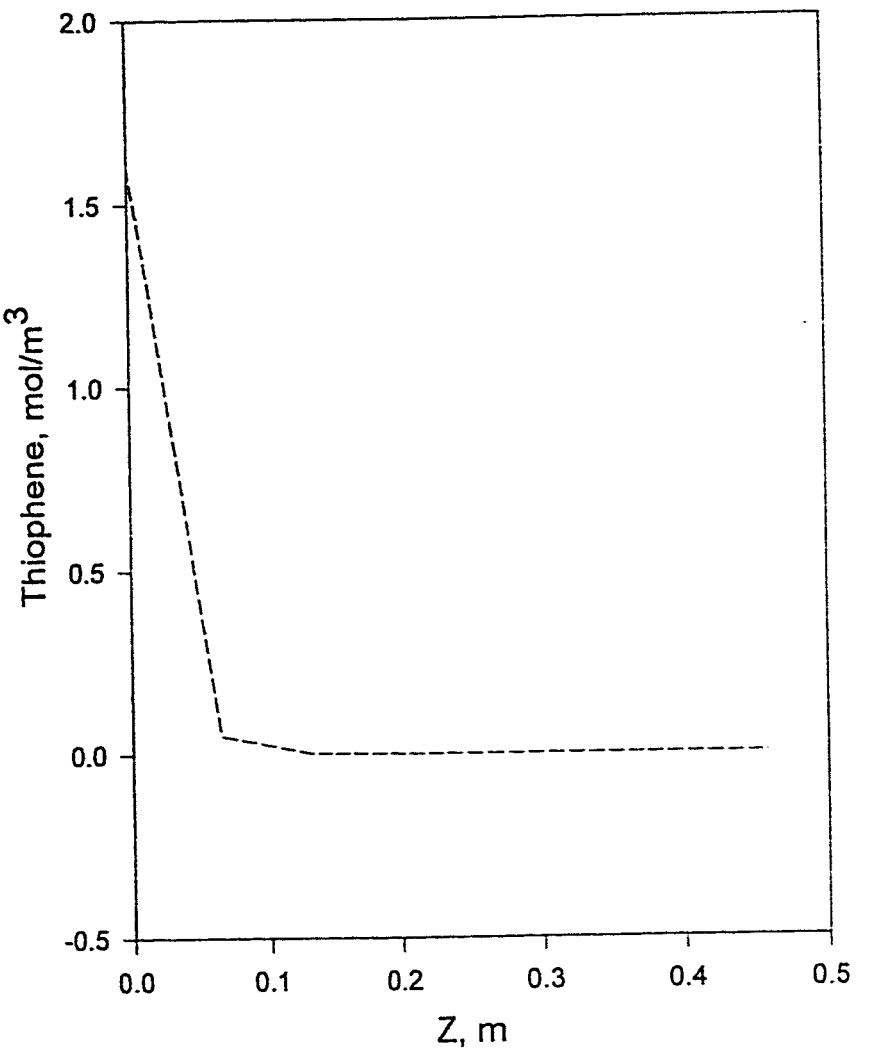

Figure 6.46. Thiophene profile at reactor bed centre. Time = 300 s. P_b=5,066.25 kPa,T_{in}=600 K, T_b=700 K, T_f=700 K, T_w=900 K. y_A =0.05.

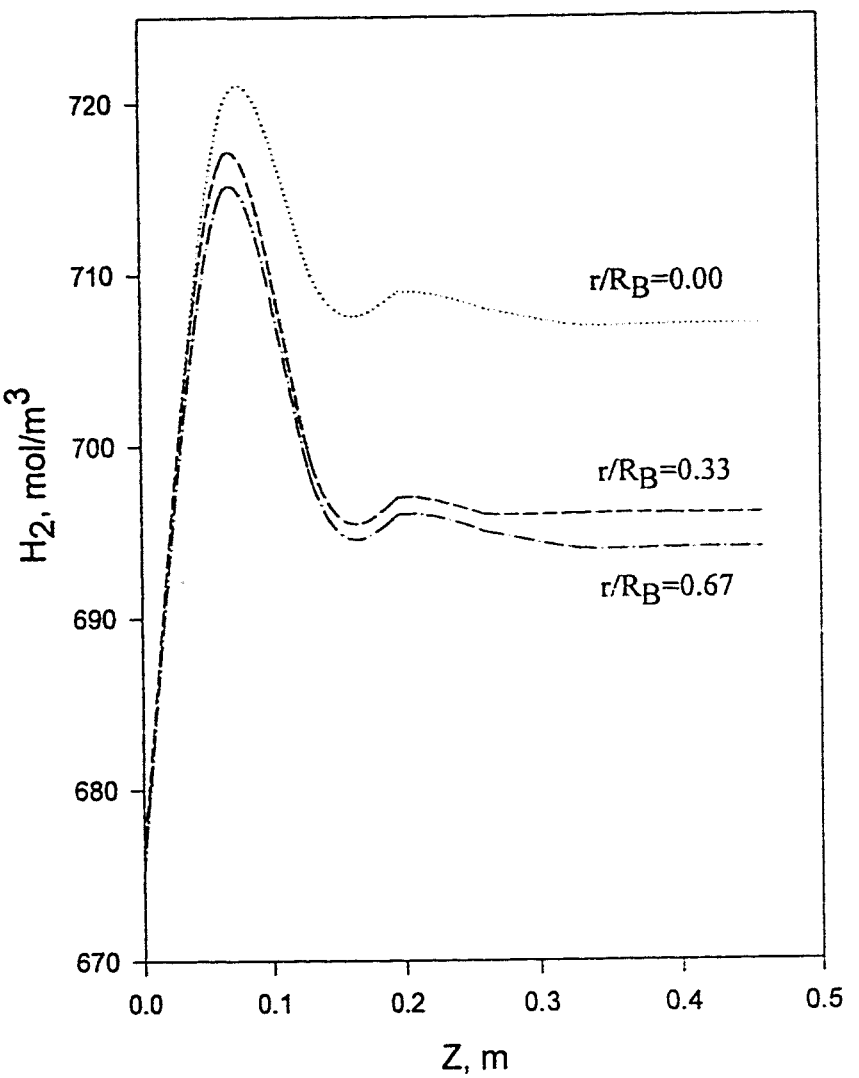

Figure 6.47. H_2 concentration profile at time=30 s. P_b=5,066.25 kPa, T_{in}=600 K, T_b=700 K, T_f=700 K, T_w=900 K. X_A =0.05.

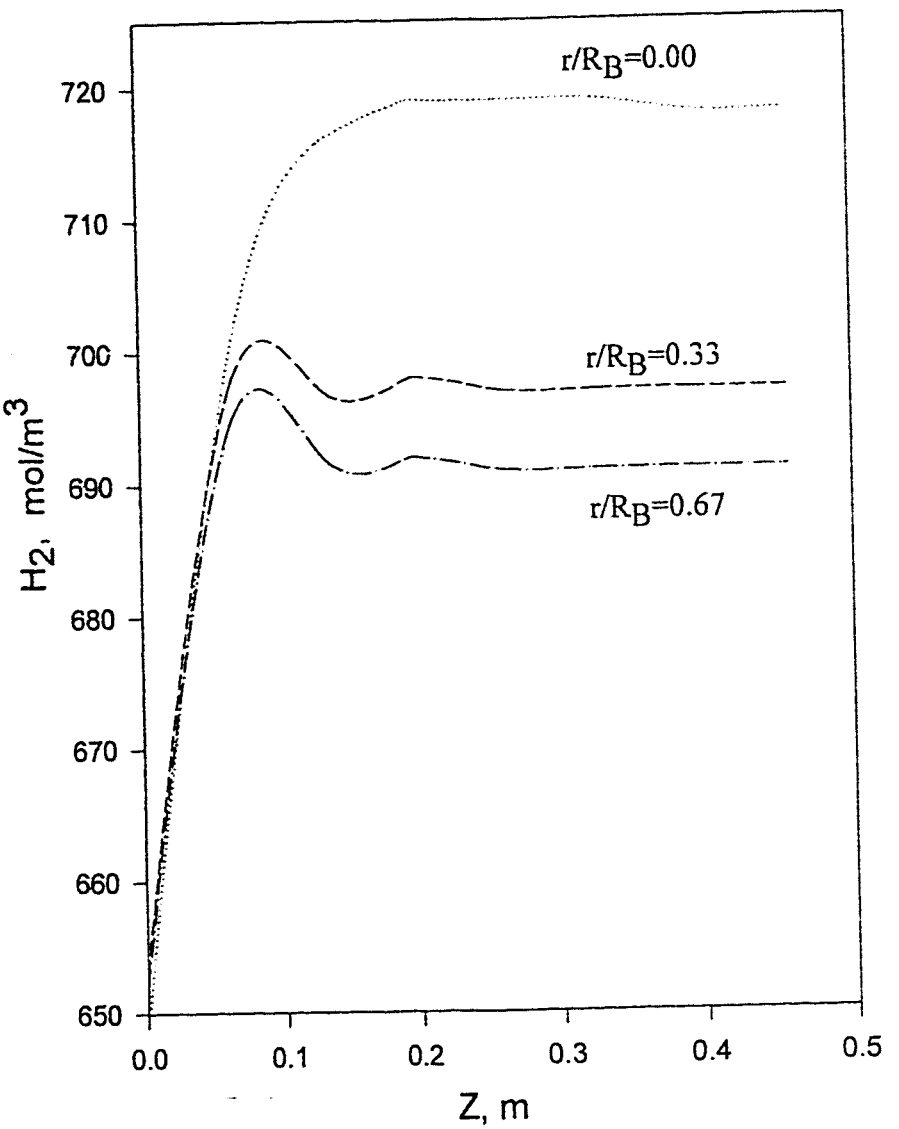

Figure 6.48. H_2 concentration profile at time=60 s. P_b=5,066.25 kPa, T_{in}=600 K, T_b=700 K, T_f=700 K, T_w=900 K, y_A =0.05.

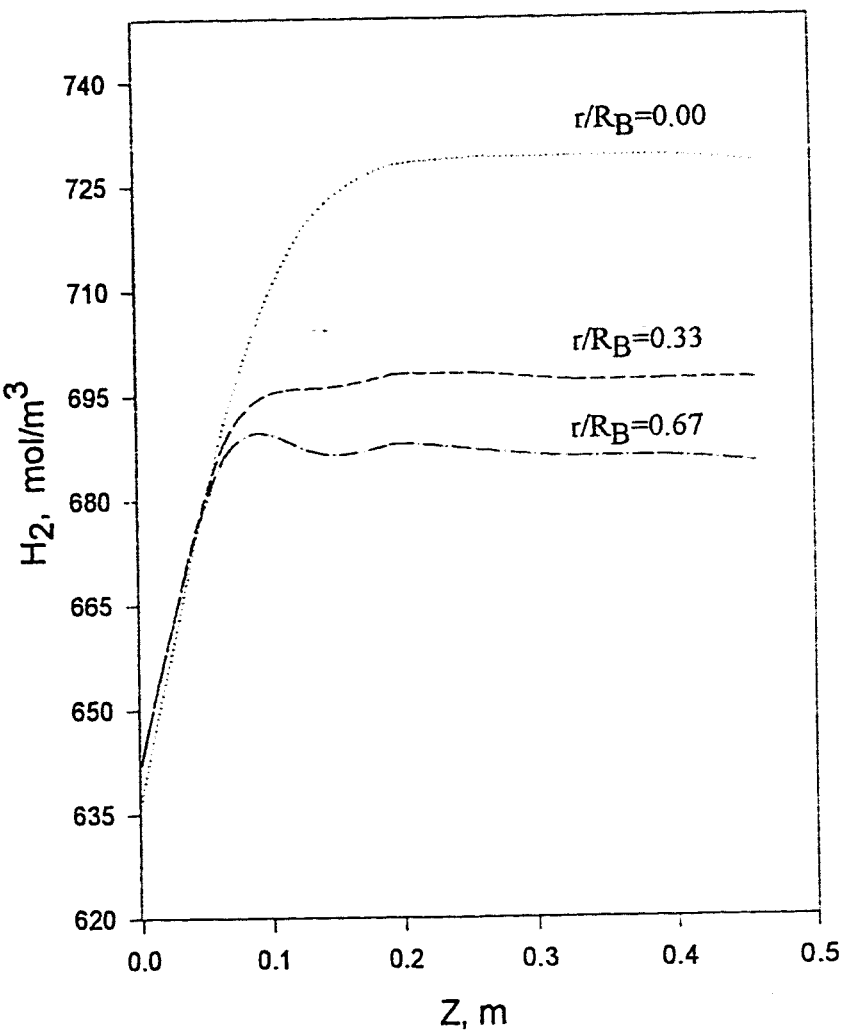

Figure 6.49. H_2 concentration profile at time = 90 s. P_b=5,066.25 kPa, T_{in}=600 K, T_b=700 K, T_f=700 K, T_w=900 K, y_A =0.05

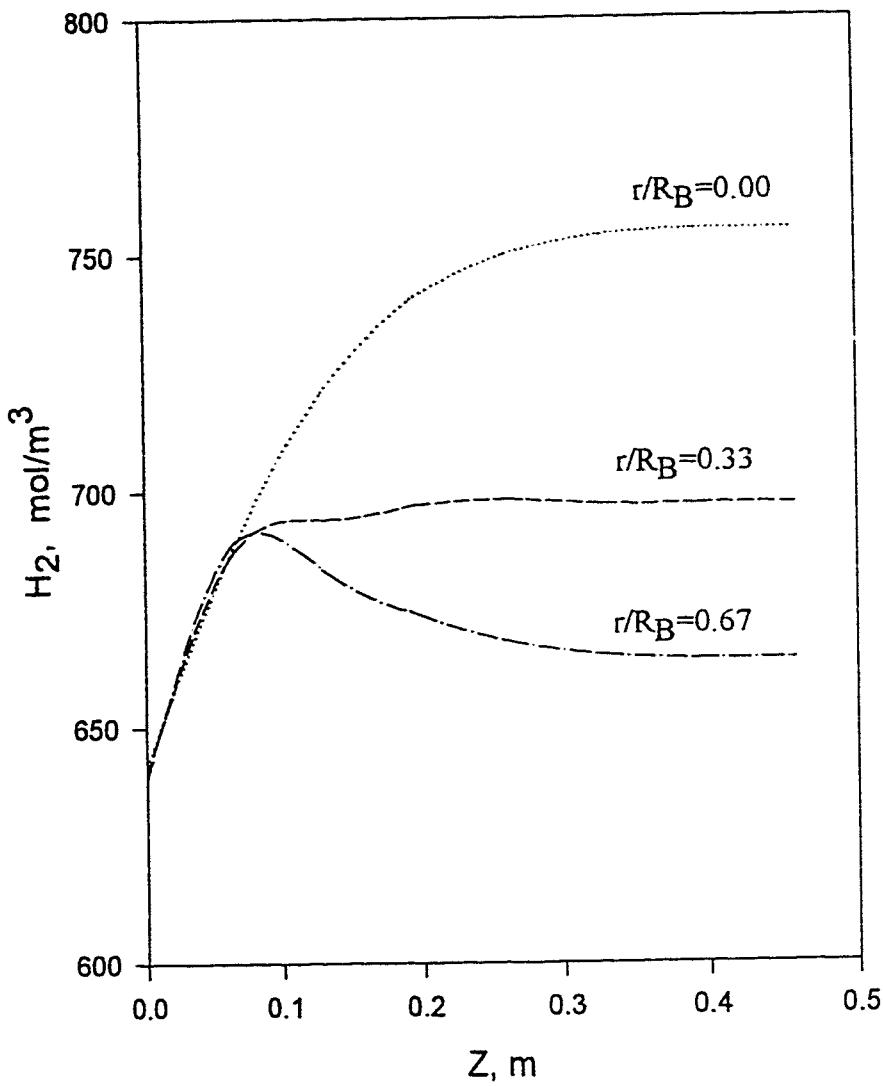

Figure 6.50. H_2 concentration profile at time = 200 s. P_b=5,066.25 kPa, T_{in}=600 K, T_b=700 K, T_f=700 K, T_w=900 K, y_A =0.05.

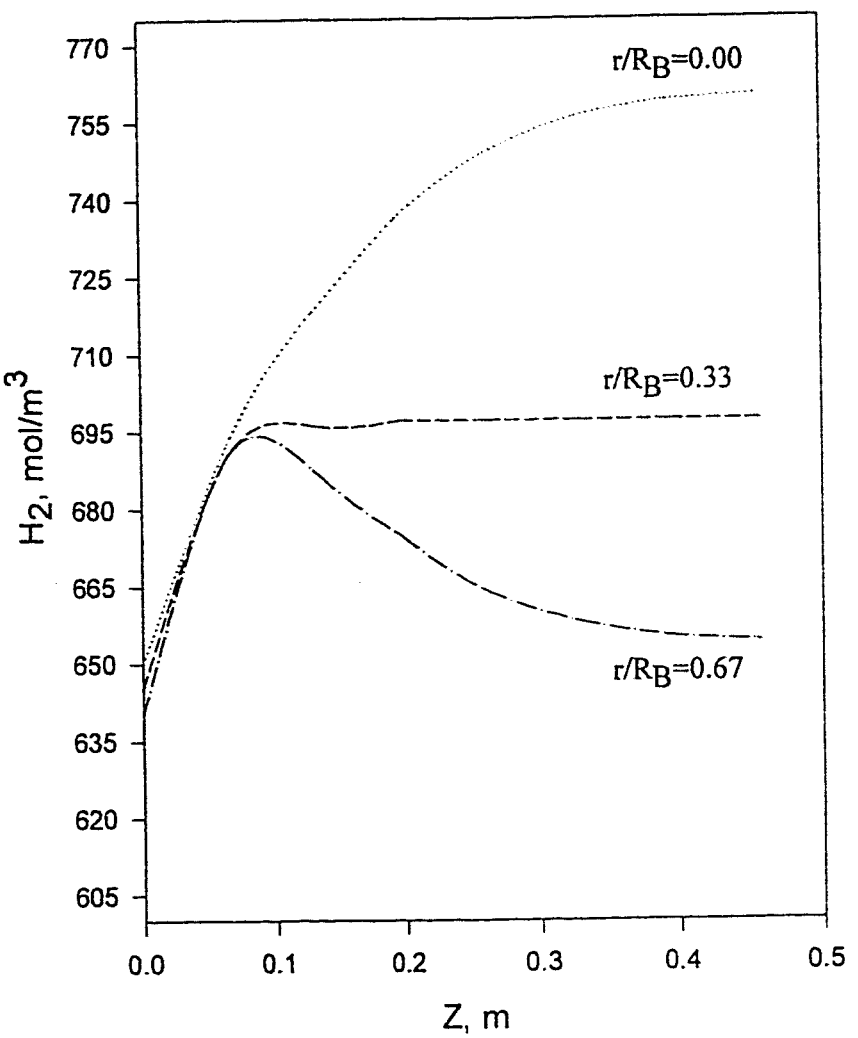

Figure 6.51. H_2 concentration profile at time=300 s. P_b=5,066.25 kPa, T_{in}=600 K, T_b=700 K, T_f=700 K, T_w=900 K, y_A =0.05.

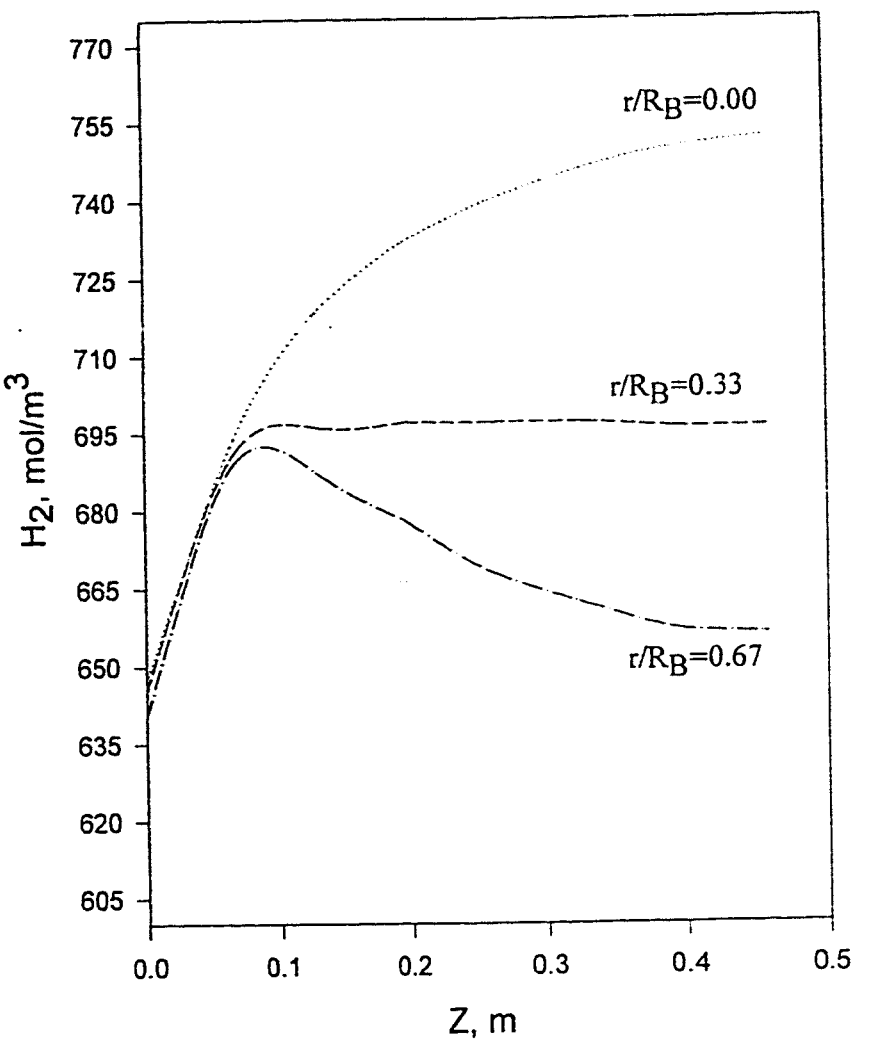

Figure 6.52. H_2 concentration profile at time = 400 s. P_b=5,066.25 kPa, T_{in}=600 K, T_b=700 K, T_f=700 K, T_w=900 K, y_A =0.05.

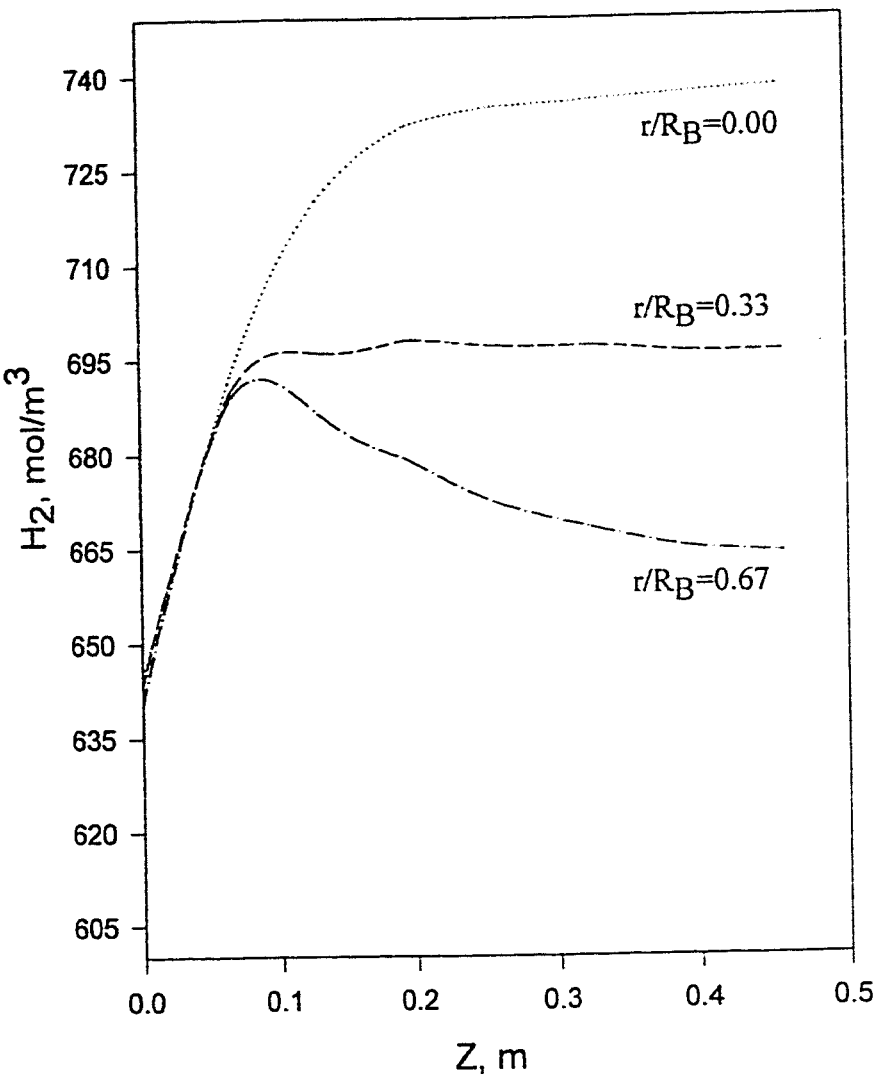

Figure 6.53. H_2 concentration profile at time = 500 s. P_b=5,066.25 kPa, T_{in}=600 K, T_b = 700 K, T_f= 700 K, T_w=900 K, y_A = 0.05.

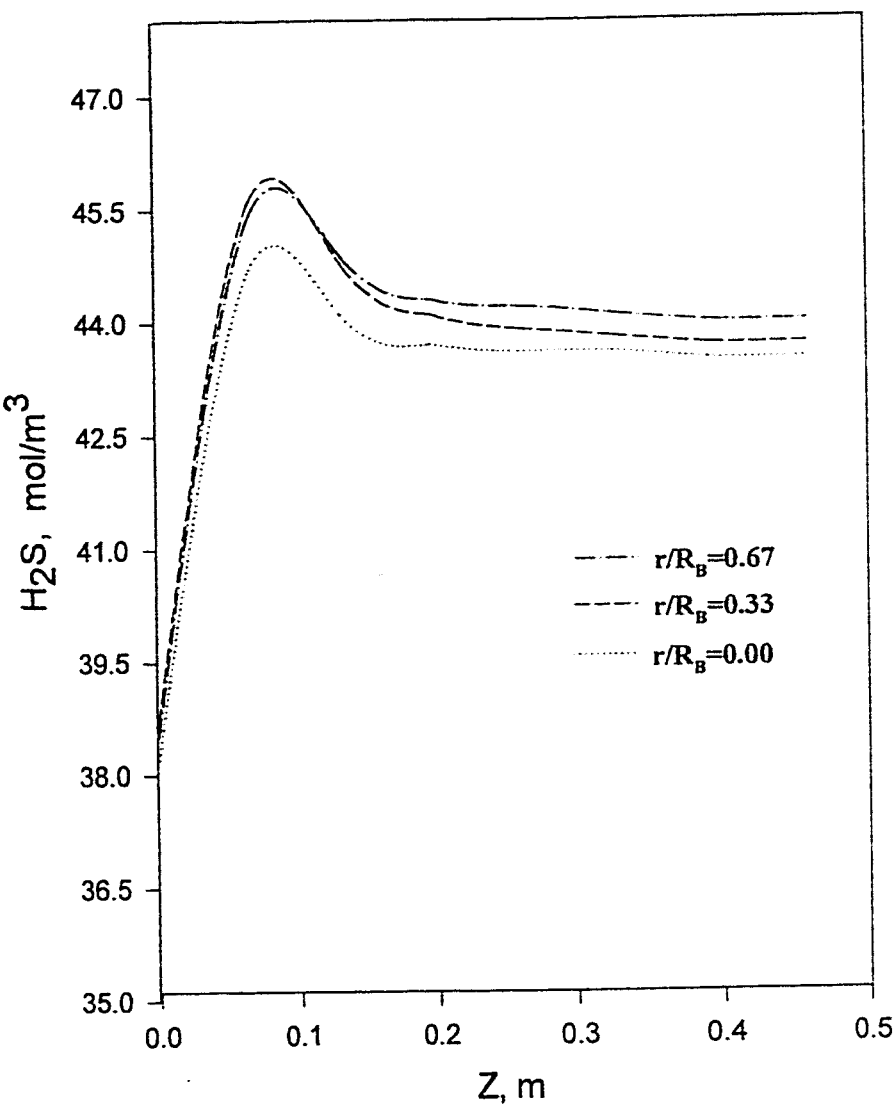

Figure 6.54. H_2S concentration profile at time = 30 s. P_b = 5,066.25 kPa, T_{in} = 600 K, T_b = 700 K, T_f = 700 K, T_w = 900 K, y_A = 0.05.

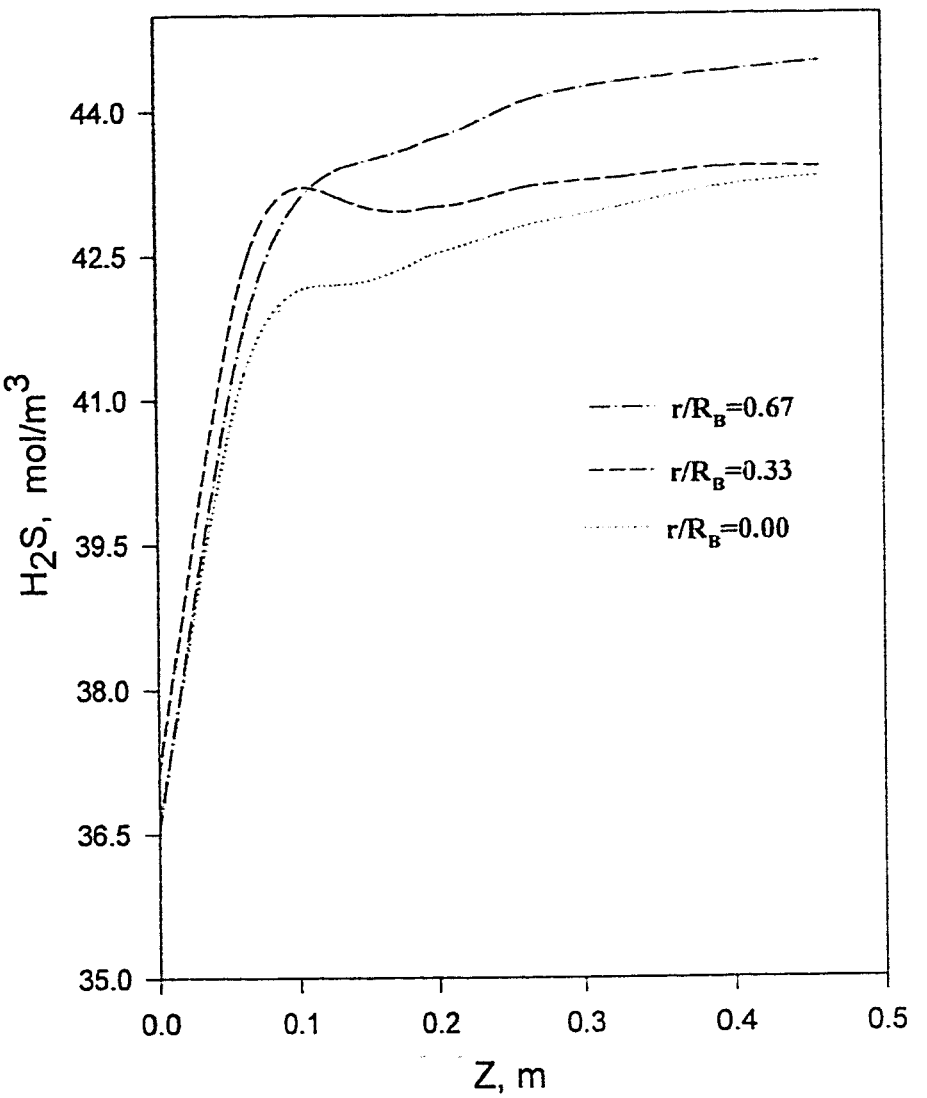

Figure 6.55. H_2S concentration profile at time = 60 s. P_b = 5,066.25 kPa, T_{in} = 600 K, T_b = 700 K, T_f = 700 K, T_w = 900 K, y_A = 0.05.

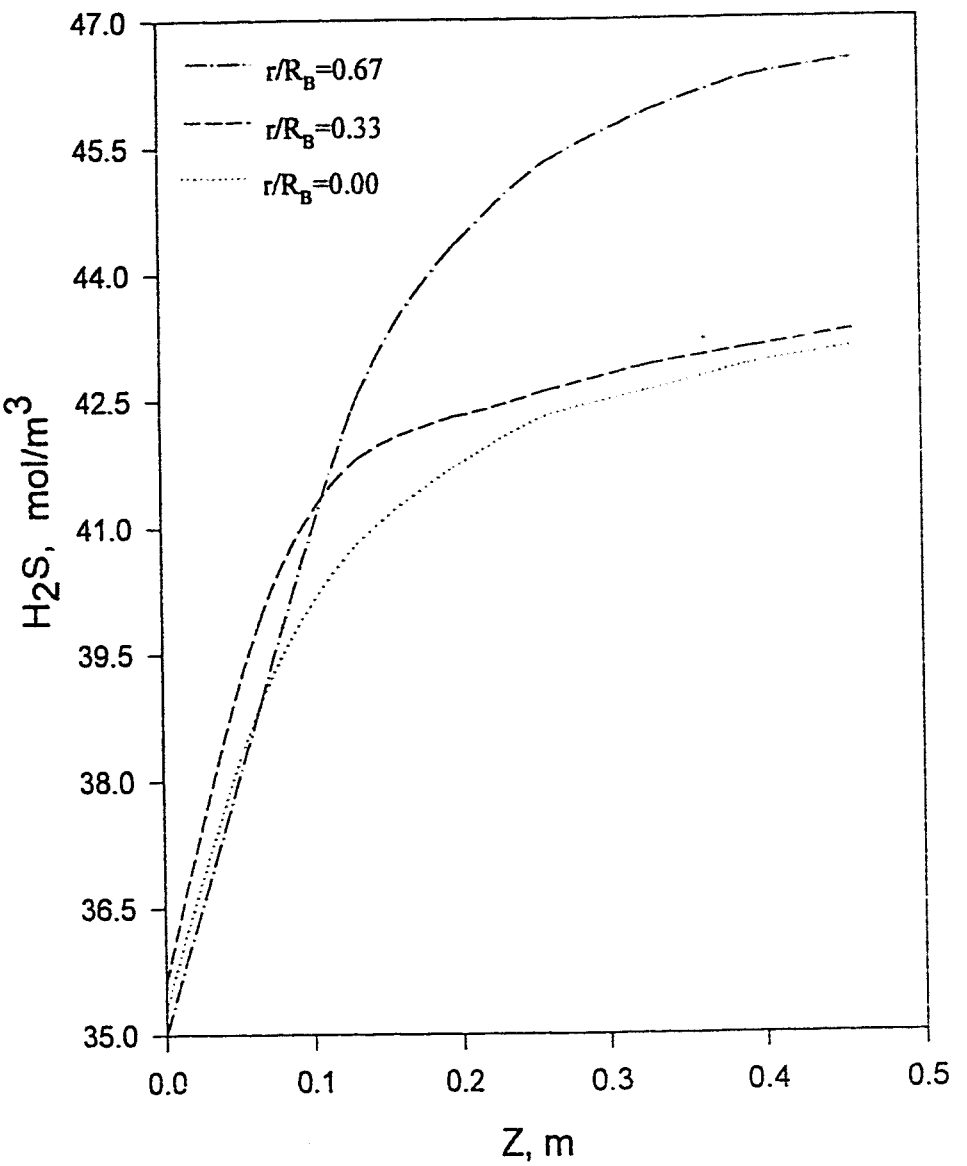

Figure 6.56. H_2S concentration profile at time = 120 s. P_b = 5,066.25 kPa, T_{in} = 600 K, T_b = 700 K, T_f = 700 K, T_w = 900 K, y_A = 0.05.

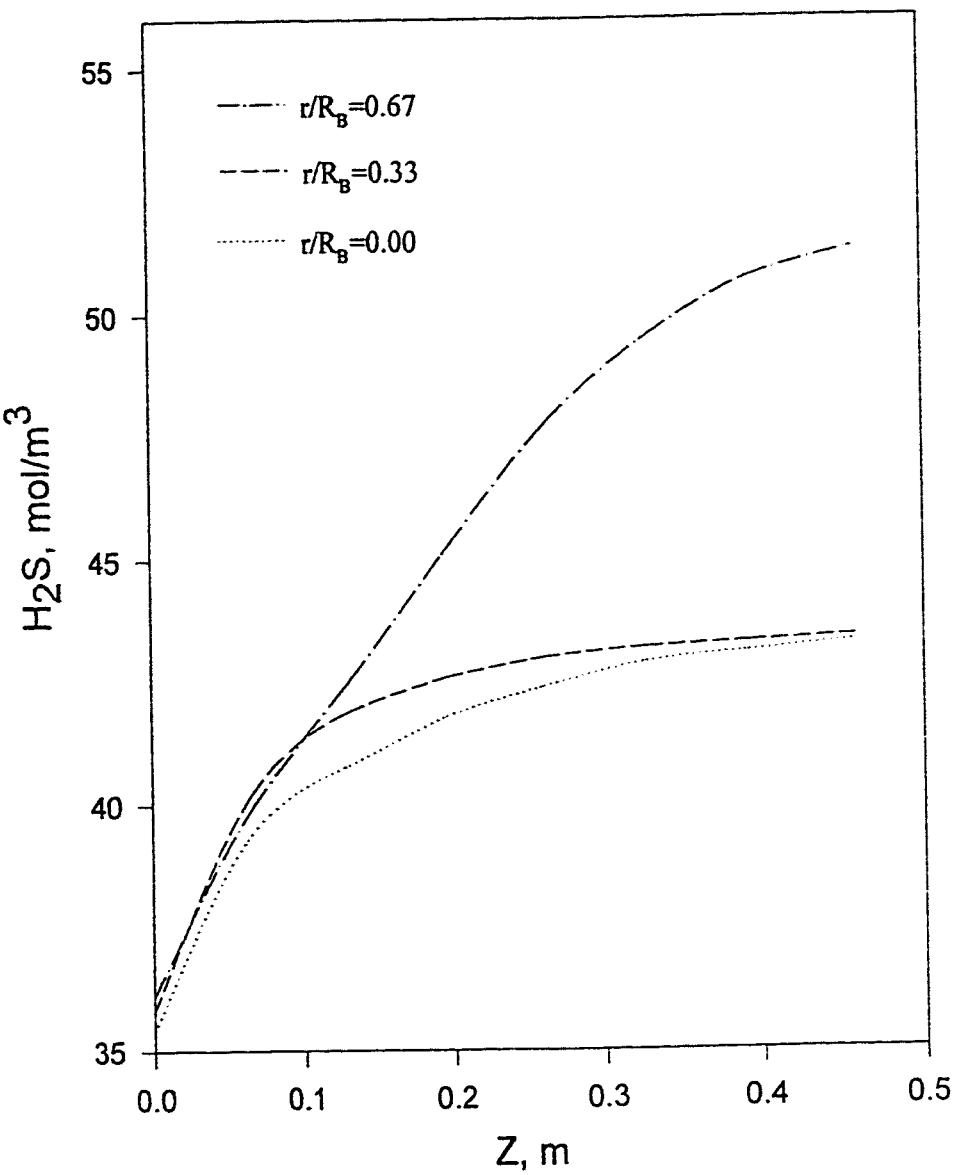

Figure 6.57. H_2S concentration profile at time = 300 s. P_b = 5,066.25 kPa, T_{in} = 600 K, T_b = 700 K, T_f = 700 K, T_w = 900 K, y_A = 0.05.

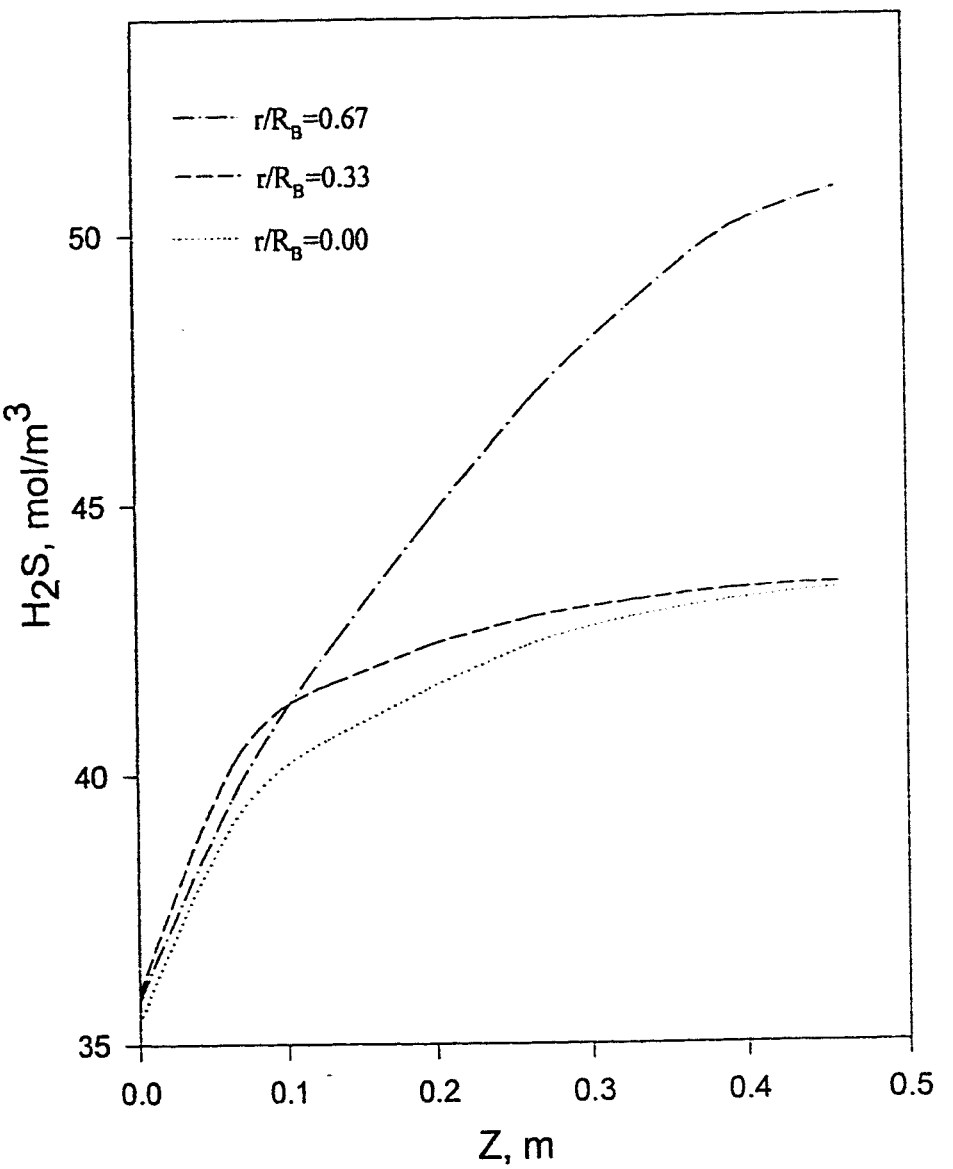

Figure 6.58. H_2S concentration profile at time = 400 s. P_b = 5,066.25 kPa, T_{in} = 600 K, T_b = 700 K, T_f = 700 K, T_w = 900 K, y_A = 0.05.

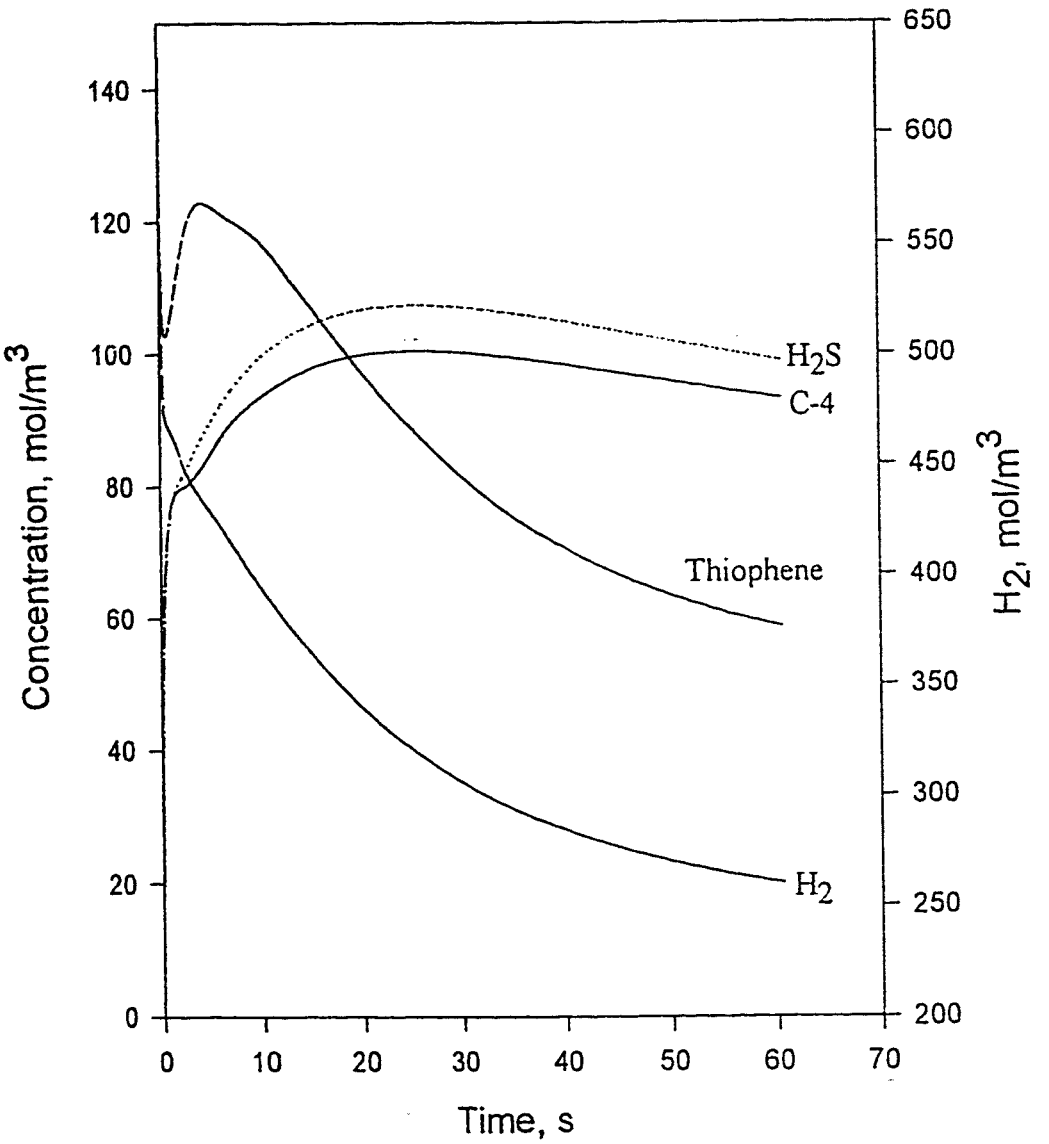

Figure 6.59.Concentration profiles in the reactor at position (1,2),
$P_b = 5{,}066.25$ kPa, $T_{in} = 600$ K, $T_b = 700$ K, $T_f = 700$ K,
$T_w = 900$ K, $y_A = 0.05$.

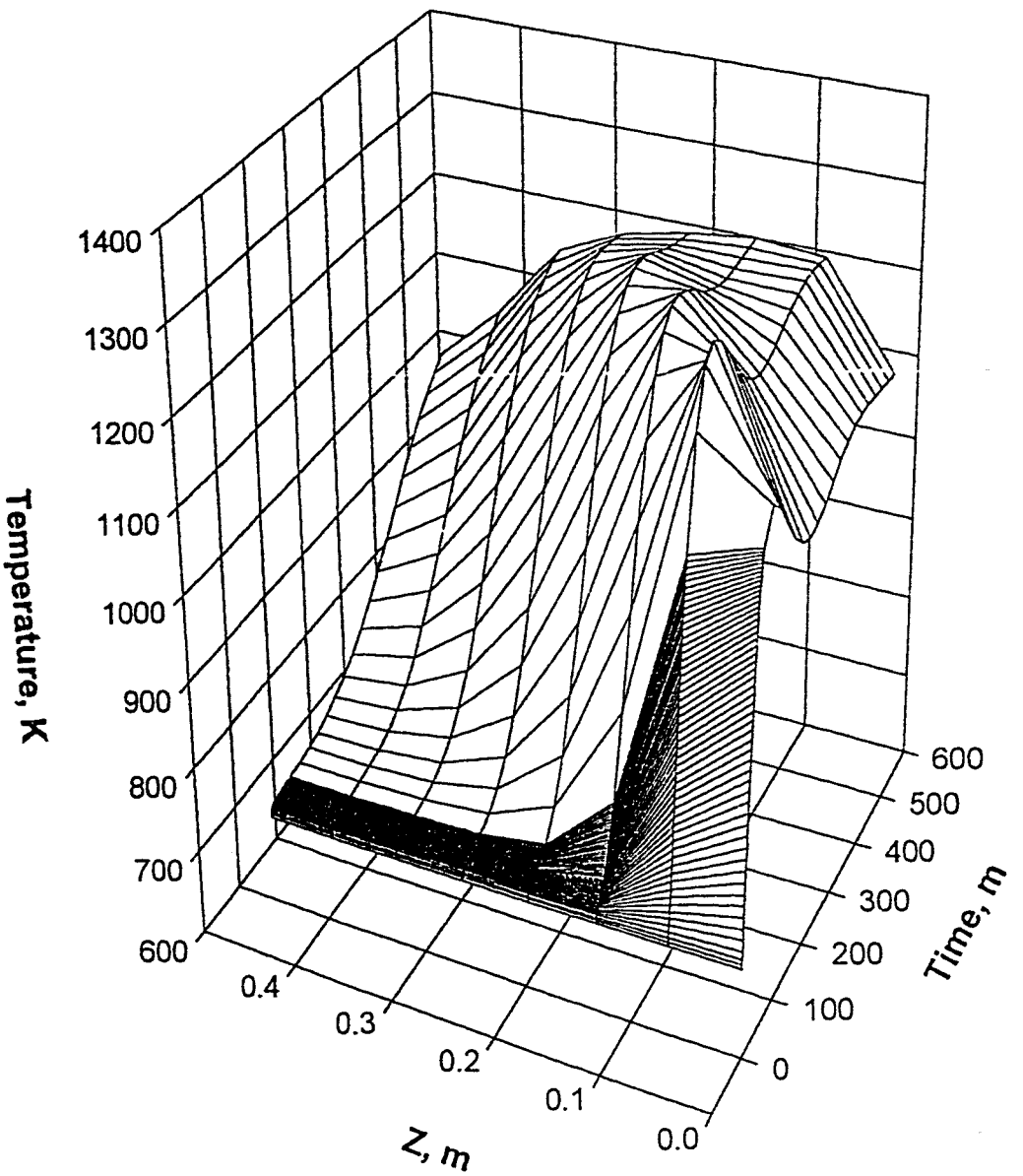

Figure 6.60. A 3D temperature profile in the reactor at position (1,2), $P_b = 5{,}066.25$ kPa, $T_{in} = 600$ K, $T_b = 700$ K, $T_f = 700$ K, $T_w = 900$ K, $y_A = 0.05$.

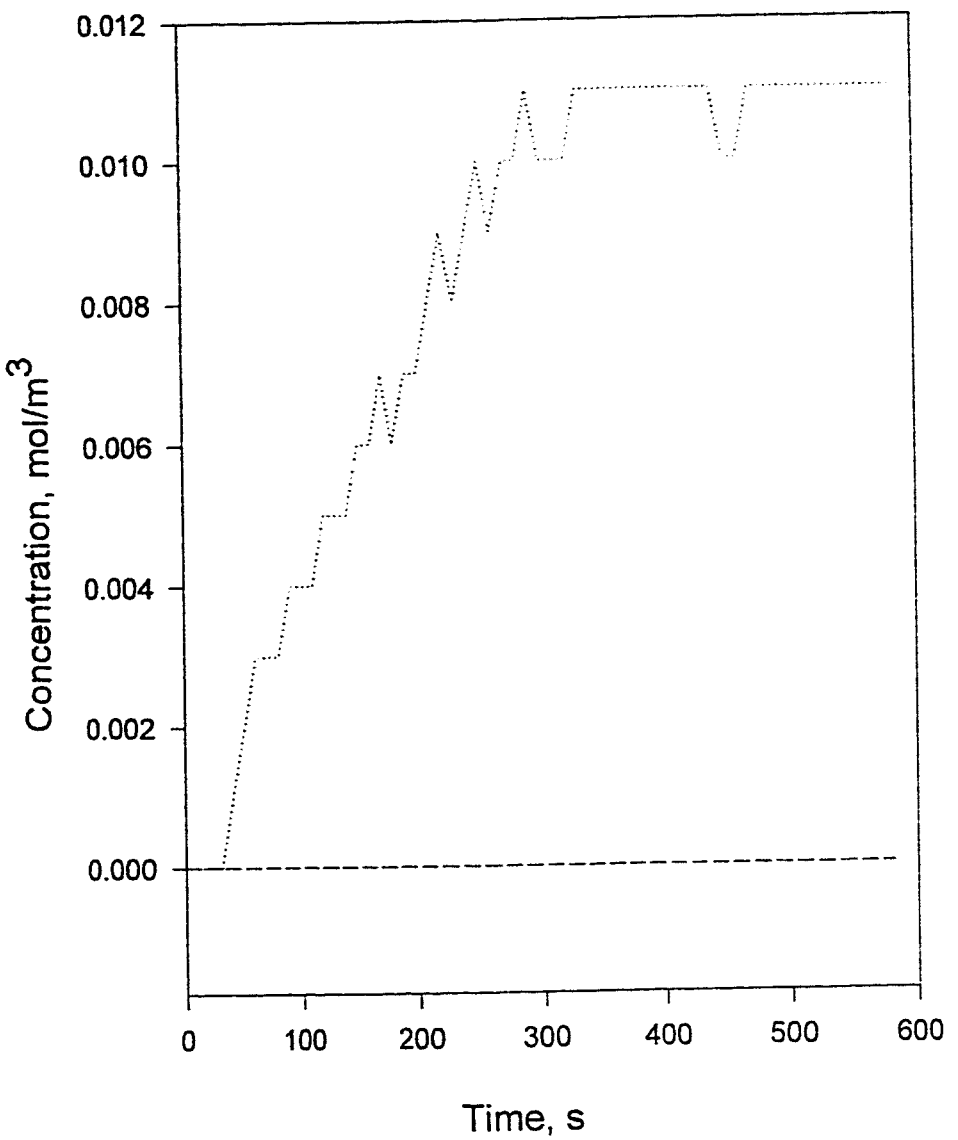

Figure 6.61. Deviation in thiophene concentration due to pertubation in T_{in} from 700 to 600 K, P_b = 5,066.25 kPa, T_b = 700 K , T_f = 700 K, T_w = 700 K.

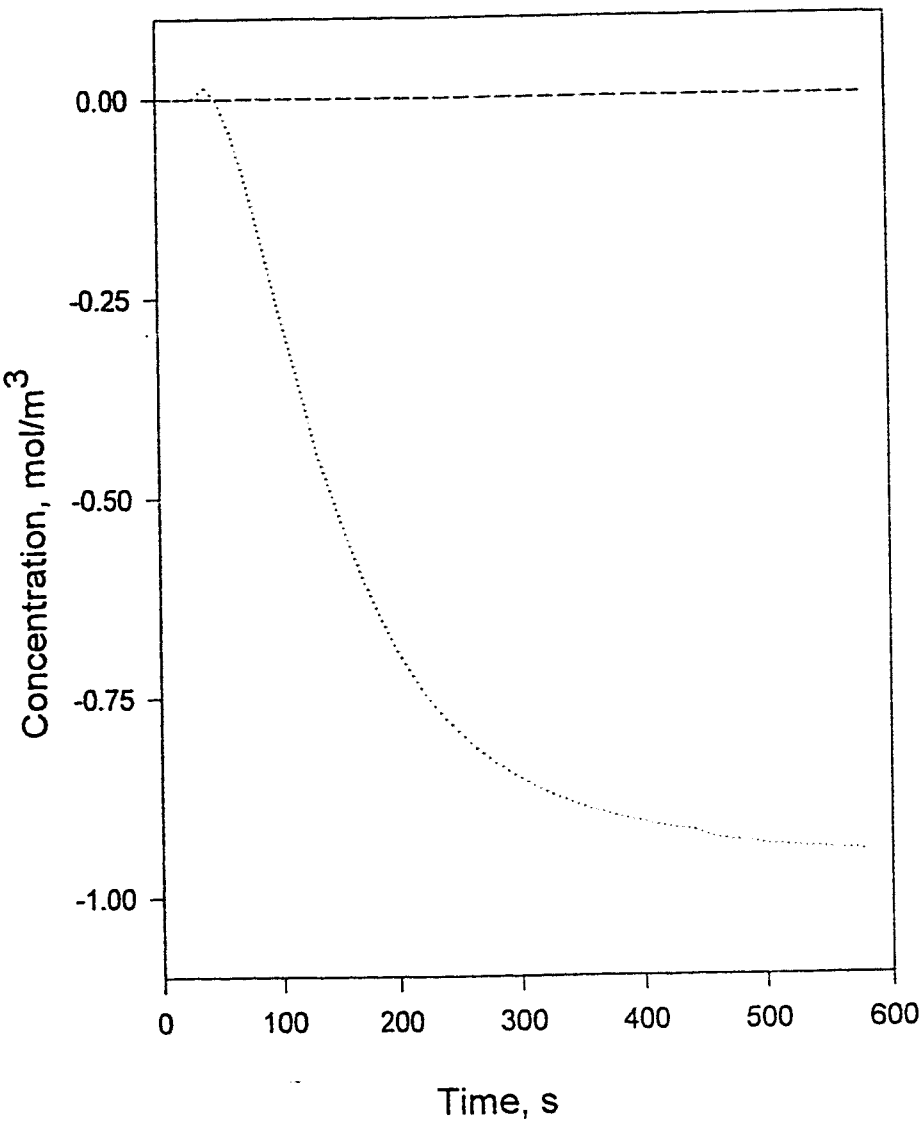

Figure 6.62. Deviation in .H_2S concentration due to pertubation in T_{in} from 700 to 600 K, P_b = 5,066.25 kPa, T_b = 700 K , T_f = 700 K T_w = 700 K.

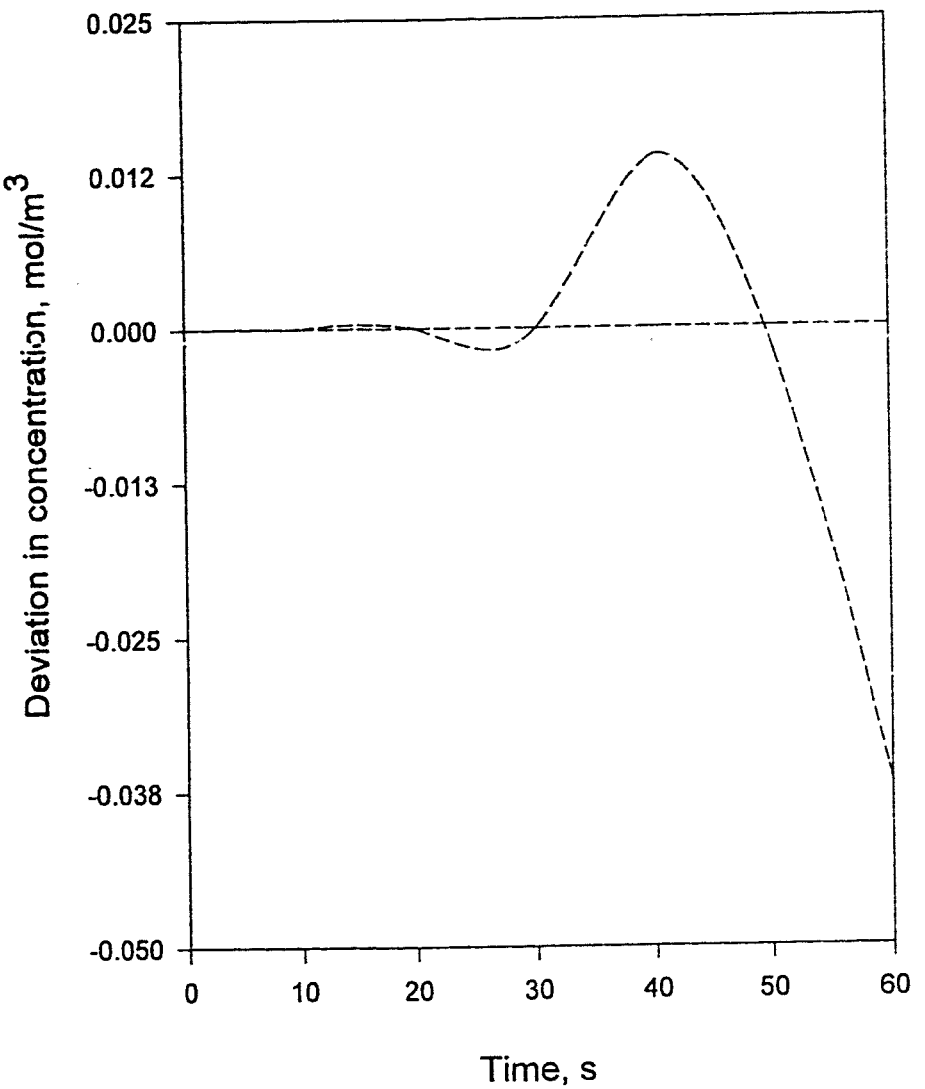

Figure 6.63. Deviation in H_2S concentration due to pertubation in T_{in} from 700 to 600 K. $P_b = 5{,}066.25$ kPa, $T_b = 700$ K , $T_f = 700$ K $T_w = 700$ K, (showing the first 1 min.).

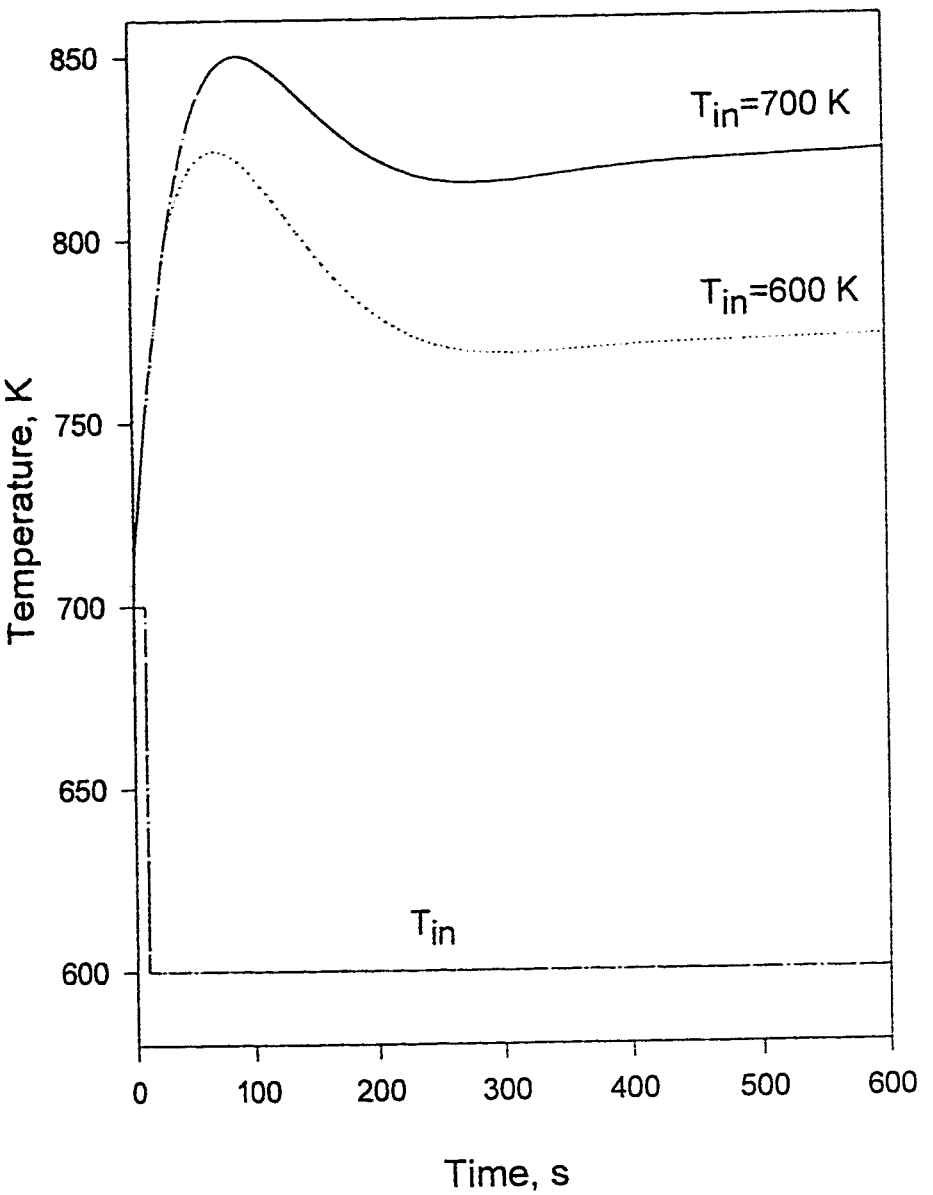

Figure 6.64. Deviation in temperature at bed centre due to pertubation in T_{in} from 700 to 600 K, P_b = 5,066.25 kPa, T_b = 700 K , T_f = 700 K T_w = 700 K.

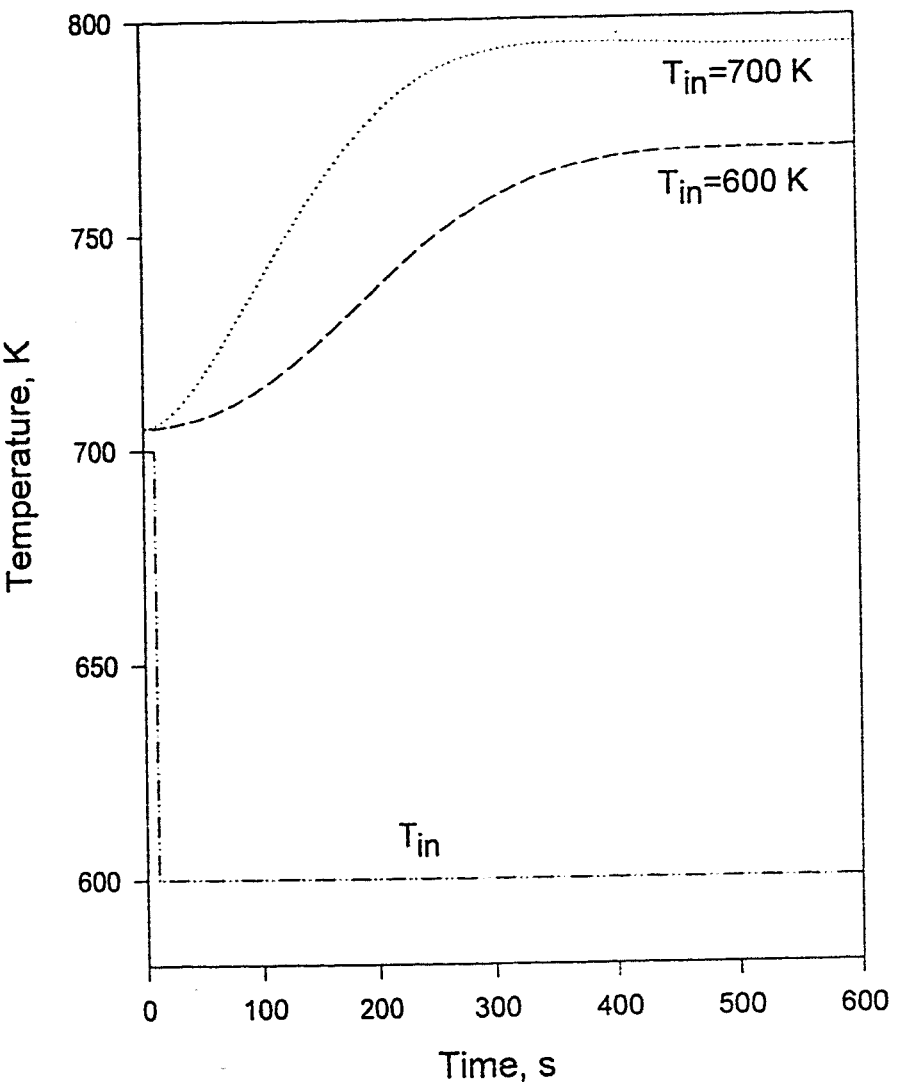

Figure 6.65. Deviation in temperature near bed wall due to pertubation in T_{in} from 700 to 600 K, P_b = 5,066.25 kPa, T_b = 700 K, T_f = 700 K, T_w = 700 K.

CHAPTER 7

CONCLUSIONS AND RECOMMENDATION

7.1 CONCLUSIONS

The conclusions which could be drawn from the modeling studies in this work are the following:

1. A model of multicomponent gas-solid reactions occurring in a fixed-bed reactor was developed. This model avoids many of the simplifying assumptions of earlier models for such type of reaction. Most of the important factors at both the reactor bed and pellet levels were taken into consideration. It is shown that the understanding of the pellet level behavior is especially important since it is very essential in understanding the bed behavior.

2. Steady state experimental data of fixed-bed reactor hydrodesulfurization (HDS) has been used to validate the model at the bed level. Non-availability of transient experimental data in the open literature, has prevented a comparison of the predicted transient profiles of this model with the actual phenomena occurring in a fixed-bed reactor Therefore, further test on the model was performed by generating the transient net concentration of each component. It has been shown that these net amounts reached zero level at steady state as expected. On the pellet level the model has successfully predicted the experimental conversion/time data for carbon gasification, metal oxide reduction, and wood pyrolysis obtained by TGA experiments.

3. A representative case of naphtha hydrodesulfurization was simulated in this work. The profiles of system parameters are performed. These give good insight into the behavior of the system variables.

4 The numerical simulation of HDS with perturbation in the inlet gas concentration and temperature are performed. This has demonstrated the stability of the model. It has revealed that temperature rises in the reactor may be brought under control by varying these parameters, they may also be used in determining the optimum operating conditions of the reactor without undue instability.

5. Transient studies have shown the importance of the internal particle/pellet gradient. There was a significant difference in temperature between the surface and center of the pellet. This was neglected in many studies.

6. The axial and radial variations in temperature and concentration are shown to be important in the cases studied. One or both of these have been neglected in some studies.

7. The significance of the wall heat transfer coefficient was demonstrated. Neglecting the convective transfer from the wall leads to misleading conclusions.

7.2 RECOMMENDATION

1. The model was developed for transient studies, but validated with the steady state experimental data due to non-availability of the transient data. It is recommended that transient experiments should be performed for further studies of the model.

2 The model did not include changes in the catalyst activities with time. It is recommended that catalyst degeneration due to coke and impurities deposition etc. be incorporated in the model.

3. The model was developed in dimensional form. This give a clear idea about the magnitude and variation in the parameters under study. It could therefore be extended for studies on control of gas-solid reactions in a fixed-bed reactor by incorporating appropriate subroutines. For the control studies the number of calculations for transport and physical properties in each time steps may be reduced without much adverse affect on the accuracy of the result. This is because in control, the speed of response of the model is very important

4. Although multi-steady states are not observed, it is recommended that the model be studied for multiplicity in steady state.

NOMENCLATURE

a	interfacial area between pellets and bulk fluid, m^2/m^3
A,a	reactant/product gas and its stoichiometric coefficient
B,b	reactant/product solid and its stoichiometric coefficient
B_o	parameter defined in equation (14a) in Section 3.3.4
C_G	concentration of G, mol/m^3
C_p^e	pellet effective specific heat capacity, J/m^3K
C_{pr}	specific heat capacity of component r, J/mol K
D,d	product solid and its stoichiometric coefficient
D_{kr}	Knudsen diffusivity of component r, m^2/s
d_p	pore diameter, m
D_{rs}	binary diffusivity between components r and s, m^2/s
f_i	rate for surface reaction, mol/m^2s
F	rate of homogeneous reaction, mol/m^3s
F	shape factor
G	dummy component
ΔH	heat of reaction, J/mol
h_m, h_r	convective and radiation heat transfer coefficients, W/m^2K
k	thermal conductivity, W/mK
k_c	mass transfer coefficient, m/s
M_B	molecular weight, kg/kmol
M_{GR}	flux of G in the packed tower radial direction, mol/m^2s
M_{GZ}	flux of G in the packed tower axial direction, mol/m^2s
N_c, N_B	Number of gaseous and solid components
N_G	flux of G in the pellet, mol/m^2s

N_r Number of surface reactions

P pressure, Pa

q_z, q_r heat flux, W/m^2

Q volumetric flow rate, m^3/s

r radial position in the pellet, r

r_g, r_c grain radius and reaction front in the grain, m

R_g universal gas constant, 8.314 N.m/mol.K

r_o initial grain radius, m

r_p pellet radius, m

R_p,R_B radial position and radius in the packed tower, m

R_W Reactor wall

Re Reynolds number

Δr, Δz increment in radial and axial directions, m

S_i Surface area of a solid i

Sc Schimdt number

t, delt time and time step, s

T temperature, K

T_b bulk temperature, K

T_S surface temperature, K

v superficial fluid velocity, m/s

V_Z fluid velocity in axial direction, m/s

x_i,X_i,X_{it} local, pellet and tower overall conversion for solid

y mole fraction

z, Z axial position and tower height, m

Greek symbols

ε	porosity
ϕ_{ij}	parameter defined in Section 3.4, equation (25)
η	fraction of solids in a pellet
μ	viscosity, kg/m.s
θ	emissivity
ρ	density, kg/m^3
σ	Boltzmann constant, $5.735\times10^{-8} W/m^2.K^4$
Ω_D	dimensionless collision integral for diffusion

REFERENCES

Abba, A. I., M. Sc. Thesis, King Fahd University of Petroleum and Minerals, Dhahran, Saudi Arabia (1995).

Abdel-Hadi, E. A. A., and Hsu, T. R, "Computer Modeling of Fixed Bed Underground Coal Gasification Using the Permeation Method", J. Energy Resources Technol. Trans. ASME **109**, 11-20 (1987).

Acharya D. R. and Hughes, R., "Modeling of Butene-1 Dehydrogenation in a Fixed-Bed Reactor - Bed and Pellet Profiles", Can. J. Chem. Eng., **68**(2),89-96 (1990).

Almeida-Costa, C. A., Ferreira, R. M. and Rodrigues, A. E. "Wrong-Way Behavior in Packed-Bed Reactor with 'Large-Pore' Catalysts", Chem. Eng. Sci., **49**,(24B) 5571-5583 (1994).

Bhattacharya, A., Salam, L., Dudukovic, M. P. and Joseph, B. "Experimental and Modeling in Fixed-Bed Char Gasification", Ind. Eng. Chem. Res. Des. Dev., **25**, 988-996 (1986).

Bird, R. B., Stewart, W. E. and Lightfoot, E. N. "Transport Phenomena", 3rd. ed. McGraw-Hill Book Company, New York. (1977).

Borio, D. O., Menendez, M. and Santamaria, J., "Simulation and Optimization of a Fixed-Bed Reactor Operating in Coking-Regeneration Cycles", Ind. Eng. Chem. Res., **31** 2699-2707 (1992).

Bussche, K. M. V., Neophytides, S. N., Zolotarskii, I. A. and Froment, G. F., "Modeling and Simulation of the Reversed Flow Operation of a Fixed-Bed Reactor for Methanol Synthesis", Chem. Eng. Sci., **48**, 3335-3345 (1993).

Carberry, J. J. "Chemical and Catalytic Reaction Engineering", McGraw-Hill Inc., USA (1976).

Carnahan, B., Luther, H. A. and Wilkes, J. O., "Applied Numerical Methods", John Wiley and Sons Inc. New York (1969).

Chilton, T. H. and Colburn, A. P., Ind. Eng. Chem. **26**, 1183 (1934).

Chiuping, L., Chen, Y. W., Shien-Jen, Y. and Wu, J. C., "Hydrodesulfurization Reactions of Atmospheric Gas Oil Over CoMo/Alumina-Aluminium Borate Catalysts", Ind. Eng. Chem. Res. **32**, 1573-1578 (1993).

Cropley J. B., "Development of Optimal Fixed-Bed Catalytic Reaction Systems", Chem. Eng. Progress, Feb. 32-39, (1990).

Doraiswamy, L. K. and Sharma, M. M., "Heterogeneous Reactions: Analysis, Examples and Reactor Design, Gas-Solid and Solid-Solid Reactions", vol. 1, John Wiley and Sons, New York (1984).

Efthimiadis, E. A and Sotirchos, S. V., "Experimental Validation of a Mathematical Model for Fixed-Bed Desulfurization", AIChE J., **39**(1), 99-110 (1993).

Ferreira, R. M. Q, Costa, A. C. and Rodrigues, A. E., "Dynamic Behavior of Fixed-Bed Reactors with 'Large-Pore' Catalysts: A Bidimensional Heterogeneous Diffusion/ Convection Model", Computers Chem. Engng, **16**(8), 721-751 (1992).

Froment, G. F. and Hofmann, H. P. K., "Design of Fixed-Bed Gas-Solid Catalytic Reactors", eds Carberry, J. J. and Varma, A., p. 373, Marcel Dekker Inc., New York (1987).

Froment, G. F., Depauw, G. A. and Vanrysselberghe, V., "Kinetic Modeling and Reactor Simulation in Hydrodesulfurization of Oil Fractions", Ind. Eng. Chem. Res., **33**, 2975-2988 (1994).

Grozev, G. G., Sapundzhiev, C. G. and Elenkov, D. G., "Unsteady-State SO_2 Oxidation: Practical results", Ind. Eng. Chem. Res., **33**, 2248-2250 (1994).

Hassam, M. S., "Studies in Gas-Solid Reactions", M. Sc. Thesis, University of Calgary, Canada (1987).

Hastaoglu, M. A. and Berruti, F, "A Gas-Solid Reaction Model for Flash Wood Pyrolysis", Fuel, **68**, 1408-1415 (1989).

Hastaoglu, M. A, "Transient Modeling of a Packed-Tower: Mass and Heat Transfer with Reaction", Fuel, **74**(11), 1624-1631 (1995).

Hastaoglu, M. A. and Hassam, M. S., "A Gas-Solid Reaction Model - Variable Temperature, Pressure and Structural Parameters", Can. J. Chem. Eng., **66**, 419-427 (1988).

Hobbs, M. L., Radulovic, P. T. and Smoot, L. D., Process Energy Combust. Sci. **19**, 505. (1993).

Hobbs M. L., Radulovic, P. T. and Smoot, L. D., "Modeling Fixed-Bed Coal Gasifiers", AIChE J., **38**(5), 681-702 (1992).

Hoebink, J. H. B .J., Couwenberg, P.M. and Marin, G. B., "Fixed-Bed Reactor Design for Gas Phase Chain Reactions Catalyzed by Solids: The Oxidative Coupling of Methane", Chem. Eng. Sci., **49**, 5453-5463 (1994).

Jackson, R. "Transport in Porous Catalysts", Chem. Eng. Monograph, New York, Elsevier (1977).

Khandavalli, V. R., Rao, V. D., Ramakanth, M. V. and Athota, K. V., "Evaluation of Stability of a Catalytic Fixed-Bed Reactor from a Steady-State Model", Chem. Eng. Sci., **48**,(21) 3677-3681(1993).

Mason, E. A. and Malinuaskas, A. P., "Gas Transport in Porous Media: The Dusty Gas Model", Chem. Eng. Monograph, New York, Elsevier (1983).

Radulovic, P. T., Ghani, M. U. and Smoot, L .D, "An Improved Model for Fixed-Bed Coal Combustion and Gasification", Fuel **74**(4), 582-593 (1995).

Reid, R. C., Prausnitz, J. M. and Sherwood, T. K., "The Properties of Gases and Liquids", 3rd ed, McGraw-Hill Comp., New York (1977).

Richard, J. R., Al-Majthoub, M., Aho, M. J. and Pirkonen, P. M., "Separate Effects of Pressure and some other Variables on Char Combustion under Fixed-Bed Conditions", Fuel **74**, 485, (1993).

Rowe, P. N. and Claxton, K. T., Trans. Inst. Chem. Eng., **43**, T231,(1965).

Satterfield, C. N. and Robert, G. W., "Kinetics of Thiophene Hydrogenolysis on a Cobalt Molybdate Catalyst", AIChE J. **14**, 159 (1968).

Segall N. L., MacGregor, J. F. and Wright J. D., "Collocation Methods for Solving Packed-Bed Reactor Models with Radial Gradients", Can. J. Chem. Eng., **62**(12), 808-817 (1984).

Silveston P. L., Hudgins R. R., Bogdashev, S., Vernijakovskaja, N. and Matros, Y. S., "Modeling of a Periodically Operating Packed-Bed SO_2 Oxidation Reactor at High Conversion", Chem. Engng., **49**(3), 335-341 (1994).

Smith, J. M., "Chemical Engineering Kinetics", 3rd ed., McGraw-Hill Book Company, Singapore, (1981).

Sotirchos, S. V and Zarkanitis S., "Pellet-Model Effects on Simulation Models for Fixed-Bed Desulfurization Reactors", AIChE J., **35**(7), 1137-1147 (1989).

Szekely, J. and Hastaoglu, M. A., "Reduction of Nickel Oxide / Hematitie Mixture with Hydrogen", Trans. Inst. Mining Met., **C78**, 85(1976).

Szekely, J. and Evans, J. W., "Structural Model for Gas-Solid Reactions with Moving Boundary", Chem. Eng. Sci., **25**, 1091 (1970).

Taylor, R. and Krishna, R., "Multicomponent Mass transfer", pp. 19-23, 78-110, John Wiley & Sons, Inc.(1993).

van Parijs, I. A. and Froment, G. F., "Kinetics of Hydrogenation on a CoMo/alpha-Alumina Catalyst. 1. Kinetics of the Hydrogenolysis of Thiophene", Ind. Eng. Chem. Prod. Res. Dev., **25**, 431-436 (1984).

Wedel, M. and Luss, D., "Steady State Multiplicity Features of an Adiabatic Fixed-Bed Reactor with Langmuir-Hinshelwood Kinetics; CO, or CO_2 Methanation", Ind. Eng. Chem. Fundam., **23**, 280-288 (1984).

Wu, P. C., "The Kinetics of Reaction Carbon with Carbon Dioxide, D.Sc. Thesis, M.I.T., Cambridge (1949).

Yu, H. C. and Sotirchos, S. V, "A Generalized Pore Model for Gas-Solid Reactions Exhibiting Pore Closure", AIChE J., **33**(3), 382-393 (1987).

APPENDICES

APPENDIX A

GENERATION OF THE TERMS FOR THE THOMAS ALGORITHM FOR SYSTEM EQUATIONS.

In this section the generation of the terms for the Thomas algorithm for the solution of the model equations is outlined. As an illustration of the procedure used in solving the equations, a representative case of heat conservation equation in the pellet is used.

The pellet heat conservation equation (section 3.2.4) may be reproduced here as

$$C_P{}^e \frac{\partial T}{\partial t} = \nabla k^e \nabla T - \sum_j^{N_g} N_j C_{Pj} \nabla T - \sum_i F_i \Delta H_i - \sum s_i f_i \Delta H_i \qquad \text{(A1)}$$

This equation can be expressed at a point *i* in the pellet as

$$C_P{}^e \frac{\partial T}{\partial t} = \frac{1}{r}\frac{\partial}{\partial r}\left(k^e r \frac{\partial T}{\partial r}\right) - \sum_j^{N_g} N_j C_{Pj} \frac{\partial T}{\partial r} - \sum_i^{N_{r1}} F_i \Delta H_i - \sum_i^{N_r} s_i f_i \Delta H_i \qquad \text{(A2)}$$

This may simplified into equation (A3) if the variations of k in the radial direction is neglected in the pellet,

$$C_P{}^e \frac{\partial T}{\partial t} = \frac{k}{r}\frac{\partial T}{\partial r} + k\frac{\partial^2 T}{\partial r^2} - \sum_j^{N_r} N_j C_{Pj} \frac{\partial T}{\partial r} - \sum_i^{N_{r1}} F_i \Delta H_i - \sum_i^{N_r} s_i f_i \Delta H_i \qquad \text{(A3)}$$

In the following, the subscript *i* is used to indicate position in the radial direction, in the pellet, * indicate position in the time direction at t+1, with t dropped for

simplicity. A finite difference approximation descritizing the first four terms using the Crank-Nicolson implicit scheme, gives:

$$C_P^{\,e}\frac{\partial T}{\partial t} = C_{pn,j}^{e}\frac{T_i^* - T_i}{\Delta t} \tag{A4}$$

$$\frac{k}{r}\frac{\partial T}{\partial r} = \frac{k}{2r_{pi}}\left(\frac{T_{i+1}^* - T_{i-1}^*}{2\Delta r} + \frac{T_{i+1} - T_{i-1}}{2\Delta r}\right) \tag{A5}$$

$$k\frac{\partial^2 T}{\partial r^2} = \frac{k}{2}\left(\frac{T_{i+1}^* - 2T_i^* + T_{i-1}^*}{(\Delta r)^2} + \frac{T_{i+1} - 2T_i + T_{i-1}}{(\Delta r)^2}\right) \tag{A6}$$

$$\sum_j^{N_r} N_j C_{Pj}\frac{\partial T}{\partial r} = \sum_j^{N_r} N_j C_{Pj}\left(\frac{T_{i+1}^* - T_{i-1}^*}{2\Delta r} + \frac{T_{i+1} - T_{i-1}}{2\Delta r}\right) \tag{A7}$$

The descritized form of equation (A3) is given by the combination of equations (A4), (A5), (A6). and (A7).

$$C_{pn,j}^{e}\frac{T_i^* - T_i}{\Delta t} =$$

$$\frac{k}{2r_i}\left(\frac{T_{i+1}^* - T_i^*}{\Delta r} + \frac{T_{i+1} - T_i}{\Delta r}\right) + \frac{k}{2}\left(\frac{T_{i+1}^* - 2T_i^* + T_{i-1}^*}{(\Delta r)^2} + \frac{T_{i+1} - 2T_i + T_{i-1}}{(\Delta r)^2}\right)$$

$$-\sum_j^{N_r} N_j C_{Pj}\left(\frac{T_{i+1}^* - T_{i-1}^*}{2\Delta r} + \frac{T_{i+1} - T_{i-1}}{2\Delta r}\right) - \sum_i F_i\Delta H_i - - \sum_i s_i f_i \Delta H_i \tag{A8}$$

After rearranging, collecting, and preparing all the unknown Temperature values at *, (t+1) time step on the left-hand side, one can arrange the terms in equation (A8) in the form of Thomas algorithm which is based on Gaussian elimination using tridiagonal matrix. The resultant equations are cast in the following form:

$$AT_{i-1} + BT_i + CT_{i+1} = D \tag{A9}$$

A_i, B_i and C_i are lower, main, and upper diagonals respectively of the diagonal matrix used together with values of D (which are known) in Gaussian elimination for evaluating the unknowns, T_{i-1}, T_i, and T_{i+1}.

The following definitions are used so that the coefficients; A, B, C and D do not appear cumbersome.

$$X1(i) = \frac{k\Delta t}{4r_p(i)C_p^e\Delta r} \qquad \text{(A10)}$$

$$X2(i) = \frac{k\Delta t}{2r_p(i)C_p^e(\Delta r)^2} \qquad \text{(A11)}$$

$$X3(i) = \frac{\Delta t\sum_j^{N_r} N_j C_{pj}}{4C_p^e\Delta r} \qquad \text{(A12)}$$

$$A(i) = [X1(i) - X2(i) - X3(i)] \qquad \text{(A12)}$$

$$B(i) = [1 + X2(i)] \qquad \text{(A13)}$$

$$C(i) = [-X1(i) - X2(i) + X3(i)] \qquad \text{(A14)}$$

$$D(i) = -A(i)T_{i-1} + (1 - 2X2(i))T_i - C(i)T_{i+1} - \sum_i^{N_{r1}} s_i f\Delta H_i - \sum_i^{N_r} F_i\Delta H_i$$

(A15)

Equation (A9) is for $1 < I < N$, while 1 and N indicate the center and surface of the pellet respectively. For the points 1 and N the equation is modified based on the boundary conditions.

At the center, r=0, i=1, the coefficients are modified as follows:

$$B(1) = [X2(1) - X3(1)]$$

$$C(1) = [1 - X2(1) + X3(1)] \qquad \text{(A16)}$$

$$D(1) = C(1)T_1 + B(1)T_2 - \sum_i^{N_{r1}} s_i f\Delta H_i - \sum_i^{N_r} F_i\Delta H_i$$

At the surface, r = N, and $T_{N+1} = T_{N-1}$

$$A(N) = 2[-X2(N) + X3(N)]$$
$$B(N) = [1 + 2X2(N) - 2X3(N)] \qquad \text{(A17)}$$
$$D(N) = B(N)T_{N-1} + C(N)T_N - \sum_i^{N_{r1}} s_i f \Delta H_i - \sum_i^{N_r} F_i \Delta H_i$$

T_N refers to the surface temperature. The same procedure was applied to other model equations.

These equations and coefficients form a set of 2N simultaneous linear equations with 2N values of the mass and temperature at the t+1 step as unknowns. This assumes that all the values at the present time level are known. This follows directly from initial conditions at t = 0, equations (19a)-(19c). Each set of equations has a tridigonal coefficient matrix and each can be put in the form of:

$$MT = D^T \qquad \text{(A18)}$$

for example for the heat balance. Here, M is the matrix of the coefficient,
T is the matrix of the unknown temperatures and D is the matrix of the known values from the previous time step.

This method of solution as the name implies is due to Thomas. It is both fast and efficient in minimizing round-off error propagation (Mcquire and Lapidus, 1965).

APPENDIX B

PROGRAM DESCRIPTION

The mathematical model developed in Chapter 3 and discretized in Chapter 4 in finite difference form was programmed in FORTRAN 77. A completely self-contained program was designed to calculate the transient equations of the pellet and reactor bed subject to the initial conditions and any perturbations in the desired variables. The model was simulated using an IBM compatible 486, 100MHz computer.

The program reads all the input data: system parameters, initial conditions, and the values of all the initial distribution of variables for the bed, pellet and grain for onward calculations. There are different subroutines for calculations / evaluations at different segments of the program. The program roughly runs in the following sequence: it evaluates some essential preliminaries, such as grid point and initial volume of grains; it then increases the time step by Δt; it calculates the bed properties, bed fluxes, mass and heat transfer coefficients. On this basis it vectorizes the three dimensional pellet variables.

Three dimensional vectorization is done in the pellet because of the bed axial, and bed and pellet radial directions. At this stage the program "enters" into a pellet. Here all the physical and transport properties (as noted in Section 3.4) are calculated. It then calculates the concentration of each component and temperature profiles based on reaction rate expressions and pellet conditions. The changes in grain radii or reaction fronts in case of chemically reacting solids are also

evaluated. The important relationship among grain, pellet and bed are given in Section 3.2.

The pellet serves as a source or sink for temperature and concentration for the bed. The bed temperature and concentration profiles are then evaluated. After a specified number of steps the program prints desired variables. Some important variables are transient concentration of each component and temperature along the axial and radial directions for the bed and pellet as the case my be.

The maximum reaction time is specified as desired. A variable time step is used. It is increased by roughly 10% at each step until a maximum value is reached which is then maintained till the end of the run period. This is particularly important since more values of the results could be printed and observed at the initial stage of the simulation run. The reactor used in the simulation contains 64 cells, (only 32 are used due to symmetry) the time for the calculation of next set of profiles at time step $t+\Delta t$ requires about 1 sec. Each pellet is divided into 5 internal radial increments for the computation time in order to increase the speed of response of the system. A preliminary investigation has shown that the number of grid points or cells chosen gives accurate and stable results for the system.

The flowchart of the program is presented in Figure B.1 below.

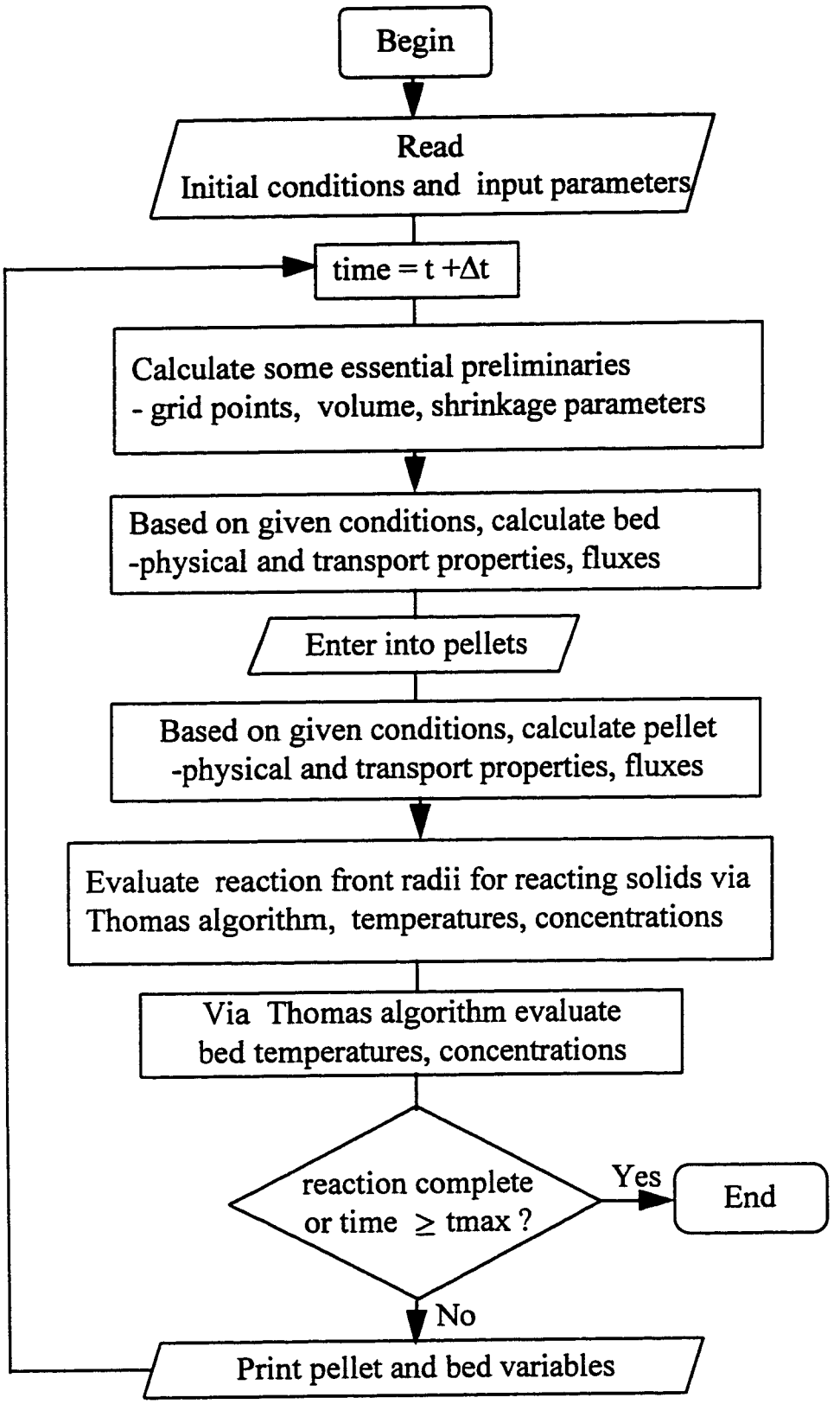

Figure B.1 Flowchart of the program

APPENDIX C

SAMPLE INPUT DATA FOR THE PROGRAM

Sample data for the program for one of the simulations are presented below. The relevant read statements follow the data.

```
1, 4, 1
5, 0.0002, 1000.1
1., 1., 3., 1., 523.15, 50.6625D+6
523.15, 523.15, 50.6625D+6
0.05, 0.0, 0.95, 0.0
1.88E+14, 125200.0
5.53E-4, 44600.0
7.23E-1, 0.0
91.2, 0.0
0.566, 0.0015, 0.005E-6, 800.0E-6, 0.0015, 8.31439
1800, 1800, 12., 12.
0.05, 0.0, 0.95, 0.0
84.,34.,2.,58.
0.4854, 0.3623, 0.2823, 0.5265
432.3, 301.1, 59.7, 323.
579.4, 373.2, 33.2, 419.6
56.2,  88.2,  12.8, 39.7
2.50E-5, 0.027
2.264E+5, 600., 0.,0.,0.,0., 18.90, 1.46
-7.310,1.070E-1, -9.009E-5, 2.992E-8
7.629, 3.431E-4, 5.809E-6, -2.810E-9
6.483, 2.215E-3, -3.298E-6, 1.826E-9
-0.715,8.436E-2, -4.754E-5, 1.066E-8
1.E-7, 1.E-8, 0.01
1.E-7, 1.E-7, 0.1
0.8, 5.676E-8
0., 0.35, 4.6E+7
0.4575, 0.0135
8,4
1
500., 500., 500., 500., 500., 500., 500., 500.
```

```
READ (5,*) N, DELT, TMAX
READ (5,*) B,C,D,E,TB,PB
READ (5,*) TFLUID,TINP,PPIN
READ (5,*) PYAIN,PYCIN,PY2IN,PY4IN
READ (5,*) AK10,EA1
READ (5,*) AK20,EA2
READ (5,*) AK30,EA3
READ (5,*) AK40,EA4
READ (5,*) EPSI,RP,RO,PWI,PEL,RGAS
READ (5,*) DENB,DEND,WMB,WMD
READ (5,*) XAB,XCB,X2B,X4B
READ (5,*) WMA,WMC,WM2,WM4
READ (5,*) RMSA,RMSC,RMS2,RMS4
READ (5,*) EMAA,EMAC,EMA2,EMA4
READ (5,*) TCA,TCC,TC2,TC4
READ (5,*) PRCA,PRCC,PRC2,PRC4
READ (5,*) FLOW,PIPEID
READ (5,*) HR1,TR1,HR2,TR2,HR3,TR3,TKM,CPS
READ (5,*) CPA11,CPA12,CPA13,CPA14
READ (5,*) CPA21,CPA22,CPA23,CPA24
READ (5,*) CPA31,CPA32,CPA33,CPA34
READ (5,*) CPA41,CPA42,CPA43,CPA44
READ (5,*) TOL1,TOL2,TOL3
READ (5,*) DCA,DCC,DXT
READ (5,*) EMI,SIGMA
READ (5,*) PFLAG
READ (5,*) BETA
READ (5,*) EPSD,PEPS,ANAREA
READ (5,*) ZPACK,RPACK
READ (5,*) NI,NJ
READ (5,*) IWALL
READ (5,*) (TW(I),I=1,NI)
```